NASA CR-935094

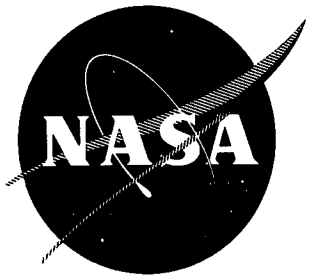

SURFACE CRACK GROWTH IN FIBER COMPOSITES

by

J. Im, J.F. Mandell, S.S. Wang, and F.J. McGarry

MASSACHUSETTS INSTITUTE OF TECHNOLOGY

prepared for

NATIONAL AERONAUTICS AND SPACE ADMINISTRATION

NASA Lewis Research Center
Grant NSG 3044

DISCLAIMER NOTICE

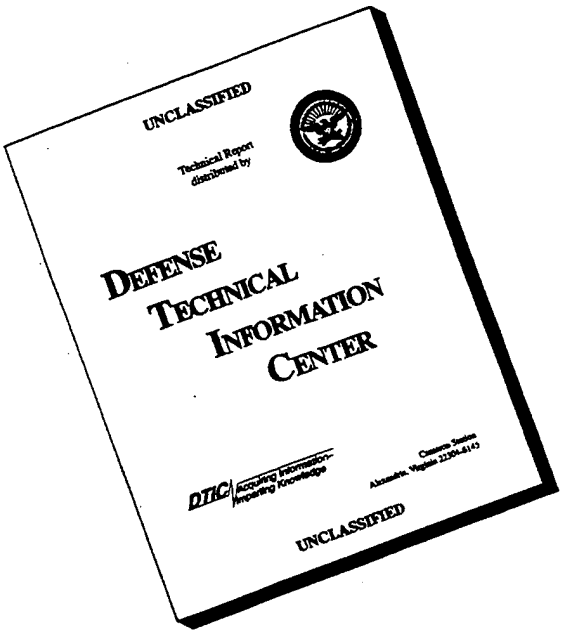

THIS DOCUMENT IS BEST QUALITY AVAILABLE. THE COPY FURNISHED TO DTIC CONTAINED A SIGNIFICANT NUMBER OF PAGES WHICH DO NOT REPRODUCE LEGIBLY.

1. Report No.	2. Government Accession No.	3. Recipient's Catalog No.
NASA CR 935094		

4. Title and Subtitle	5. Report Date
Surface Crack Growth in Fiber Composites	September 1976
	6. Performing Organization Code

7. Author(s)	8. Performing Organization Report No.
J. Im, J. F. Mandell, S. S. Wang, F. J. McGarry	10. Work Unit No.

9. Performing Organization Name and Address	11. Contract or Grant No.
Department of Materials Science and Engineering Massachusetts Institute of Technology Cambridge, MA 02139	NSG 3044
	13. Type of Report and Period Covered
12. Sponsoring Agency Name and Address National Aeronautics & Space Administration Washington, DC 20546	Interim
	14. Sponsoring Agency Code

15. Supplementary Notes

Project Manager, C. C. Chamis
Materials and Structures Division
NASA-Lewis Research Center
Cleveland, OH 44135

16. Abstract

The results of an experimental study of damage extension and failure in glass and graphite/epoxy laminates containing partially through-thickness surface cracks are presented. The laminates studied are divided between those containing four plies, 90/0/0/90, 15/-15/-15/15, and 45/-45/-45/45, and those containing 12-16 plies of the general configurations 0/90, $\pm$45, and 0/$\pm$60. Most of the results are for surface cracks of various lengths and several depths. Stable damage extension in laminates containing surface cracks is predominantly delamination between plies, and tends to be much more extensive prior to failure than is the case with through-thickness cracks, resulting in approximately notch-insensitive behavior in most cases. A greater tendency for notch-sensitive behavior is found for 0/90 graphite/epoxy laminates for which stable damage extension is more limited. The rate of damage extension with increasing applied stress depends upon the composite system and ply configuration as well as the crack length and depth. An approximate semiempirical method is presented for estimating the growth rate of large damage-regions.

17. Key Words (Suggested by Author(s))	18. Distribution Statement
Fiber composites, surface cracks, flaw growth, failure, delamination, glass, graphite, flaw-growth rate, experimental, approximate analysis	Unclassified, Unlimited

19. Security Classif. (of this report)	20. Security Classif. (of this page)	21. No. of Pages	22. Price*
Unclassified	Unclassified	130	

* For sale by the National Technical Information Service, Springfield, Virginia 22151

FOREWORD

This report summarizes experimental efforts for the period 1 February, 1975 through 1 May, 1976. The study was conducted for the NASA-Lewis Research Center by members of the Department of Materials Science and Engineering at the Massachusetts Institute of Technology. The Principal Investigator in the study is Prof. F.J. McGarry; other major participants are J. Im, J.F. Mandell, and S.S. Wang. The NASA-LeRC Project Manager is Dr. C.C. Chamis, Mail Stop 49-3.

Efforts in this study are primarily directed towards the development of finite element analyses for the study of flaw growth and fracture of composites. The experimental work described in this report is meant to complement the analytical efforts by providing test data for comparison purposes, as well as to advance the general understanding of the subject.

ABSTRACT

The results of an experimental study of damage extension and failure in glass and graphite/epoxy laminates containing partially through-thickness surface cracks are presented. The laminates studied are divided between those containing four plies, 90/0/0/90, 15/-15/-15/15, and 45/-45/-45/45, and those containing 12-16 plies of the general configurations 0/90, ±45 and 0/±60. Most of the results are for surface cracks of various lengths and several depths. Stable damage extension in laminates containing surface cracks is predominantly delamination between plies, and tends to be much more extensive prior to failure than is the case with through-thickness cracks, resulting in approximately notch-insensitive behavior in most cases. A greater tendency for notch-sensitive behavior is found for 0/90 graphite/epoxy laminates for which stable damage extension is more limited. The rate of damage extension with increasing applied stress depends upon the composite system and ply configuration as well as the crack length and depth. An approximate semiempirical method is presented for estimating the growth rate of large damage-regions.

CONTENTS

LIST OF TABLES

LIST OF FIGURES

INTRODUCTION

The confidence with which any material may be employed in a structural capacity depends, among other considerations, upon the degree of understanding and the predictability of its response to the variety of damage and pre-existing stress concentrators which it may encounter in service. The wealth of experience with homogenous materials in this regard stands in contrast to the relatively unknown behavior of fiber reinforced composites in the presence of any but the most basic types of damage, consisting almost entirely of through-thickness cracks or holes under uniaxial loading. The objective of the study described in this report was to obtain detailed data on the response of some common laminate types to damage which does not completely penetrate through the thickness (surface flaws or cracks). The data are to be used in conjunction with the development of a three-dimensional finite element analysis in another part of the study as well as to advance knowledge in this field.

Background

Studies of the fracture resistance of composites have largely adopted the techniques available from the existing technology of homogenous materials. Primary attention with homogenous materials is focused on dominant, through-thickness cracks [1]. This emphasis is logical for several reasons: (1) through-crack geometries are more simple to treat both experimentally and analytically, (2) through-cracks are generally the most severe, (3) other crack geometries, such as surface cracks, propagate in a similar manner, often growing to become through-

cracks, and (4) if the material is isotropic, it has a similar resistance to any type of crack. The study of failures in homogenous materials is simplified by the characteristic features of a dominant spreading crack which is colinear and self similar, and whose extension is resisted by an identifiable material property, the fracture toughness, subject primarily to variations in the degree of triaxiality of the stress field.

The behavior of fiber reinforced composites containing through-thickness cracks is in some respects similar to that of homogenous materials. Depending upon the fiber, matrix and ply configuration involved, the crack may be colinear and self similar on a macroscale, and classical brittle fracture criteria may be applicable [2]. Composites may also display a "quasi-ductile" behavior, reaching complete notch-insensitivity [3]. The fracture behavior, like other properties, is highly anisotropic, and may vary from brittle to notch-insensitive for specimens cut in various directions from the same plate of material [3].

While the behavior of some composites containing through-cracks may resemble homogenous materials on a macroscale, the local stress and fracture characteristics of crack extension are considerably different. The high degree of anisotropy, particularly within each ply, results in a complex array of local damage at the main crack tip. For laminates composed of unidirectional plies with fibers oriented in various directions, the damage tends to occur on the weakest planes, resulting in a local system of cracks running parallel to the fibers of each ply and between plies [4]. This damage zone grows in extent as the applied stress is increased, until complete fracture finally occurs, often catastrophically. As long

as the damage zone remains localized near the crack tip region, the extension of the damage and the conditions of fracture appear to be governed at least approximately by the classical stress intensity factor, K_I (opening mode). If the inter and intraply damage becomes global, spreading far ahead of the original crack, then the behavior becomes notch-insensitive. Figures 1,2 and 3, taken from Reference [4], give the size and geometry of the damage region for graphite fiber reinforced epoxy laminates similar to those used in the present study. The 90/0/0/90 and 15/-15/-15/15 laminates in Figures 1 and 2 were notch-sensitive, as the damage remained localized until fracture occurred; the 45/-45/-45/45 laminate in Figure 3 was notch-insensitive, as the damage became global prior to fracture. Damage zones in laminates of other ply configurations may be even more complex, involving fiber breakage and buckling in some cases, as well as multiple resin cracking parallel to the fibers [3].

The characteristics of the damage zone in Figs. 1 - 3 are in sharp contrast to a single crack in a metal, with a yielded zone at the tip. The cracks within one ply of the laminate do not generally penetrate adjacent plies, but terminate at the ply interface or at an interfacial crack. The material within the damage zone remains generally elastic and continuous except for the individual cracks. Early three-dimensional finite element results have shown the complex mechanics of stress transfer within the damage zone which lead to a relaxation of the in-plane stresses relative to those existing in the absence of such damage [5]. These results also indicate the mechanisms tending to cause damage zone

extension and the constraints on extension provided by neighboring plies.

The high degree of anisotropy evident in damage zones at through-thickness crack tips may be anticipated to have even greater influence with cracks which do not penetrate completely through the laminate. Existing literature on this topic is limited to very simple cases, but the important problem of the unwinding of a rocket motor case illustrated in Figure 4 is typical of unwinding from surface flaws encountered in many pipe and pressure vessel applications. The geometry of the crack in Figure 4 is indicative of partial through-thickness cracks in general. These cracks have a strong tendency to propagate parallel to the fibers causing unwinding, and seldom penetrate further through the thickness. If unwinding of the type in Figure 4 is extensive and stress concentrations are not signficant, propagation of the crack may be predicted by assuming that the crack tip stress field remains constant as the crack extends, leading to the approximation [6]

$$G_c = \frac{ct_1}{c+t_1}\left(\frac{\sigma_c^2}{2E_h}\right) \tag{1}$$

where G_c is the critical strain energy release rate for peel-off-type delamination, E_h is the elastic modulus in the hoop direction, and σ_c is the critical hoop stress. For $t_1 << C$ this gives

$$G_c = \frac{t_1 \sigma_c^2}{2E_h} \tag{2}$$

The above relationships suggest a possible method of prediction for the extension of global damage zones which primarily involve delamination between plies, and such an approach has been pursued in the present case.

Scope

The approach taken in this study was exploratory in nature, since little was known about partially through-thickness cracks in laminates containing plies oriented in various directions. Relatively simple geometries such as that in Figure 4 were not considered, thus eliminating cases where only the surface ply was damaged. The interest in the present study was in crack geometries where free peeling or unwinding as in Figure 4 is constrained by neighboring plies having fibers which cross over one another.

The work is divided between relatively simple laminates containing four plies, in the configurations 90/0/0/90, 15/-15/-15/15, and 45/-45/-45/45 (the ply angle is the direction of the fibers relative to the load, with the initial crack cut perpendicular to the load direction), and laminates containing a greater number of plies in the configurations 0/90, ± 45, and $\pm 60/0$. Both graphite/epoxy and E-glass/epoxy are used in the four-ply laminates, with E-glass/epoxy used for the thicker laminates. Crack geometries are primarily surface cracks of varying depth and length, with embedded cracks used in only a few cases for comparison.

Emphasis in this experimental phase of the work is in two areas: (1) gathering precise data for damage extension from precut cracks to be used later in comparisons with analytical predictions, and (2), a broader characterization of damage geometry, growth characteristics and fracture behavior of laminates with a range of ply configurations and crack lengths. This was done in order to gain a more general and in-depth understanding of the behavior of fiber composite laminates containing such cracks. As a result, data are given and discussed in greatest detail for the 0/90 laminates, with less emphasis on quantitative damage growth rates in the other cases. Tables 1 and 2 list the ply configurations and geometries tested.

EXPERIMENTAL METHODS

Materials

All materials used in this study were obtained from 3M Company as prepeg, and were compression molded using a bleeder cloth arrangement. The graphite/epoxy was SP288-T3 (Thornel 300 fibers), a medium-modulus material. Two types of E-glass/epoxy were used: Type 1002 was to be used for the entire study, but this line was discontinued midway through, so Type 1003 was substituted. Type 1003 has a slightly lower ply thickness. The switch from Type 1002 to 1003 required considerable retesting since the properties were not identical.

Specimens containing surface cracks were prepared according to the following procedure:

1. Pieces were cut to the desired size out of a roll of prepeg.
2. If a surface crack, m plies deep was to be included, then only m plies were joined together by hand, in the desired ply sequence. This is called Assemblage I.
3. Using a commercial razor blade, the assemblage was cut to form the desired crack geometry as shown schematically in Fig. 5.
4. Once this was done, the Assemblage II which would constitute the remainder of the specimen was layed up similarly, but without razor cuts.

5. Assemblages I and II were stacked together, making one plate.

6. If a surface crack was also needed on the other surface of the specimen, the same operation as was followed with Assemblage I was repeated to produce Assemblage III as shown in Fig. 5. The Assemblage III was then put together with the other two. Care was exercised to locate the two cracks as nearly opposite to each other as possible.

7. On each side of the plate was placed a layer of permeable Teflon-coated fiberglass, followed by one layer of bleeder cloth (Mochburg Type CW1850) per every two plies of the laminate, followed by a layer of impermeable Teflon-coated fiberglass next to an aluminum mold plate.

8. The whole assembly was placed in a press, in order to cure the laminate. The cure conditions were

	glass/epoxy	graphite/epoxy
preheat	330°F(166°C)	300°F(149°C)
contact pressure and duration	40 psi(276 KN/m^2) for 2 min.	40psi(276KN/m^2) for 2 min.
gradual increase in pressure to	100 psi(690 KN/m^2)	100 psi(690 KN/m^2)
within	2 min	2 min
curing time	45 min	2 hrs.

9. The cured plate was machined by rough cutting with a diamond-edged wheel, and finished with a Tensilekut router to the desired dimension. Care was exercised to have the suface crack as nearly centered as possible.

The structure of graphite/epoxy was very sensitive to the molding conditions. A series of specimens were molded by changing only the time duration at contact pressure while keeping the other conditions the same. The two-minute contact time gave the best quality laminates yielding the fewest voids, so this condition was maintained throughout the study in molding the test specimens. The quality under these conditions was good as indicated by a typical cross-section in Figure 6. The interlaminar shear strength measured by short beam bend tests averaged 13.0 ksi (89.6 MN/m^2).

Glass/epoxy laminates are relatively difficult to observe using the optical microscope because the fiber boundaries are less distinguishable than with graphite. The fibers were made more observable by etching the specimen with 1% hydrofluoric acid (diluted in water) for 5-7 seconds. The effect of etching on the matrix surface was insignificant so that fine cracks, when present, could be viewed without distortion. A micrograph of a cross section using this technique is shown in Fig. 7 for Type 1002 Scotchply in the virgin state. Unlike graphite/epoxy, there appear to be numerous large voids, but apparently no temperature cracks. This quality is typical of previous experience with Type 1002 Scotchply, and efforts to decrease the void content were unsuccessful. The average interlaminar shear strengths for glass/epoxy were 6.0 Ksi(41 MN/m^2) for Type 1002 and 6.2 Ksi(43 MN/m^2) for the Type 1003.

The cracks introduced by cutting the prepeg prior to molding showed good retention of their original geometry. The crack flanks appeared straight by visual inspection, and the tips of the crack were relatively sharp where fibers were cut. Figure 6 shows a micrograph of a surface crack as molded; the crack tip radius is in the range of 10^{-3} in. (2.5×10^{-3} cm).

Testing Procedure

Tests were performed using an Instron universal testing machine with the cross-head speeds of 0.05 and 0.02 in/min. (.13 and .05 cm/min) for glass/epoxy and graphite/epoxy, respectively. The ultimate tensile strength specimens for various ply sequences were prepared by bonding tapered fiberglass tabs on the grip surfaces of the straight-sided strips for four-ply laminates; a dog-bone shape was used for the thicker laminates with a reduced width of 1.5 in (3.81 cm). The appearance of the precracked plates prior to load was not different from the uncracked plates, because the razor cuts were completely closed up by flowing resin during cure. However, the cracks opened up at applied stresses in the range of 7 to 11 ksi (48 to 76 MN/m^2) for glass/epoxy and 14 to 18 ksi (97 to 124 MN/m^2) for graphite/epoxy.

For the purpose of investigating the characteristics of damage which developed due to the presence of precut cracks, the specimens were loaded to some predetermined stress level before being unloaded and removed from the testing machine. In the notch region of the preloaded glass/epoxy, black india ink was applied, which stained delamination interfaces and penetrated into splits. In selecting staining agents, consideration was given to penetrability, washability and

color. Although some of the dyes normally used for biological purposes were excellent in the speed of penetration, they were too easily washed out during wet-sanding. The india ink chosen would not penetrate as fast as the above, but it spread sufficiently after a duration of time, and moreover was hard to wash away completely. The low interlaminar shear strength of glass-epoxy made it possible to peel off one layer after another, instead of sanding, in order to examine interfacial delaminations. Wet sanding and polishing were employed when splits within a ply were to be measured.

The staining technique was not effective for graphite/epoxy because of the opaqueness of the specimens. Instead, a fluorescent dye (Zyglo, Magnaflux Corp.) was sprayed on the preloaded, notched specimen. After waiting until the dye had penetrated and dried, the specimen was bonded to a flat surface of a solid plastic piece for better holding and handling. It was wet-sanded, polished and viewed under ultraviolet light so that the regions containing the dye were evident. Exposing delamination by sanding and polishing was a tedious process. If the plane of the surface being polished wasn't kept parallel to that of the laminate interfaces, the fluorescent dye was removed at one portion of delamination while other portions were still unexposed. Also the polishing had to be stopped at the right moment when the dye still remained at the valleys existing due to the waviness of the delamination surface. The dye could easily be lost completely by slightly more polishing.

The wet sanding, polishing and viewing were repeated sequentially through the entire specimen. As the damage was usually extensive for both glass and graphite/epoxy, viewing was either direct or with the aid of a 10X magnifier.

FOUR-PLY LAMINATES

Introduction

Four-ply laminates were chosen as the subject of a significant portion of the study due to their relative simplicity both for experimental observation and analytical modelling. Before considering the actual results for four ply laminates it is instructive to consider the general nature of damage which is observed for surface cracks in a variety of laminates. Figure 8 (a) indicates schematically that damage extending from from a laminate with a surface crack completely across the width is similar to that in Figure 4: the primary damage takes the form of a delamination crack propagating along the length of the specimen. In many cases the delamination spreads completely into the grips, leaving the uncut plies to carry the full load. In some cases, particularly with graphite/epoxy, the entire specimen may fail at some lesser value of ℓ. Figure 8(b) indicates schematically a similar, but more complex damage geometry for cases of surface cracks with $2C < W$. There is still a strong tendency to form a large delamination, but now the growth of the delamination is constrained by plies with transverse fibers, and a complex damage pattern may develop, possibly resulting in some lengthening of the original crack in the precut plies.

E-Glass/Epoxy Laminates

Results were obtained for Type 1003 Scotchply using three different ply sequences : 90/0/0/90, +15/-15/-15/+15 and +45/-45/-45/+45 which contained surface cracks half-way through the thickness, and of various lengths.

Figures 9 (a) - (c) show test results of nominal fracture stress vs. normalized crack length. The notch insensitive lines represent the nominal fracture stress level which would be calculated if the stress state were uniform at the time of fracture, as opposed to a state with concentrated stress near the cracks. Noting that the net-section (measured at the notch) then would attain a stress approximately equal to the UTS (ultimate tensile strength) of the same material without a notch, ignoring the effects of nonsymmetry, etc., the notch insensitive stress can be represented as

$$\text{notch insensitive stress} = \text{UTS} \left(\frac{A_{net}}{A_{gross}} \right) \tag{3}$$

where A_{gross} is the cross-sectional area of a straight edged strip measured away form the notched section and A_{net} is the area at the notch. The notch insensitivity as approached by the data in Fig.9 can be attributed to steady, extensive growth of damage such as delaminations and splits which effectively eliminate the stress concentrations that would be expected at the precut cracks. While ±45 laminates tend to be notch insensitive even for through-cracks, the 0/90 laminate would be significantly notch-sensitive for through-cracks over much of the range of 2c/W [4].

Damage did not occur in a stressed specimen until the applied stress reached at least 20-30% of the UTS, the stress being lower as the crack length increased. The first damage was in the form of delamination, initiated at the center of the root of the surface crack and expanding at the interface separating the last precut layer (second layer) and the adjacent uncut layer (third layer). Although some other similarities in behavior can be observed among the three ply configurations, they are most conveniently discussed separately.

For 90/0/0/90 laminates, further growth of damage is shown schematically in Fig. 10 and photographically in Fig. 11. When the boundary of the expanding delamination reached the precut crack tips, it was pinned down there, making only vertical expansion possible from then on. However, the vertical growth itself was also constrained. The situation was analogous to a metal containing a dislocation line pinned down at two points (crack tips in the study), where the increase in area enclosed by the dislocation line comes only through the change in curvature of the line. Eventually, but well before the delamination attained a full circular shape, the stress concentration at the surface crack tips caused splits parallel to fibers within the second layer (0°) as shown by the third schematic in Fig. 10. The splits apparently played a dual role: first, that of relieving stress concentrations at the tips, so that the 0°fibers at the crack tip did not fail, and second, that of acting as boundaries within which the delamination could grow. The splits also changed the shape of the opened crack into a near-rectangle from a thin ellipse, and changed the rate of delamination growth with respect to applied stress. Since the crack opening is apparently accomplished primarily by retraction during unloading of the mid-strips separated from the body due to delamination and 0° splits, it involved the tearing off and lifting up of the last continuous material still holding the mid-strips, e.g., first layer (90°). As a result, another form of delamination was created around the main cracktips, at an interface different from the previous one. It appeared as a slender triangle beyond the crack tips with the 0° split as its longest side. The 90° layer over this region was severely damaged due to splits parallel to the fibers on its own plane; the split spacing was in the range of 0.01 to 0.03 in. (.025 to .076 cm).

Figure 12 shows a series of photographs taken by peeling off layers of the ink-stained specimen containing a surface crack of $2c/W = 0.375$, after preloading to 76% of the UTS. The first photo taken before peeling faintly shows numerous 90° splits within the region of darker triangular background. When the first layer is peeled off, the triangular delaminations can be seen to have grown almost up to the propagating fronts of the major delamination underneath. The length of the long 0° splits at the surface crack tips is concealed in this photo, but it can be noted clearly after slight polishing of the surface to remove the stain, as shown in Fig. 13. Note also from the Figure that the surface crack did not extend from its initial length (did not fail any 0° fibers), the delamination underneath was completely contained within the 0° splits, and the splits constituted the longest sides of the triangular delaminations. The last photo in Fig. 12, which was obtained by peeling off one more layer, indicates that the upper and lower delamination boundaries are far from being circular but are rather box-shaped. When the specimen in Figure 12 was again polished, the stain was completely removed and no further damage was found in the remaining uncut plies.

The principal quantitative results from the observations are presented in Fig. 14-17 . Figures 14(a)-(f) give the relation between ℓ and ℓ_s for various crack lengths. The following empirical equation relates ℓ, the central delamination length, with ℓ_s, the 0° split length, obtained by a weighted average of the coefficients from a least-squares fit of data from each crack length

$$\ell/W = 0.40\,(2c/W) + 0.98\,(\ell_s/W) \qquad (4)$$

The significance of the equation can be realized by letting ℓ_s approach zero

$$\ell/W\Big|_{\ell_s = 0^+} = 0.40(2c/W)$$

or

$$\ell/2c\Big|_{\ell_s = 0^+} = 0.40$$

This equation suggests that the aspect ratio, $\ell/2c$ of the central delamination at the time of the 0° split initiation within the second layer is approximately constant for all surface crack lengths.

The ratio, $(\frac{\ell_s/2}{a})$, the slope of the outer boundary of the triangular delaminations, was approximately 8.0 for all crack lengths except those which were long enough to cause interaction with the free edges of the strip.

Figure 15(a) - (h) give the central delamination length, ℓ, as a function of applied stress for various crack lengths. Most of the data appear to follow a power law relationship on the log.-log. plots except at low stress levels. Deviation from the straight line tends to occur at the point where the value of ℓ_s first becomes non-zero. The initiation of delamination occurs along the central portion of the precut crack as indicated in Figures 10 and 11. The value of stress when this delamination is first observed varies only slightly for different crack lengths in Figure 15 from σ/UTS of approximately 0.35 at 2c/W = .125 to .25 at 2c/W = 1.0. Thereafter the delamination grows much more rapidly for the longer cracks. The results in Figure 15 represent the extension of the primary damage in the 0/90 laminates, and will be discussed in more detail in a later section, where linear plots of the same data are also given .

The crack opening displacement (COD) at the center of the pre-cut crack has also been measured as a function of stress and crack length. Figure 16 indicates a superposition of the data on to a nearly linear power law relationship over the entire range. A gradual change in the geometry of the open crack, approaching a rectangle at high loads, has already been noted in Figures 10 and 11.

Qualitatively similar damage is observed for ±15 laminates in Figure 17. The first damage is again in the form of delamination at the interface between the second and third ply. The delamination spreads more freely in the vertical direction after the constraining effects of the intact material beyond the crack tip are released by split formation parallel to the fibers of each ply. As the splits extend along the fibers from each crack tip toward the center-line of the specimen, they evenually cross each other at the center-line. This results in two identical isosceles triangles symmetric with respect to the surface crack, above and below it. The delamination grows within the triangle boundaries as shown in Fig. 17 (b). The triangles inevitably dictate the maximum growth of the delamination, which is constrained within the cones. It slows down after a period of fast growth.

The normalized vertical delamination length, ℓ/W is plotted against σ/UTS in Fig. 18 for the two composite systems. The three domains of different growth rate are more evident when redrawn on logarithmic scale (Fig. 19), where the slope of the central region suggests an exponent of approximately 5.3. The delamination initially grows slowly, mainly due to the constraint effect, up to σ/UTS equals approximately 0.5, where splits relieve the restriction on the growth. The fast growth domain lasts until a σ/UTS value of approximately 0.63. This roughly corresponds to the instant when the delamination assumes a full circular shape. Beyond this point, the growth rate decreases again. From Fig. 19, the delamination length at the

time of fracture may be picked as approximately 0.90W. Since the crossover points of the +15 and -15 fibers above and below the crack at center line of the specimen may be calculated as approximately 1.24W when 2c/W = 0.333, this indicates that the delamination does not expand beyond the peaks of the triangles.

Returning to Fig. 17, another form of delamination exists between the first and second plies. The splits formed in the second layer subject the first layer above these splits to kinking or shearing type of loading. This is induced by the unloading of the mid-strips which are partially freed by the central delamination. This results in additional splits parallel to the fibers of the first ply in the neighborhood of the crack tips. Delamination regions between the first and second plies instantly follow in-between these splits, as shown in Figs. 17(a) and (c). Note also from the photograph and schematic, the short splits within the second layer which are lined up along the splits formed in the first layer. Immediately prior to fracture, one or both of the splits in the first layer bordering the delaminations below that layer suddenly propagated close to the edge of the specimen. At this point the mid-strips were lifted up, distorting the whole specimen.

Damage extension in $\pm 45^\circ$ specimens was not measured quantitatively for this group of laminates. The only significant damage prior to fracture was intraply splits in all plies, parallel to the fibers, with little inter-ply delamination observed.

Graphite/Epoxy Laminates

Fracture tests performed to date on a limited number of graphite/epoxy specimens indicate that laminates containing partial through-thickness cracks are notch insensitive for +15/-15/-15/+15 (Fig. 20 (b)) and +45/-45/-45/+45 (Fig. 20 (c) configurations, similar to glass/epoxy in Figure 9. A relatively greater notch sensitivity is evident for the 90/0/0/90 configuration in Figure 20 (a).

Damage in the 90/0/0/90 laminates was not as massive as for glass/epoxy of the same ply sequence (given in Figure 11). However, the characteristics, e.g., central delamination between the second and third plies followed by vertical splits within the second ply at the main crack tips, followed by triangular delamination behind the tips but this time in between the first and second plies, etc. --- were identical for both materials.The origin of the increased notch sensitivity in the case of 0/90 laminates as compared with glass/epoxy is apparently directly related to the decreased stable damage extent at fracture. This was most evident in the case 2c=W, where the graphite epoxy specimens failed after an average delamination growth, ℓ/W, of .23 rather than propagating the delamination all the way to the grips. Figure 21 shows the left half only of a preloaded specimen which was later dyed, wet-sanded and polished down to different depths. The vertical split is clearly shown to limit the main crack extension and sidewise expansion of the delamination underneath. The polishing technique was not successful in revealing the delaminations situated at the crack tips in between the first and second plies , probably because the zones are so tiny and it is very difficult to stop polishing at the precise moment when the zones just appear but are not yet removed. These delaminations were observed on cross-sections only.

The only damage growth data obtained for 90/0/0/90 graphite/epoxy was the relation, ℓ/W vs. σ/UTS which is plotted to log scales in Fig. 22. The slope is Fig. 22 is approximately 6.2 at high stress levels. The slope wasn't estimated at low stress levels because of the lack of data, but it is evidently smaller than at high stress levels unlike glass/epoxy (Fig. 15).

Although Fig. 20 (b) indicates that the +15/-15/-15/+15 laminates are notch insensitive, the final fracture came catastrophically. The appearance of the fracture paths is shown in Fig. 23 for laminates containing two types of initial cracks - surface and embedded. For the specimens containing surface cracks, the fracture paths did not touch the initial cracks, indicating a very high degree of notch insensitivity. This was true of 45/-45/-45/45 laminates as well.

Two series of photographs are given in Figs. 24 (a) and (b), which were taken at different depths through the +15/-15/-15/+15 specimens containing surface cracks (the specimens were cut in half lengthwise along the center line after preloading). At the lower load (Fig. 24 (a)), the damage is restricted to the crack tips and the interfaces which separate the pre-cut plies from the remainder. The third and fourth plies are uncracked. The resultant cross-section in this case is shown in Fig. 25. When higher loads are applied, the previously intact layers are damaged by splits throughout the central region (Fig. 24 (b)). The growth rate of the central delamination is compared with that for glass/epoxy of the same geometry in Figs. 18 and 19. Three aspects are noteworthy from these Figures: (1) the delamination for graphite/epoxy is as extensive as for the glass, (2) when the applied stresses are normalized by the respective UTS, the data points almost superimpose, and (3) there are three regions differing in growth rate in Fig. 19 as was discussed for glass/epoxy.

The central delamination of +15/-15/-15/+15 laminates containing ebedded cracks developed at two interfaces within a specimen - between the first and second plies and between the third and last plies. Fig. 26 shows the damage appearance in different layers. There appear to be short splits within the two outermost plies along the line of the embedded crack. The second and third plies, which can act together as a unit (they have the same orientation), possess just one common split at the tip, apparently with no other damage. The central delaminations in these plies are small. Even at final fracture, the splits developed within the two mid-plies do not seem to play a role at the delamination boundaries. The delamination lengths plotted in Fig. 22 are an order of magnitude smaller than the corresponding lengths for the surface cracks shown in Fig. 19. Despite this localization of damage, the laminates containing embedded cracks were still notch-insensitive.

Introduction

The approach taken in this portion of the study is similar to that with four-ply laminates. Experimental observations made on several different ply sequences are described and quantitative results are presented for damage development and growth. Emphasis is on laminates with more layers than in the previous chapter, in some cases with matching cracks on each surface.

Damage in multi-ply composites is more complicated than in four-layered composites, in part because there exist more layers and interfaces. As a result, there are additional damage characteristics not recognized in thin composites, and data reduction is often difficult due to increased scatter.

This section is concerned entirely with surface crack phenomena. Embedded cracks are not specifically discussed. While the investigation is limited to E-glass/epoxy (both Type 1002 and 1003), new variables such as crack depth and specimen width are introduced.

Notch Sensitivity

Figures 27 and 28 give fracture test results for 90/0 laminates containing five layer deep surface cracks on one surface only and on both surfaces, respectively. The specimen width, when varied from one to two inches, did not affect the nominal fracture stress as long as the normalized

initial crack length, 2c/W was kept the same. The notch insensitive lines were obtained using the definition given in Equation (3), but the A_{net} and A_{gross} were replaced by the respective cross-sectional areas of the 0° layers only because the load carrying capacity of the 90° layers is expected to be insignificant. The approximate notch insensitivity revealed in both figures is, as in the four-layer laminates, a phenomenon not probable in the respective through-thickness crack cases, where the fracture stress is still governed by a brittle fracture criterion [3]. Consistent with the notch insensitivity, the crack tip damage was large enough to be comparable in size to the specimen width. The actual damage zone geometeries and the meaning of the second peak stress lines shown in the figures will be discussed in the following sections.

Figure 29 compares the tendency for notch sensitivity among specimens having various crack depths. The fracture stress deviates considerably downward from the notch insensitive line only when the crack is seven layers deep on both surfaces of a specimen, leaving only one uncut 0° layer.

Figures 30 and 31 show results for ±60/0 laminates containing four and five layer deep surface cracks, respecitvely, on one side of the specimen. As in the case of the 90° plies, the notch insensitive prediction lines are drawn without considering the contribution of the +60° or -60° plies. For the material considered here, the transverse ply strength is so low that it makes only a few percent difference at most in calculating the notch insensitive stress. The fracture stresses in Fig. 30 deviate somewhat from the notch insensitive line, while Fig. 31 shows considerably more downward deviation. The immediate departure of the data from the notch insensitive line in the latter figure, although not so severe, resembles the behavior of a specimen with a through-

thickness crack. Considering that not just one, but two ineffective layers (60°) are separating the assembly of pre-cut layers from the counterpart of exactly the same configuration, it may be that the results in Fig. 31 are a combination of the pre-cut assembly behaving in a brittle fashion, like a specimen with a through-thickness crack, while the remaining portion behaves like an unnotched specimen. The data in Figs. 30 and 31 fall between the NI prediction and a prediction based on the UTS of the uncracked plies only (the second peak stress).

Presented in Figs. 32 and 33 are the fracture test results for ±45 laminates with surface cracks on one and both surfaces, respectively. The behavior in each case is clearly notch-insensitive, as is by now anticipated for ±45° laminats.

Damage Formation and Growth

As in the four-layered composites, the first form of damage in multi-layered composites for all ply configurations was the delamination inititated at the center of the root of the surface crack, which then expanded at the interface separating the last pre-cut layer and the adjacent un-cut layer. This separation is designated as the central delamination. The delamination was then followed by split formation at the crack tips accompanied by delaminations at the other interfaces.

Figure 34 (a) is a schematic of the central delamination and 0°splits for 90/0 laminates at low load. As the load is increased (Fig.34(b)), the crack tip damage becomes severe and complicated. Figures 35 (a) and (b) present two sets of photographs showing damage throughout the thickness of specimens

which were preloaded to 68 and 79% of the UTS, respectively. The 1-2 interface, the interface between first and second plies of the first set shows two relatively small dark areas representing delaminations at the crack tips. Hidden below the stain are vertical splits as shown in 2 (the second ply). This was obtained by removing the surface stain with slight polishing. The polished surface of the third ply (designated by 3) shows 90° splits within the ply, but the vertical extent of the splits is not clear from the photograph. Note from both sets of photographs that the horizontal extent of delamination at interfaces (1-2), (2-3), and (3-4) and of splits within ply (2) are similar. The vertical extent is also similar between the delaminations at (1-2) and (2-3), but much more elongated for (3-4). These are illustrated schematically in Fig. 34 (b). Also shown in the figure is the horizontal extent of the remainder of the damage; e.g. splits within ply (4) and delaminations at interfaces (4-5) and (5-6) which progress together, lagging behind the other regions. This was observed for all load levels, as shown clearly in Fig. 36. Here, the farthest splits from the initial crack tips within the fourth layers coincide with the delaminations underneath. Another significant phenomenon illustrated in the figure is that the 0° fibers within the distance between the original crack tips and the last splits are actually being broken, which was not observed in four-layer laminates. Although the split lengths in the fourth ply (as well as in the second ply) vary irregularly, the first splits right at the initial crack tips are invariably long. Figure 34 (c) shows cross-sectional micrographs depicting the splits in the plies, although it is difficult to see all of the damage without adjusting the microscope focus.

In contrast to the irregular variation of the split lengths, the delaminations spreading within the regions bordered by the splits (e.g. interface 3-4) take on a definite shape when fully developed. Note the similarity in shape between that shown in Fig. 37 and interface (3-4) in Fig. 35. The large extent of the delaminations and splits, having dimensions on the order of the specimen width, apparently rendered the 90/0 laminates notch insensitive as shown earlier in Fig. 26.

Figures 38 and 39 compare the characteristics of damage in ±60/0 laminates containing four and five plies deep surface cracks, respectively. For cases with the crack four plies deep (including only one 0° layer), the damage grew relatively unrestrained. The central delamination (4-5) expanded, maintaining an approximately circular shape, and the horizontal propagation fronts of the other damage originating at the crack tips spread simulatneously. Although the splits parallel to fibers in each ply were also observed in the remaining layers previously uncut, actual fiber breakage was limited to the second ply, and occurred near the original crack tips.

For ±60/0 laminates with five plies deep surface cracks, the fifth ply (0°) played a major role in keeping the damage small compared with the above. Ply (5) in Fig. 39 shows no damage except the two splits, one at each tip, which block the extension of the precut crack in this ply. Since the fibers in thsi ply constrain damage in the other plies, their damage regions were consequently smaller than before, due to the avoidance of fiber failure in this case. However, in the second ply (also 0°), three plies away from ply (5), the main crack continuously

extended by the breaking of fibers within the ply. A new development not seen previously in any of the configurations was the presence of two central delaminations - one at the usual interface demarcating the precut and uncut plies , and the other at interface 7-8 within the uncut plies as shown in Fig. 39. A schematic showing the cross-section of the specimen is given in Fig. 40 (a), while the micrographs taken at Section B-B are shown in Figs. 40 (b) and (c) in order to emphasize the role of the two aforementioned splits at the tips in the fifth plies.

The results for the ±45 laminates are given in Fig. 41. These photographs indicate that the damage in the precut plies is localized around the crack tips, while extensive delamination and splitting is present in the uncut layers in the entire region between the crack tips. This is an unusual example of the most severe damage occurring in the uncut plies.

Residual Strength After Precut Ply Failure

The load -extension curves recorded on the Instron chart during fracture tests exhibited two distinct peaks as shown schematically in Fig.42 This phenomenon was absent in ±45 laminates; but it was dominant in the other configurations, especially when the surface crack lengths were long. The first peak was associated with unstable fracture of some of the precut plies and the second peak was the load at final fracture of the residual cross-section. As will be discussed later, the first peak was not necessarily higher than the second.

In connection with the 90/0 laminates, it was stated earlier that the main crack extension associated with fiber failure propagated further in the second ply than in the fourth (Fig. 34 (b)). The first peak load

occured when the crack in the second ply suddenly extended to completely fail the ply all the way to the edge of the specimen. The load suddenly dropped because the compliance of the specimen was increased while the displacement was maintained. Figure 43 (a) shows schematically the residual net-section after the first peak, indicating that the outer three plies are completely broken. The remainder of the fourth and twelfth plies is still intact and continue to act tegether with the inner (uncracked) layers. After the first peak, the load rises agian steadily as the displacement is increased, up to the second peak. The fourth ply, which had been fracturing more slowly than the second before the first peak, does not break further in this interval, so that the net section shown in Fig. 43 (a) is maintained between the peaks. The variation of the ligament width in the fourth ply relative to initial crack length, was not studied in detail beyond the first load peak.

Figures 44 and 45 give the experimental results of the residual strength for 90/0 laminates containing surface cracks on one and both sides, respectively. The significant scatter of the data necessitated a large number of tests in order to confirm the general trends. The second peak stresses were mostly unrecognizable from the Instron chart when the initial crack size, 2c/W was small. This is apparently because the first peak stresses are so high that dynamic effects resulting from the initial breaks lead to total specimen failure. As the initial crack size, $2c_o/W$ approaches 1.0, the first peak stress decreases and the second peak stress approaches the value of the notch insensitive stress at $2c_o/W = 1.0$. The trend lines in Figs. 44 and 45 were drawn such that they not only hit the NI streses at $2c_o/W = 1.0$, but also passed through the averages of the

data as closely as possible. The lines so obtained were redrawn in Figs. 27 and 28. The lines, however, played only a minor role in the figure because the 90/0 laminates were approximately notch insenstitive and the notch insensitive predictions were a close approximation of the fracture stresses for almost all crack lengths.

For ±60/0 laminates with four-ply deep surface cracks, the damage in the precracked plies (including fiber breaks in the 0° ply) was shown to expand relatively rapidly toward the free edges of a specimen (Fig. 38). The first peak occurred upon complete separation of the precut plies along the plane of the main crack. Complete separation was achieved regardless of the initial crack length because: (1) the ±60° plies backing up the second (0°) ply weren't strong enough to effectively constrain the latter without being split, and (2) the two consecutive -60° layers (e.g., third and fourth) virtually isolated the second ply (0°) from the main body. Therefore, the net sections prior to the total fracture assume an identical shape independent of the initial crack length, as shown schematically in Fig. 43 (b). The prediction made of the residual section strength under the assumption that the net section would fracture at its UTS was a slight overestimation as shown in Fig. 46. When the average line (instead of the prediction) obtained from Fig. 46 is incorporated into the fracture test results (Fig. 30), one notes that the residual strength line is an approximate limit load for large crack lengths, while the notch insensitive prediction is appropriate for small ones. For intermediate crack lengths, they serve as a lower and upper bounds, respectively.

Finally, for ±60/0 laminates with five ply deep surface cracks, the residual net section is as shown schematically in Fig. 43 (c). The fifth ply (0°) that was precut did not fracture at all at the tips, which can be seen from Figs. 39 and 40. The residual strength prediction based on the same assumption as before was also an overestimation as shown in Fig. 47 . Referring to Fig. 40, the second peak stress line is seen to closely approximate the actual fracture stresses even when the initial crack lengths are very large.

For ±45 laminates, the second load peak phenomenon was nonexistent. This can be attributed to the fact that the central regions of the plies previously uncut are not immune from damage (Fig. 41 (a)).

Damage Extension in 90/0 Laminates

The rate of extension of damage has been determined only for the 90/0 laminates in this group, and is given for various crack lengths and locations in Figures 48-51. Data in these figures are given for both types 1002 and 1003 Scotchply. The major difference in mechanical properties between the two materials in the 90/0 configuration is that the 1003 has a UTS approximately 27% higher than 1002: 70 ksi ($483 MN/m^2$) vs. 55 ksi ($379 MN/m^2$).

Figure 48 gives the central delamination length as a function of applied stress. These results are similar to those found for 90/0/0/90 laminates in Figure 15, with very similar growth rates at the same values of 2c/W. The data for Type 1002 in Fig. 48 (b) fit in well with the data for 1003.

when normalized by the UTS. As in Figure 15, the data appear to show a shift in this case when the fibers begin to break in the precut plies ($\Delta C=0^+$); more detailed data at lower stress levels might also show a shift when the splits in the 0° plies initiate. It is of interest that the growth rates at higher stress levels are similar to those of the four-ply laminates despite the additional factor of fiber failure (Δc) in the present case.

Figure 49 indicates the relationship between the central delamination length and the amount of crack extension, Δc, in the fourth, 0° ply, which results from fiber fracture. The figures clearly indicate that the initiation of Δc will not take place until the delamination has grown significantly. Also shown in the figures are least-square fit curves which approximate each set of data, through a second degree polynomial represented by:

$$\text{Fig.49(b): } y = 0.30 + 39.1x - 298x^2$$

$$\text{(c): } y = 0.61 + 42.7x - 412x^2$$

$$\text{(d): } y = 0.735 + 34.4x - 288x^2$$

$$\text{(e): } y = 0.39 + 18.1x - 78.2x^2$$

where $x = \Delta c/W$ and $y = \ell/W$.

The values of ℓ/W at which the intitiation of Δc takes place can be determined from the above equations at x=0. The results are summarized in Table 3. The last column in the Table suggests that the aspect ratio of the central delamination, $\ell/2c_o$, at the initiation of Δc may be uniform for a given material, regardless of the initial crack length. Taking the averages,

$$\text{Average of } \ell/2c_o \Big|_{\Delta c = 0^+} \begin{cases} \simeq 1.20 \text{ for Type 1003} \\ \simeq 1.04 \text{ for Type 1002} \end{cases}$$

This means that the delamination at the initiation of Δc must have grown to a full circular shape for 1002 Scotchply and a slightly more elongated shape for 1003 Scotchply which is stronger.

Figure 50 shows the rate of the crack tip delamination growth at the interface between third and fourth plies. Although a great deal of scatter is evident, the data for ℓ_v and ℓ_h roughly follows linear relationship indicated by the straight line drawn in the figure with the slope of 1.0. If so, the aspect ratio of the delamination, ℓ_v/ℓ_h would be constant of approximately 5.0 throughout the applied stress range.

Figure 51 gives approximate inter-relationships among ℓ/W, and $\Delta c/W$, ℓ_v/W, and ℓ_h/W for 1002 Scotchply. It is suggested that the results be treated as only qualitative. The figure shows that $\Delta c/W$ increases more rapidly than ℓ_h/W, but the former will not overtake the latter before the first peak load which occurs when the ℓ_h/W becomes 0.31; that is, when the delamination reaches the free edges of a specimen. Thus the ligaments in the fourth ply will be left still partially intact as shown in Fig. 43 (a) until the final fracture of the residual cross-section.

APPROXIMATE ANALYSIS FOR LARGE DAMAGE ZONES

Introduction

The prevalent notch-insensitive conditions at failure for partially through-thickness cracks suggest that the stress fields associated with extensive delamination growth are relatively uniform, and without major stress concentrations around the cracks and damaged regions. This condition approaches that assumed in the estimation of the critical stress for the unwinding of rocket motor casings discussed in the first section of this report. The present section describes an attempt to predict the growth rate of large damage zones by a similar simplified analysis based upon an energy balance at the border of the propagating damage for the relatively simple damage observed in 90/0/0/90 laminates. Prior to that derivation, the simpler case of a surface crack in a unidirectional laminate is considered. The results obtained are extended to crossplied laminates with a surface crack completely across the width of the specimen.

It is essential to keep in mind that these approximate derivations are relevant only to cases of very large damage zones, where the stresses are nearly uniformly distributed. The critical early development and growth of damage is impossible to treat in this fashion and a complete three-dimensional analysis is necessary in this more complex case. It may prove to be convenient if large damage regions can be treated in an approximate manner, since a precise analysis of such geometries would be difficult.

Unidirectional Laminates

Consider the model shown in Fig. 52. The model is subdivided into three domains, A,B,C, for convenience. Assume the strips C are stress free and the domains A and B retain uniform stresses within each domain. Then the stresses in A and B at applied stress σ are

$$\sigma_A = \sigma$$

$$\sigma_B = \left(\frac{tW}{tW - 2ct_1}\right)\sigma = \frac{\sigma}{\left(1-\frac{2c}{W}\ \frac{t_1}{t}\right)} \tag{6}$$

The elastic stored energy,

$$U_A = \int\int_A \sigma_A\, d\varepsilon_A\ dv = \frac{\sigma^2}{2E_o}\ tW(L-\ell) \tag{7}$$

$$U_B = \left(\frac{\sigma^2}{2E_o}\right)\left[\frac{tW}{\left(1-\frac{2c}{W}\ \frac{t_1}{t}\right)}\right]\ell$$

where v is the volume, and E_o is the elastic modulus in the loading direction. The total energy, U is

$$U = U_A + U_B = \frac{\sigma^2}{2E_o}\ tW\ \left(L + \frac{\frac{2c}{W}\ \frac{t_1}{t}}{1-\frac{2c}{W}\ \frac{t_1}{t}}\ \ell\right) \tag{8}$$

As it should, the L term representing a uniformly stressed body of uncracked specimen increases without bound as $L \to \infty$. So the energy difference between the cracked and uncracked body,

$$\Delta U = \frac{\sigma^2}{2E_o} \frac{2ct_1 \ell}{(1 - \frac{2c}{W} \frac{t_1}{t})} \tag{9}$$

The area created during delamination,

$$A = (2c + 2t_1)\ell \tag{10}$$

Hence

$$G = \frac{\Delta U}{A} = \frac{2ct_1}{(2c+2t_1)} \frac{\sigma^2}{2E_o} \frac{1}{(1 - \frac{2c}{W} \frac{t_1}{t})} \tag{11}$$

When $2c/W \to 0$, $t \to t_1$ and Eq. (11) reduces to Eq. (1), the unwinding problem. If $2c/W = 1$, Eq. (10) must be revised to include only the 2c term, and the subsequent equation for G is

$$G = \frac{t_1 \sigma^2}{2E_o} \frac{1}{(1 - t_1/t)}, \quad 2c/W = 1 \tag{12}$$

Although the uniform stress assumptions are more tenuous, Equation (12) may be applied to composites of different orientations when E_o is replaced by E_c, where E_c is the composite modulus in the loading direction. Letting $t_1 = t/2$ suitable to the four ply specimens in this study, Eq.(12) becomes

$$G = \frac{t\sigma^2}{2E_c} \; , \; 2c/W = 1 \; , \; t_1 = t/2 \qquad (13)$$

In the case of a 90/0/0/90 laminate, the contribution of the two outer plies to the strain energy is negligible, especially when the load is high enough to produce splits throughout the specimen faces within the 90° layers. The G suitable to the situation can be derived similarly,

$$G = \frac{t\sigma^2}{E_L} \qquad (14)$$

where E_L is the elastic modulus along the direction of fibers in a unidirectional ply, and σ is the applied stress based on the total cross-sectional area, $\sigma = P/tW$.

Referring to Table 4 for E_L and Fig. 54 for σ at spontaneous delamination expansion, the G_c for the 90/0/0/90, 1003 glass/epoxy is

$$G_c = \frac{(0.032)\ (29.7 \times 10^3)^2}{6.6 \times .10^6} = 4.28 \text{ lbs/in.} \qquad (15)$$
$$(750 \text{ N/m})$$

This compares favorably with a value of G_c determined by interlaminar cleavage [7] of 4.18 lbs./in. (732 N/M) for Type 1002 Scotchply.

90/0/0/90 Glass/Epoxy Laminate with Surface Crack

Before initiating the derivation, it is helpful to list some of the experimental observations relevant to the problem.

1. The vertical splits, at the surface crack tips in the second ply, act as vertical boundaries of the delamination underneath (Fig. 13).

2. The initial surface crack does not extend, so there are no regions of broken fibers in the second ply (Fig. 12 and 13). In fact, there are no regions of broken fibers in the entire specimen until the final fracture.

3. The propagating fronts of the central delamination are arc-shaped, but far from being semi-circular (Fig. 12).

4. The triangular delaminations occurring at the interface between the first and second ply are well contained within the boundaries composed of the side ℓ_s and height a (Figs. 12 and 13).

5. The ratio, vertical split length to transverse split length, $(\ell_s/2)/a \tilde{} 8.00$

6. The segments within the first ply, over the triangular delaminations, act as ligaments connecting tongue-shaped central strips to the main body (Figs. 10 and 12).

7. The material is notch insensitive (Fig. 9 (a)).

8. The central delamination length, ℓ and vertical split length, ℓ_s, are related by a simple equation (Eq. (4)): $\ell/W = .40(2c/W) + .98\ (\ell_s/W)$.

Taking advantage of these empirical observations, the system is converted to a simplified model shown in Figs. 53 (a) and (b), and through incorporation of the model, the follwoing assumptions are made:

1. The 90° plies make negligible contribution to total elastic energy, except the portions above the triangular delaminations where the segments are shear loaded by a constant stress, q_o.

2. There are no stress concentrations in the body so that when the model is subdivided into Regions 1 to 6, the tensile stress in each region, $\sigma_j = \sigma_j$ (y only).

3. The central delamination fronts are box-shaped.

4. In Region 4, the tensile stress changes linearly in the domain $\xi = 0$ to $(\ell - \ell_s)/2$.

5. The Region 6 is exactly triangular so that the boundaries are straight lines.

6. q_o= const.

7. There exists a material property, G_c, which is defined as the critical strain energy release rate for delamination.

8. The G_c's associated with creation of the central and the triangular delamination are identical.

Details on the derivation of an equation relating ℓ/W to σ are presented in Appendix A using the above assumptions and empirical damage geometry. Rewriting the result,

$$\frac{q_o^2}{4} Y^2 - \left(\frac{2c}{W}\right)\{(.97\sigma - .06\, q_o)q_o + \frac{1}{4}\left(1 - \frac{1}{2}\frac{2c}{W}\right)$$

$$\left(S - \frac{E_L}{8G_{LT}} q_o^2\right)\} Y$$

$$+ \left(\frac{2c}{W}\right)^2 \{.13\,(8\sigma - q_o)\sigma - 1.92$$

$$\left(1 - \frac{1}{2}\frac{2c}{W}\right) S \} = 0 \qquad \text{(A16)}$$

where $$S = G_c E_L / t \qquad \text{(A17)}$$

$$Y = \ell/W - .40(2c/W) \qquad \text{(A18)}$$

and

$E_L / G_{LT} \tilde{\sim} 8.0$ from Table 4, $t = .032$ in. from Table 1.

In applying the equation, it is necessary to keep the units consistent. The units of σ and q_o must be the same, and the units of S must be the square of these. To determine the constants S and q_o, actual experimental values chosen randomly from Fig. 10 (b) are substituted into Eq. A 16 as follows:

2c/W	σ/UTS	σ	ℓ/W	Y
.25	.57	51.3	.52	.43
.25	.71	63.9	1.10	1.01

Solving the resulting equations simultaneously,

$$S = 987.5\ (\text{ksi})^2\ (46{,}946\ \text{TN}^2/\text{m}^4) \qquad (16)$$
$$q_o = 6.24\ \text{ksi} \quad (43.\ \text{KN/m}^2)$$

The values so determined are used without any modification to predict damage growth for other crack lengths. From Eq. 16 and (A16),

$$\underset{[462]}{9.77\ Y^2} - \frac{2c}{W}\left\{\underset{[42]}{6.12\ \sigma} - \underset{[111]}{2.34} + \underset{[45{,}100]}{237.0}\left(1 - \frac{1}{2}\frac{2c}{W}\right)\right\} Y$$

$$+\left(\frac{2c}{W}\right)^2 \left\{\left(\underset{[.96]}{.96\sigma} - \underset{[5.2]}{.72}\right)\sigma - \underset{[88{,}300]}{1856}\left(1 - \frac{1}{2}\frac{2c}{W}\right)\right\} = 0 \qquad (17)$$

where the top numbers are ksi based and the bottom numbers in brackets are in SI units as in Eq. (16).

The curves predicted by Eq. (17) are drawn in Fig. 54, which agree fairly well with experimental results in the intermediate range of stresses for all values of 2c/W.

The physical significance of the S can be realized if Eq. (14) is rewritten at the critical state of spontaneous delamination,

$$G_c = \frac{t\sigma_{cr}^2}{E_L} \qquad (18)$$

Comparing Eq.(18) with Eq. (A17), one notes

$$S = \sigma_{cr}^2, \quad \text{or } \sqrt{S} = \sigma_{cr} \qquad (19)$$

As discussed earlier, the value of σ_{cr} picked from Fig. 54 at constant load delamination growth is approximately 29.7 ksi (205 KN/m^2). On the other hand, the value of $\sqrt{S}$ calculated from Eq. (16) is 31.4 ksi (217 KN/m^2). This suggests that the value of σ_{cr} obtained for the best curve fit is close to the actual σ_{cr} within an acceptable margin of error.

The value of q_o is more difficult to check independently, as is the assumption that it is constant. The stress-strain curve for a 90° ply in shear is highly nonlinear, but a value of 6.24 ksi (43.KN/m^2) appears to be in a reasonable range [8].

The analysis given in this section can, in theory, be extended to other ply configurations and materials if the general shape of the damage is known empirically. It has not been applied to graphite/epoxy of the 90/0/0/90 configuration because the extent of damage was too limited at fracture, and some notch-sensitivity was evident. Although the analysis worked as well as could be expected considering the degree of approximation, the empirical input necessary reduces its usefulness relative to a method which would predict both the geometry and rate of growth of the damage.

SUMMARY AND CONCLUSIONS

The behavior of a variety of glass and graphite/epoxy laminates containing partially through-thickness(surface) cracks has been studied. The work was divided between four-ply thick glass and graphite/epoxy laminates in the configurations 90/0/0/90, 15/-15/-15/-15, and 45/-45/-45/45, and multi-ply glass/epoxy laminates of the configurations 0/90, ±45, and 0/±60. The degree of notch sensitivity and the characteristics of damage extension have been investiaged for each case, with the most detailed attention given to 0/90 laminates containing surface cracks.

Several general observations may be made about the results in addition to the detailed discussion throughout the report:

1) Almost all specimens tested approached notch-insensitive conditions at fracture. The major exceptions to this were 90/0/0/90 graphite /epoxy in which the damage region was relatively small, and 0/±60 multiply laminates in which significant crack extension occurred in the precut plies prior to failure. One other exception was 0/90 multi- ply laminates in which the deep surface cracks penetrated all but a single 0° ply.

2) Initial damage almost always occurred along the interface separating the precut plies from the remainder of the laminate. The delamination at this interface spread along and above the crack as the load was increased, and further damage initiated parallel to the fibers of the precut plies. In most cases the damage geometry, once established, remained similar in shape (self similar); the

ratio of damage extent at various locations tended to remain constant. In most cases, the damage which extended under higher loads was dominated by the central delamination between the precut plies and the remainder of the specimen, but other important damage was evident at other interfaces in the precut portion, particularly beyond the original crack tips. No significant regions of broken fibers were present in the four-ply laminates prior to fracture, but significant fiber fracturing occurred in the precut plies of the multi-ply laminates. The only extensive damage in the uncut plies occurred with the multi-ply ±45 laminates.

3) The rate of damage growth was sensitive to the ply configuration, constituent materials, and specimen geometry. The rate of extension in many cases remained relatively constant as long as the damage geometry was maintained, and transitions in rate were observed as damage initiated in different locations. Damage was less extensive for graphite/epoxy than for glass/epoxy laminates in the 90/0/0/90 configuration, but was almost identical in extent and growth rate for the 15/-15/-15/-15 configuration. Damage for embedded cracks in 15/-15/-15/15 graphite/epoxy was much more localized than for surface cracks.

4) In multi-ply laminates a portion of the precut plies tended to fail all the way to the edges of the specimen, creating a sudden drop in load. As more displacement was applied, the load again increased to a second peak, where the remainder of the specimen failed.

5) An approximate semi- empirical relationship was derived to predict damage extension for large damage zones in 90/0/0/90 laminates. Although the predictions were in good agreement with measured growth rates, the method is not useful in the absence of empirical knowledge of the damage geometry. Prediction of damage initiation and initial growth requires an accurate 3-dimensional analysis due to the complex stress fields involved.

APPENDIX A

DERIVATION OF AN EQUATION RELATING VERTICAL DELAMINATION LENGTH TO APPLIED STRESS

The model to be adopted for the derivation is shown in Fig. 53 and the underlying assumptions are given previously.

Let the subscript L in σ_{iL} and E_L stand for the direction of fibers in a unidirectional ply. The stress in each region based on the cross-sectional area which excludes that occupied by the 90° layers is

$$\sigma_{1L} = 2\sigma_\infty \equiv 2(P/tW) \tag{A1}$$

$$\sigma_{2L} = 2(q_o \frac{t}{4} \; y)/(2c \cdot \frac{t}{4}) = q_o y/c \tag{A2}$$

$$\sigma_{4L} = \sigma_{2L} + \frac{\sigma_{1L} - \sigma_{2L}}{(\ell - \ell_s)/2} \xi = \frac{q_o}{2c} \ell_s + \frac{2}{\ell - \ell_s} \left(\sigma_{1L} - \frac{q_o}{2} \ell_s \right) \xi, \quad \xi \equiv y - \ell_s/2 \tag{A3}$$

$$P = \sigma_{5L} \frac{t}{2} (W - c) + \sigma_{4L}(2c) \cdot \frac{t}{4} = \sigma_{1L} \frac{t}{2} W$$

$$\therefore \sigma_{5L} = \frac{W \sigma_{1L} - c \sigma_{4L}}{W - c} \tag{A4}$$

Also,

$$P = \sigma_{3L} \frac{t}{2} (W - c) + 2(q_o \frac{t}{4} y) = \sigma_{3L}(y = 0) \cdot \frac{t}{2}(w - c) = \sigma_{1L} \frac{t}{2} W$$

$$\therefore \sigma_{3L} = \frac{W\sigma_{1L} - q_o y}{W - c} \tag{A5}$$

Rewriting Eq. (4)

$$\ell/W = .40\ (2c/W) + .98\ \ell_s/W \tag{A6}$$

Considering only the upper half of the model, the elastic stored energy in Region 1 is

$$U_1 = \iiint_{v_1} \sigma_{1L}\ d\varepsilon_{1L}\ dv_1 = \frac{\sigma_{1L}^2}{2E_L}\ \frac{t}{2}\ W\{\frac{L}{2} - \frac{\ell}{2},$$

Replacing ℓ by ℓ_s using Eq. (A6),

$$U_1 = \frac{tW^2}{4E_L}\ \sigma_{1L}^2\ [\frac{L}{2W} - \frac{1}{2}\ (.40\ (\frac{2c}{W}) + .98\ \ell_s/W)\ ] \tag{A7}$$

Similarly,

$$U_4+U_5 = \frac{1}{2E_L}\int_o^{(\ell - \ell_s)/2} [\sigma_{5L}^2\ \ \frac{t}{2}(W - c) + \sigma_{4L}^2 \cdot \frac{t}{4}(2c)]\ d\xi$$

Substituting Eq. (A4),

$$= \frac{tW}{4E_L(1 - c/W)}\int_o^{(\ell - \ell_s)/2} (\ \sigma_{1L}^2\ - \frac{2c}{W}\ \ \sigma_{1L}\ \sigma_{4L}\ + \frac{c}{W}\ \sigma_{4L}^2)\ d\xi$$

Here,

$$\int_o^{(\ell - \ell_s)/2} \sigma_{4L}\ d\xi\ \ = \frac{1}{2}(\ \sigma_{1L} + \frac{q_o}{2c}\ \ell_s)\ \frac{\ell - \ell_s}{2}$$

$$\int_o^{(\ell - \ell_s)/2} \sigma_{4L}^2\ \ d\xi\ \ = \frac{1}{6}(\ell - \ell_s)\ \{\sigma_{1L}^2 + \frac{q_o}{2c}\ \sigma_{1L}\ \ell_s\ + (\frac{q_o}{2c})^2\ \ell_s^2\}$$

Hence,

$$U_4 + U_5 = \frac{tW}{8E_L(1-c/W)} \quad (\ell - \ell_s)\{ \sigma_{1L}^2 \ (1- \frac{2}{3} \frac{c}{w}) - \frac{1}{3} \frac{q_o}{W} \sigma_{1L} \ \ell_s + \frac{1}{12} \frac{q_o^2}{cW} \ \ell_s^2 \}$$

Eliminating ℓ using Eq.(4),

$$U_4 + U_5 = \frac{tW^2}{8E_L \ (1-c/W)} \ (-.02 \frac{\ell_s}{W} + .80 \frac{c}{W}) \ [\sigma_{1L}^2 (1 - \frac{1}{3} \frac{2c}{W}) - \frac{1}{3} q_o \ \sigma_{1L} \ \ell_s/W + \frac{q_o^2}{6(2c/W)} \ (\frac{\ell_s}{W})^2 \ ] \qquad \text{(A8)}$$

In Region 3,

$$U_3 = \frac{1}{2E_L} \int_o^{\ell_{s/2}} (\frac{W\sigma_{1L} - q_o \ y}{W - c})^2 \ \frac{t}{2} (W - c) \ dy$$

$$= \frac{tW^2}{12E_L(1-c/W)} \ \{ \frac{3}{2} \ \sigma_{1L}^2 \ (\frac{\ell_s}{W}) \ - \frac{3}{4} \ q_o \ \sigma_{1L} (\frac{\ell_s}{W})^2 + \frac{1}{8} \ q_o^2 \ (\frac{\ell_s}{W})^3 \ \} \qquad \text{(A9)}$$

Similarly,

$$U_2 = \frac{tW^2}{96 \ E_L \ (c/W)} \ q_o^2 \ (\frac{\ell_s}{W})^3 \qquad \text{(A10)}$$

$$U_6 = 2 \int_o^{\ell_{s/2}} \frac{q_o^2}{2 \ \mu_{LT}} \ \frac{t}{4} \ a(y) \ dy = \frac{tW^2}{256 \ G_{LT}} \ q_o^2 (\frac{\ell_s}{W})^2 \qquad \text{(A11)}$$

where μ_{LT} is the shear modulus of a unidirectional ply, the subscript T stands for transverse direction. The relation $\ell_s/2/a = 8.0$ was used in Eq. (A11).

The total energy in the upper half of the model,

$$U_{Tot.} = \sum_{i=1}^{6} U_i$$

The energy difference between the cracked and uncracked body is then obtained by subtracting the first term in Eq. (A7).

$$\Delta U_{Tot.} = \sum_{i=1}^{6} U_i - \frac{tW}{8E_L} \sigma_{1L}^2 L \qquad \text{(A12)}$$

Aside, the delamination area

$$A = \frac{\ell}{2}(2c) + 2\left(\frac{a.\ell_s/2}{2}\right) = W^2\left[\frac{c}{W}\frac{\ell}{W} + \frac{1}{32}\left(\frac{\ell_s}{W}\right)^2\right]$$

$$= W^2\left[\frac{c}{W}\left(\frac{\ell_s}{W} + .40\left(\frac{2c}{W}\right)\right) + \frac{1}{32}\left(\frac{\ell_s}{W}\right)^2\right]$$

$$\therefore \partial A = \frac{W^2}{2}\left[\frac{1}{8}\left(\frac{\ell_s}{W}\right) + \frac{2c}{W}\right]\partial\left(\frac{\ell_s}{W}\right) \qquad \text{(A13)}$$

Therefore

$$G_c = \frac{\partial \Delta U_{Tot.}}{\partial A} = \frac{\partial\left[\sum_{i=1}^{6} U_i - \frac{tW}{8E_L}\sigma_{1L}^2 L\right]}{\frac{W^2}{2}\left\{\frac{1}{8}\left(\frac{\ell_s}{W}\right) + \frac{2c}{W}\right\}\partial\left(\frac{\ell_s}{W}\right)}$$

or

$$\frac{W^2}{2}\left[\frac{1}{8}\left(\frac{\ell_s}{W}\right) + \frac{2c}{W}\right] G_c = \frac{\partial U_1}{\partial(\ell_s/W)} + \ldots + \frac{\partial U_6}{\partial(\ell_s/W)} \qquad \text{(A14)}$$

Partial differentiations of Eqs. (A7-A11) with respect to ℓ_s/W give

$$\frac{\partial U_1}{\partial(\ell_s/W)} = -\frac{.98tW^2}{8E_L}\sigma_{1L}^2 \qquad \text{(A15-a)}$$

$$\frac{\partial U_2}{\partial(\ell_s/W)} = \frac{tW^2}{32E_L(c/W)}q_o^2\left(\frac{\ell_s}{W}\right)^2 \qquad \text{(A15-b)}$$

$$\frac{\partial U_3}{(\ell_s/W)} = \frac{tW^2}{8E_L(1-c/W)}\left\{\sigma_{1L}^2 - q_o\sigma_{1L}\left(\frac{\ell_s}{W}\right) + \frac{q_o}{4}\left(\frac{\ell_s}{W}\right)^2\right\} \qquad \text{(A15-c)}$$

$$\frac{\partial(U_4+U_5)}{(\ell_s/W)} = \frac{tW^2}{8E_L(1-c/W)}\left[q_o^2\left(\frac{\ell_s}{W}\right)\left(.13 - \frac{.02\left(\frac{\ell_s}{W}\right)}{2(2c/W)}\right)\right.$$

$$\left. -q_o\sigma_{1L}\left(.13\frac{2c}{W} - .01\frac{\ell_s}{W}\right) - .02\left(1-\frac{1}{3}\frac{2c}{W}\right)\sigma_{1L}^2\right] \qquad \text{(A15-d)}$$

$$\frac{\partial U_6}{\partial(\ell_s/W)} = \frac{tW^2}{128G_{LT}}q_o^2\left(\frac{\ell_s}{W}\right) \qquad \text{(A15-e)}$$

Substituting Eqs. (A1) and (A15) into (A14) and rearranging,

$$\frac{q_o^2}{4}Y^2 - \left(\frac{2c}{W}\right)\left\{\left(.97\sigma_\infty - .06q_o\right)q_o + \frac{1}{4}\left(1-\frac{1}{2}\frac{2c}{W}\right)\right.$$

$$\left.\left(S - \frac{E_L}{8G_{LT}}q_o^2\right)\right\}Y$$

$$+\left(\frac{2c}{W}\right)^2\left\{.13\left(8\sigma_\infty - q_o\right)\sigma_\infty - 1.92\left(1-\frac{1}{2}\frac{2c}{W}\right)S\right\} = 0 \qquad \text{(A16)}$$

Here the ratio $E_L / G_{LT} = 8.0$ as given by Table 2 and S and Y are defined as

$$S = G_c E_L / t \tag{A18}$$

$$Y = \ell/W - .40(2c/W) = .98 (\ell_s/W) \tag{A18}$$

The Eq. A16 contains two kinds of parameters - one related to the crack geometry, 2c/W and the other associated with the material properties such as q_o, S and E_L/G_{LT}. Another geometric parameter that seems missing in Eq. (A16) is the one representing the thickness of the unloading mid-strips. This is because the particular thickness has already been converted to the total thickness , t,during the derivation.

REFERENCES

1. Irwin, G.R., and Wells, A.A., "A Continuum-Mechanics View of Crack Propagation," Metallurgical Reviews, Vol. 10 (1965), p. 223.

2. Wu, E.M., and Reuter, R.C., "Crack Extension in Fiberglass Reinforced Plastics," TAM Report No.275, Univ. of Illinois (1965)

3. Mandell, J.F., McGarry, F.J., Im. J., and Meier, U., "Fiber Orientation, Crack Velocity, and Cyclic Loading Effects on the Mode of Crack Extension in Fiber Reinforced Plastics," in Failure Modes in Composites II, The Metallurgical Society of AIME (1974), p.33.

4. Mandell, J.F., Wang, S.S. and McGarry, F.J., "The Extension of Crack Tip Damage Zones in Fiber Reinforced Plastic Laminates," J. Composite Materials, Vol. 9 (1975), p. 266.

5. Wang, S.S., Mandell, J.F., and McGarry, F.J., "Three-Dimensional Solution for a Through-Thickness Crack with Crack Tip Damage in a Crossplied Laminate, in Fracture Mechanics of Composites, ASTM STP 593, American Society for Testing and Materials (1975), p. 61.

6. Kies,J.A. and Bernstein, H.,"Recent Advances in Glass Fiber Reinforced Plastic Rocket Motors, " Proc. 17th Technical and Management Conf. of Reinforced Plastics Div., Society of the Plastics Industry (1962), Paper 6-B.

7. McKenna, G.B., "Interlaminar Effects in Fiber Reinforced Plastics," M.I.T. MS Thesis, Dept. of Civil Engineering (1971).

8. Sims,D.F. "In Plane Shear Stress Stain Response of Unidirectional Composite Material," J. Composite Materials, Vol. 7 (1973), p. 124

TABLE 1

CONFIGURATIONS AND GEOMETRIES OF FOUR-PLY SPECIMENS

Type of Crack	Material	Configuration	2c/W
Surface	graphite/epoxy	90/0/0/90	.333, 1.0
		15/-15/-15/15	.333
		45/-45/-45/45	.333
	1003 Scotchply E glass/epoxy	90/0/0/90	.125,.25,;333,.375,.5,.625,.75,1.0
		15/-15/-15/15	.333
		45/-45/-45/45	.333
Embedded	graphite/epoxy	15/-15/-15/15	.333

W_{av} = 1.5 in.(3.8cm)

t_{av} = 0.020 in.(.051 cm) graphite/epoxy
0.032 in.(.081 cm) 1003 Scotchply

Note: Surface cracks are two layers deep, and two inner layers are cut for embedded cracks,.

TABLE 2

SPECIMEN CONFIGURATIONS AND SURFACE CRACK GEOMETRIES FOR THICK LAMINATES

A. Material: Type 1002 and 1003* Scotchply E-Glass/Epoxy

B. Ply Sequence

1. 90/0/90...0/90 (15 layers)

2. +60/0/-60/-/0/+/0/-/-/0/+ (12 layers)

3. +45/-45/+/-/+/-/+/-/-/+/-/+/-/+/-/+ (16 layers)

C. Specimen width, W: 1, 1.5 and 2 in. (2.5, 3.0, and 5.1 cm)

D. Surface Crack Depth

1. 90/0 a) Five layers deep on one surface, (layers 1-5 cut)

b) Five layers deep on both surfaces, (1-5) and (1-15)

2. $\pm$60/0 a) (1-4)

b) (1-5)

3. $\pm$45 a) (1-5)

b) (1-5) and (12-16)

E. Initial Surface Crack Length:

$2c_o/W$ = .125, .25, .375, .5, .625

F. The averages thicknesses, t, for the 90/0, $\pm$60/0, and $\pm$45 laminates were .128, .102, and .136 inches (.325, . 259, and .345 cm) respectively.

---

* 1003 Scotchply was used only for 90/0 laminates

TABLE 3

ASPECT RATIO OF CENTRAL DELAMINATION, $\ell/2c_o$, at ΔC INITIATION, GLASS/EPOXY LAMINATES CONTAINING FIVE-LAYER DEEP SURFACE CRACKS ON BOTH SIDES OF A SPECIMEN

	$2c_o/W$	$(\ell/W)_{\Delta c=0^+}$	$(\ell/2c_o)_{\Delta c=0^+}$
Type 1003	.125	?	?
	.25	.30	1.20
	.5	.61	1.22
	.625	.735	1.18
Type 1002	.375	.39	1.04

TABLE 4

UNIDIRECTIONAL PLY PROPERTIES

Property	Symbols	Units	Thornel 300 Graphite/Epoxy	Type 1002 Glass/Epoxy	*Type 1003 Glass/Epoxy
Longitudinal Modulus	E_L	10^6psi	16.5	6.0	6.6
		GN/m^2	114	41.	46.
Transverse Modulus	E_T	10^6psi	1.5	1.4	1.6
		GN/m^2	10.	9.7	11.
Shear Modulus	G_{LT}	10^6psi	0.75	0.80	0.83
		GN/m^2	5.2	5.5	5.7
Longitudinal Tensile Strengh	-	10^3psi	200.	150.	190.
		MN/m^2	1380.	1035.	1311.
Fiber Volume Fraction	V_f	-	0.55	0.55	0.60

* The properties are representative values taken from manufacturer's data and various literature sources. The values for Type 1003 glass/epoxy are estimated from experimental measurements and limited information available from the manufacturer.

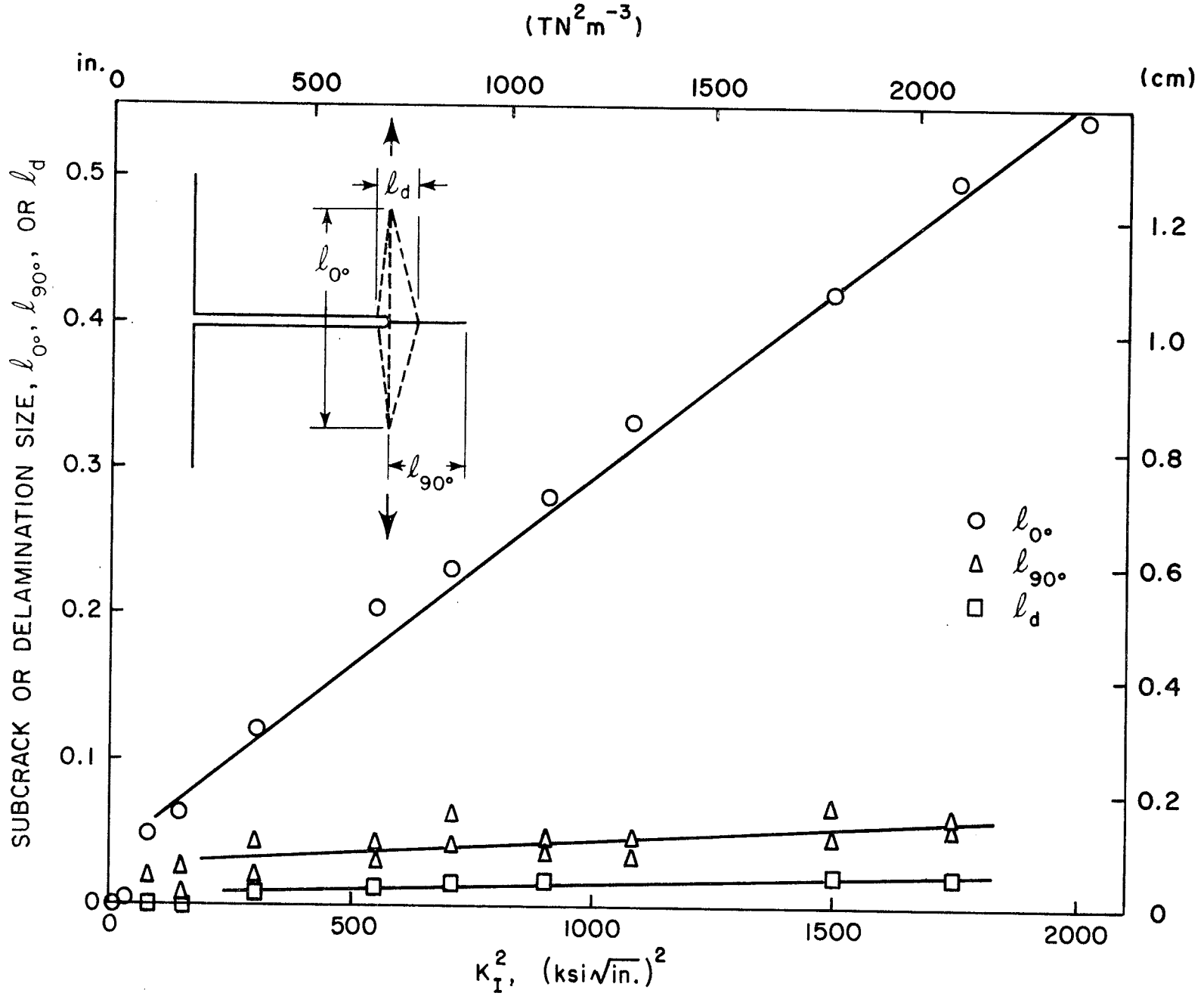

FIGURE 1.

DAMAGE ZONE SIZE vs. $(K_I)^2$, (90/0/0/90) GRAPHITE/EPOXY WITH A THRU CRACK.

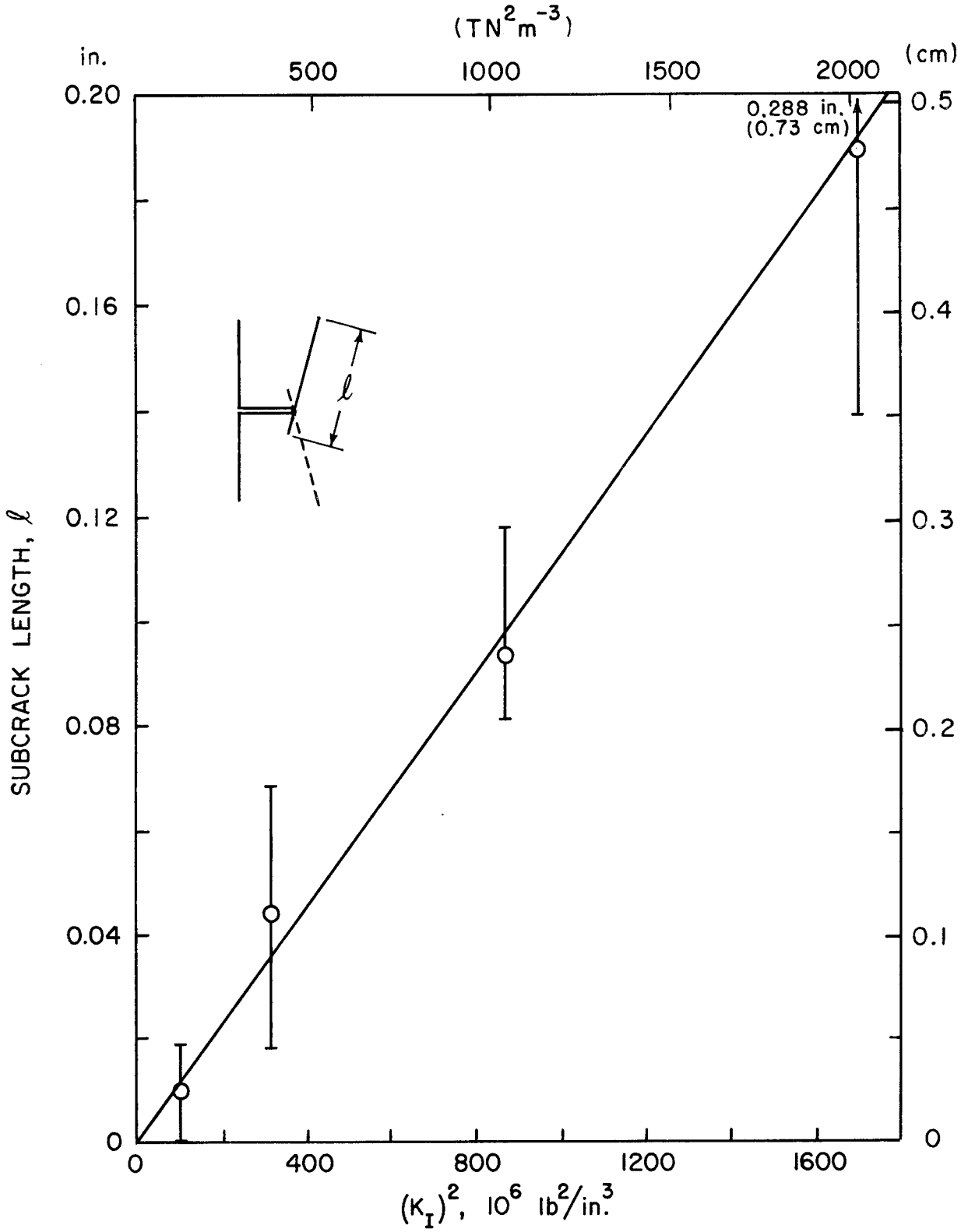

FIGURE 2.

SUBCRACK LENGTH vs. $(K_I)^2$, (15/-15/-15/15) GRAPHITE/EPOXY WITH A THRU CRACK.

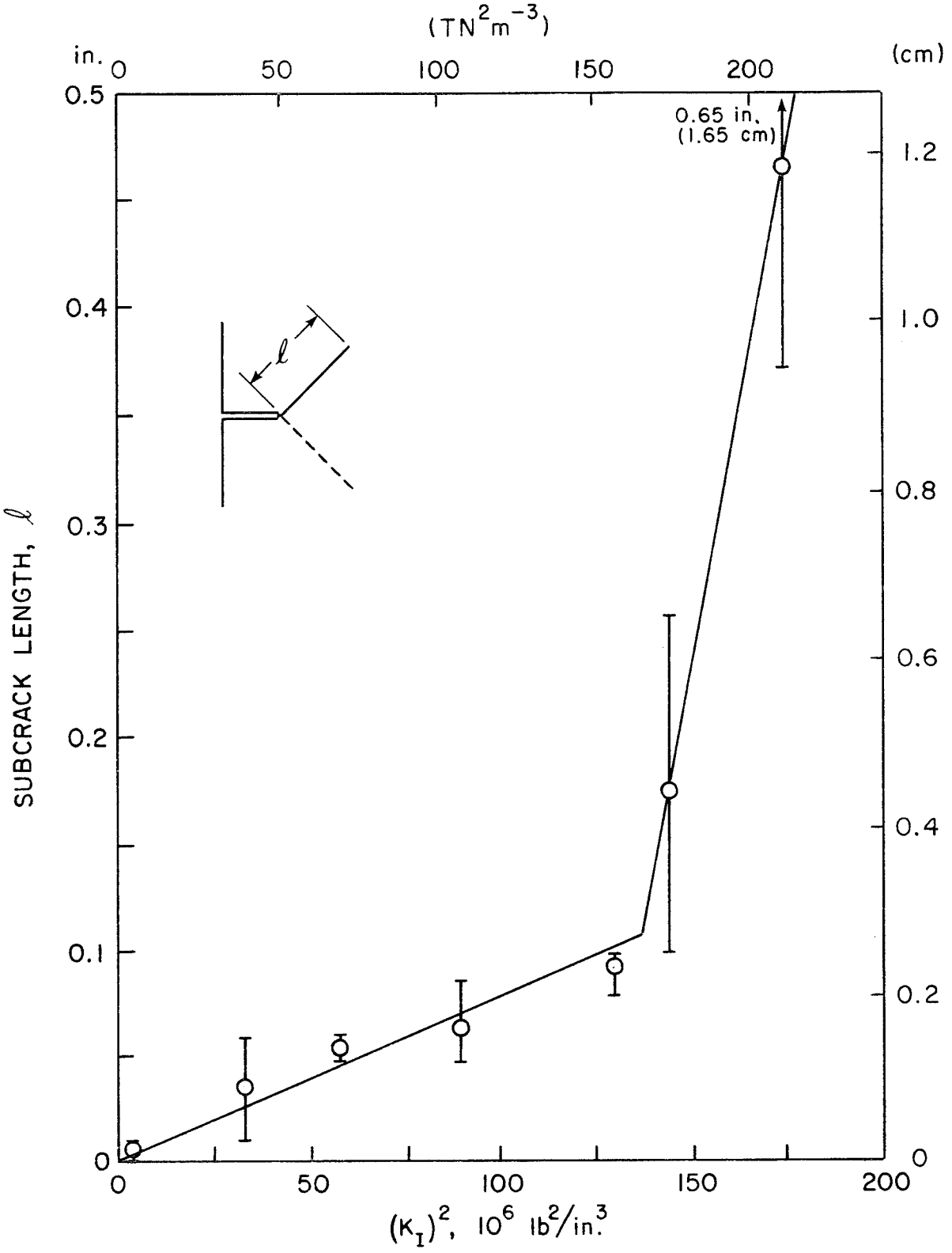

FIGURE 3.

SUBCRACK LENGTH vs. $(K_I)^2$, (45/-45/-45/45) GRAPHITE/EPOXY WITH A THRU CRACK.

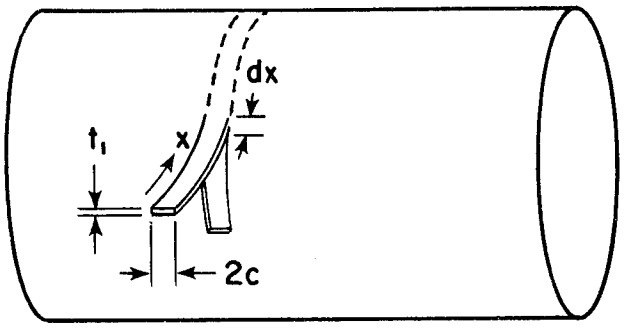

FIGURE 4.

SURFACE CRACK MODEL OF KIES AND BERNSTEIN (FROM [6]).

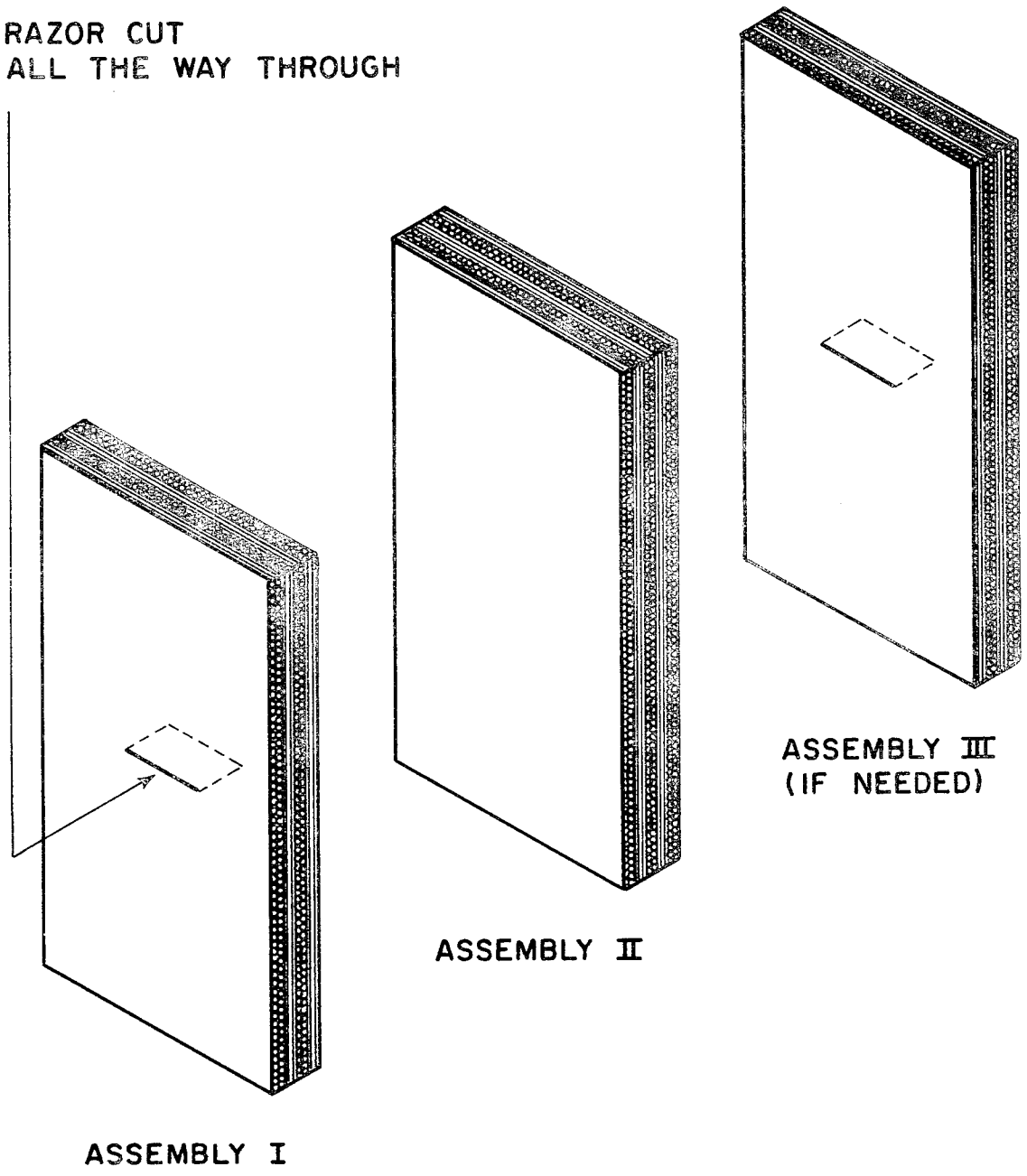

FIGURE 5.

SCHEMATICS OF LAYUPS AND RAZOR CUTS, PRIOR TO MOLDING FOR SURFACE-CRACKED SPECIMEN.

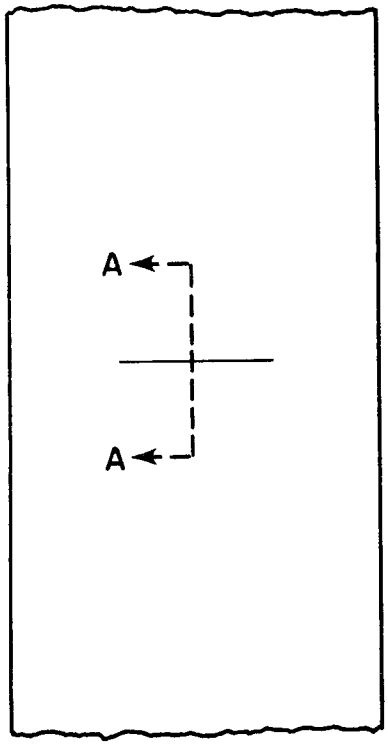

Front view of
unloaded specimen

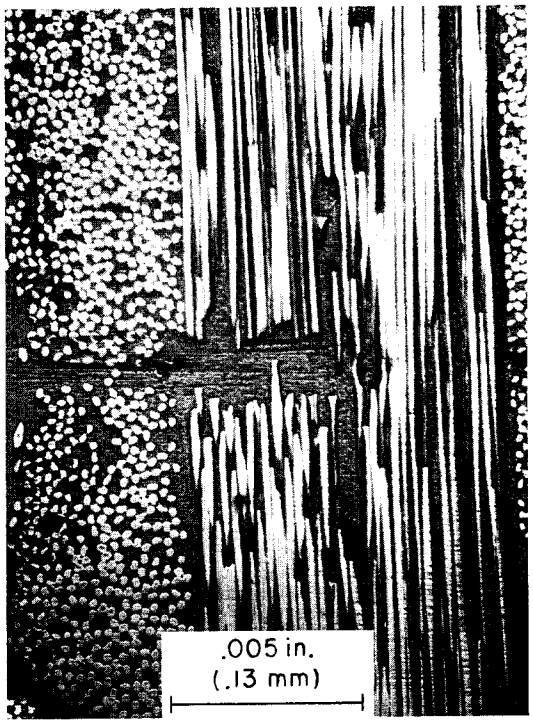

Section A-A

FIGURE 6.

MOLDED RADIUS OF RAZOR CUT,
90/0/0/90 GRAPHITE/EPOXY.

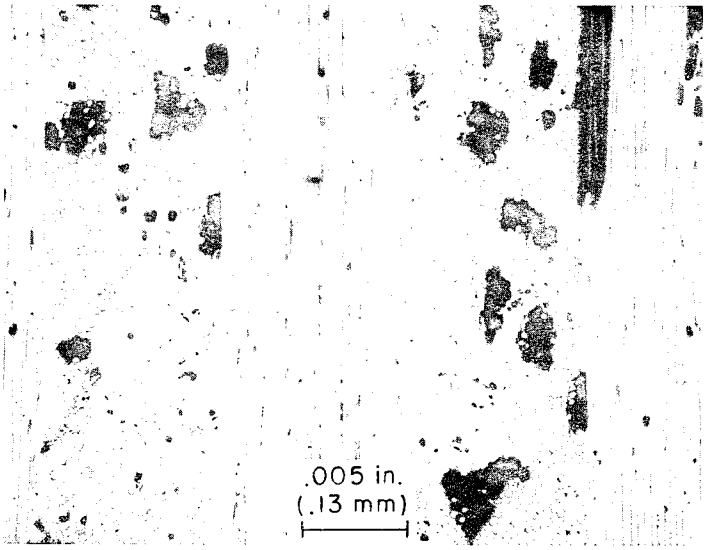

FIGURE 7.

CROSS-SECTIONAL VIEW OF 90/0, 1002 GLASS/EPOXY IN VIRGIN STATE, ETCHED 1% HF, 6 SECONDS.

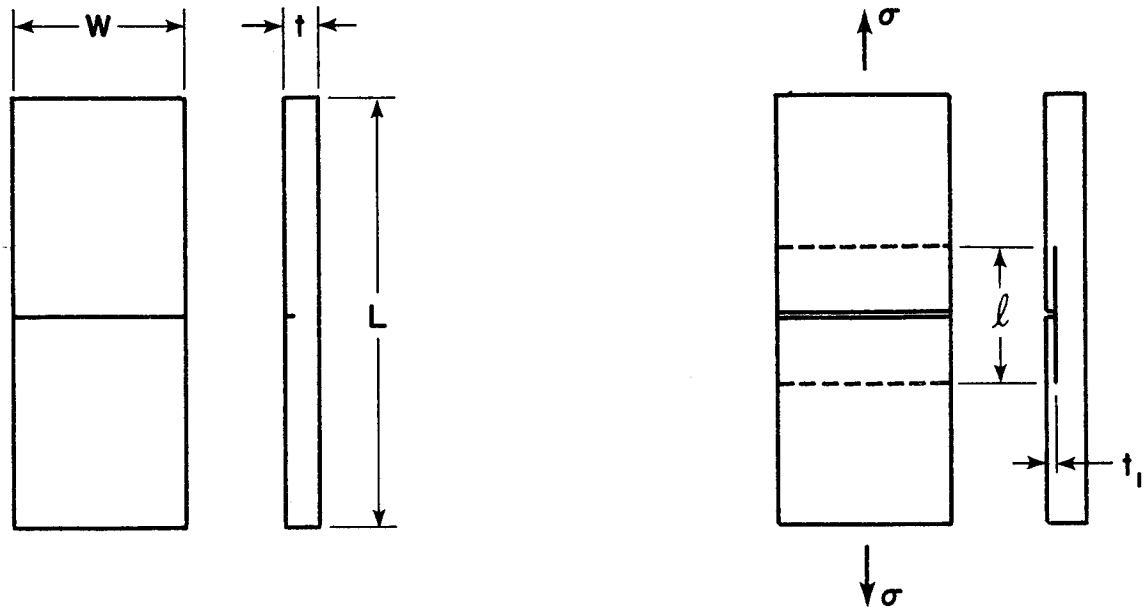

(a) Surface crack all the way across the width

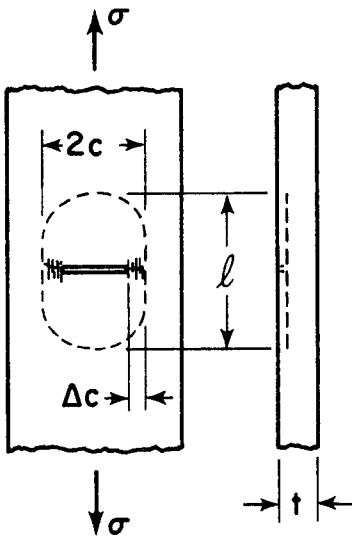

(b) Intermediate length of surface crack

FIGURE 8.

SCHEMATICS OF TYPICAL DAMAGE IN SURFACE-CRACKED COMPOSITE SPECIMEN.

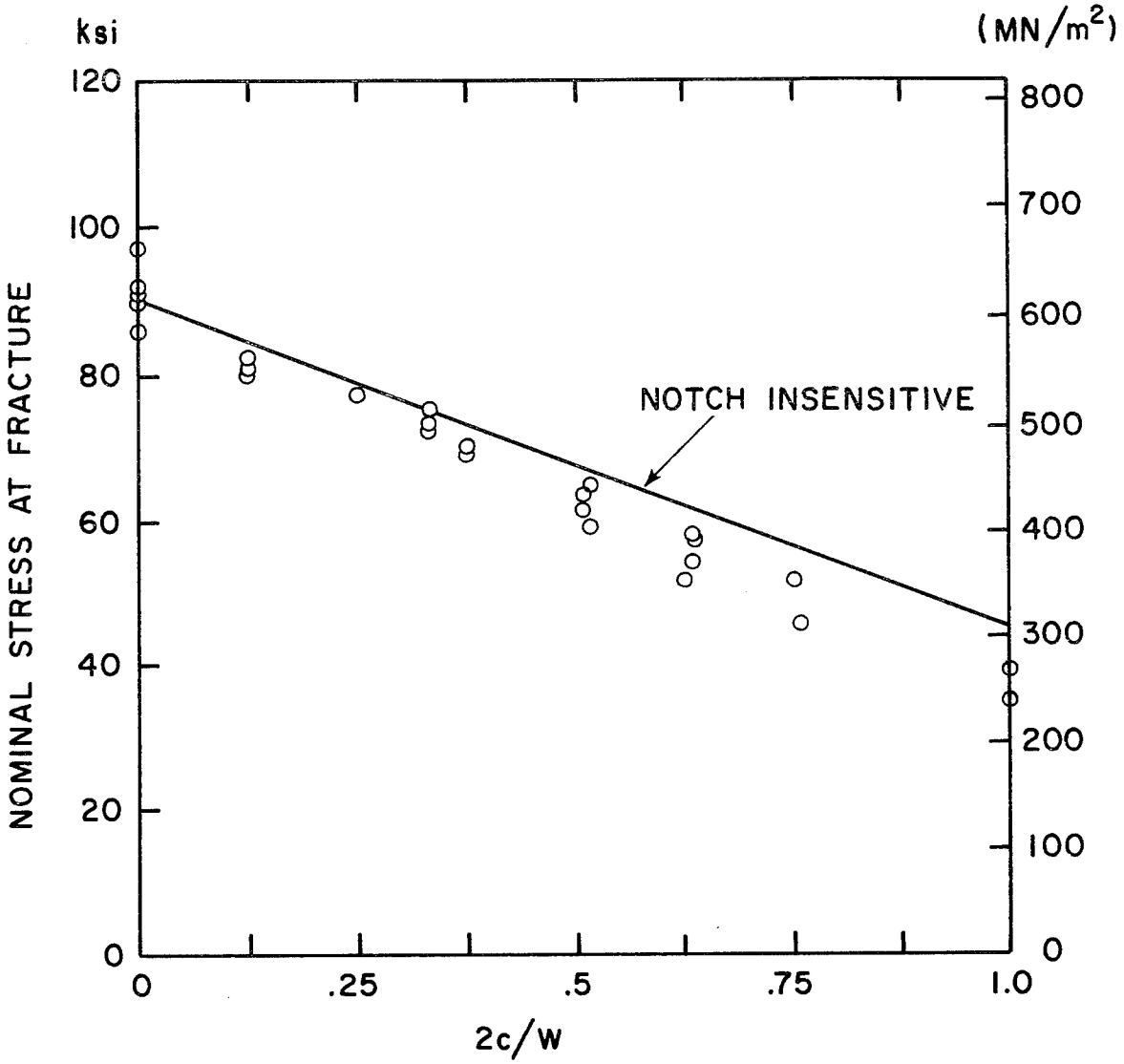

(a) 90/0/0/90

FIGURE 9.

FRACTURE STRESS vs. 2c/W, TYPE 1003 SCOTCHPLY WITH TWO-PLY DEEP SURFACE CRACK.

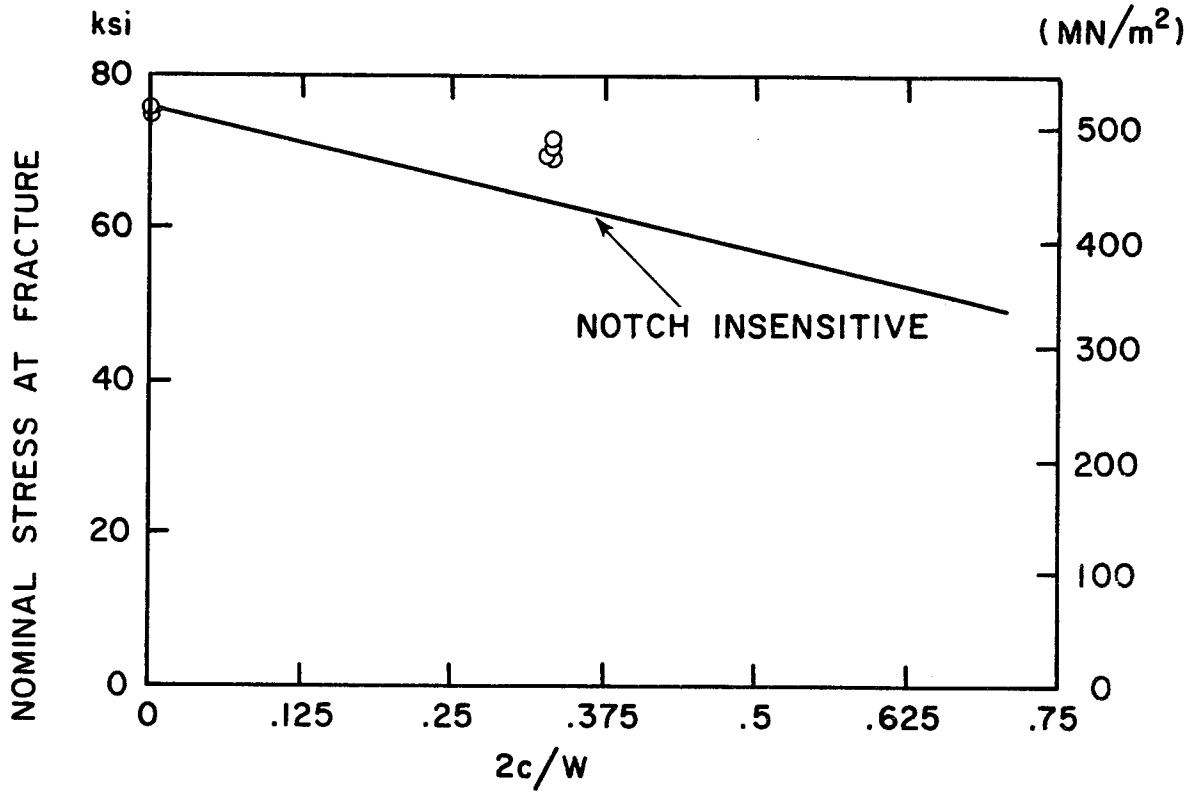

(b) 15/-15/-15/15

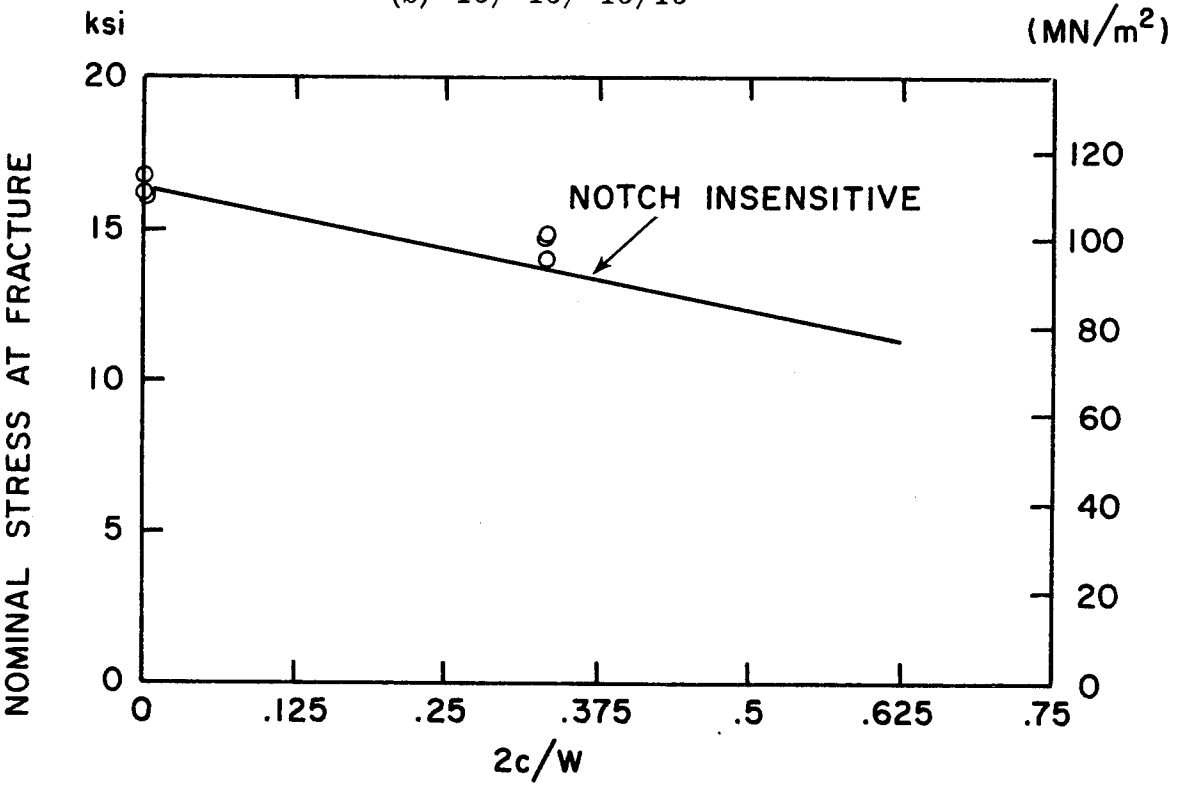

(c) 45/-45/-45/45

FIGURE 9 (continued).

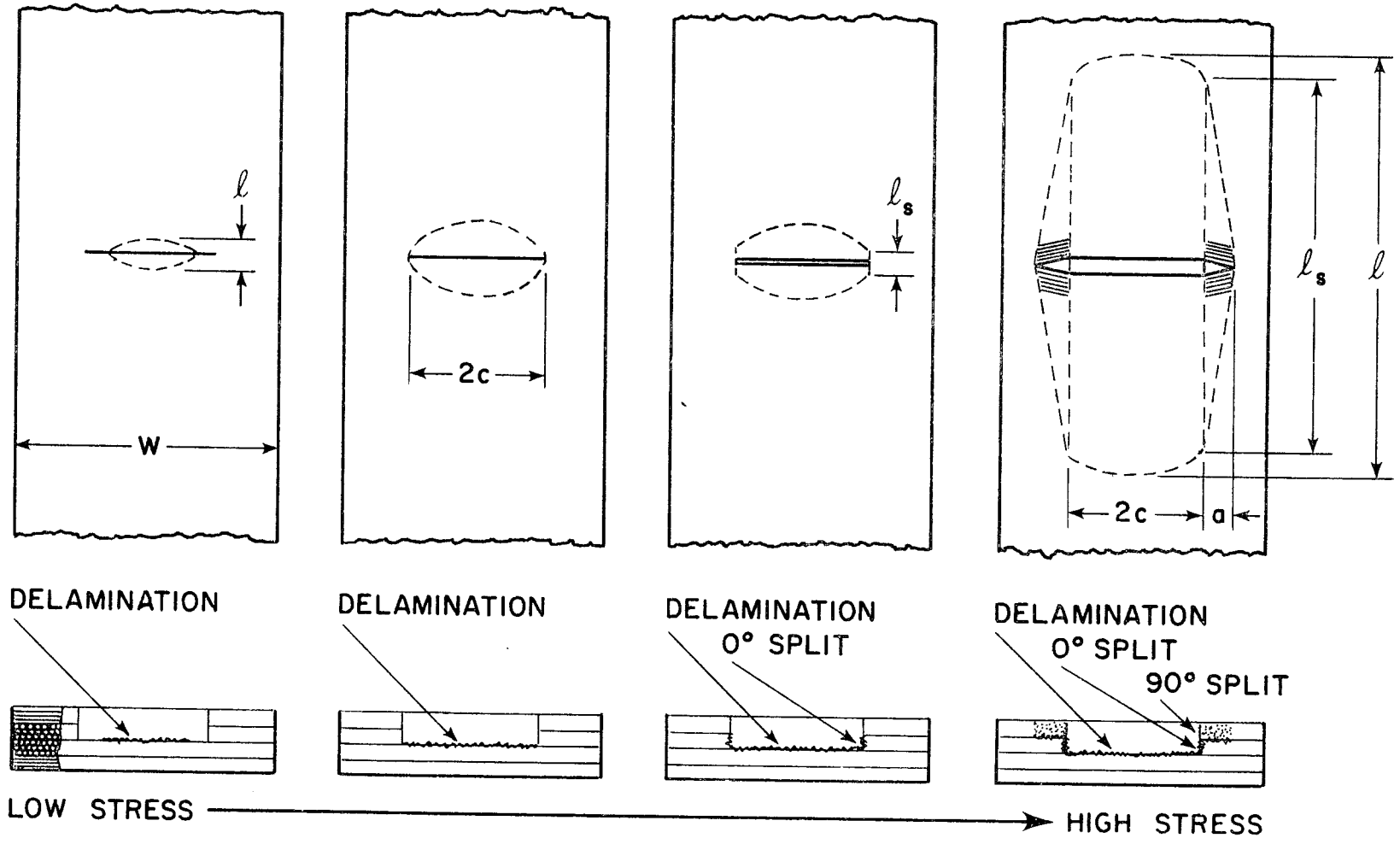

FIGURE 10.

SCHEMATICS OF DELAMINATION AND SPLIT GROWTH IN 90/0/0/90, 1003 SCOTCHPLY WITH TWO-PLY DEEP SURFACE CRACK.

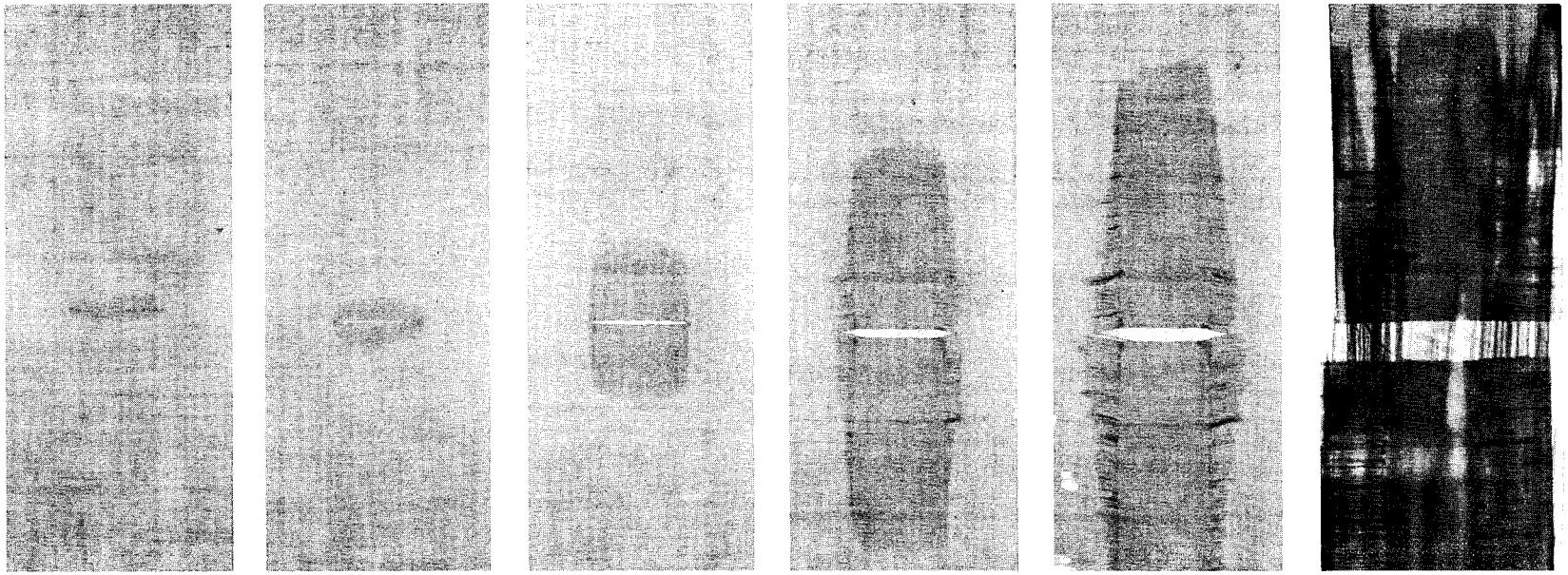

$\frac{\sigma}{UTS}$ = 0.32 0.40 0.50 0.60 0.70 0.77 (failed)

FIGURE 11.

TRANSMITTED LIGHT PHOTOGRAPHS OF SEQUENTIAL GROWTH OF DAMAGE IN 90/0/0/90, 1003 SCOTCHPLY WITH TWO-PLY DEEP SURFACE CRACK, 2c/W = 0.375.

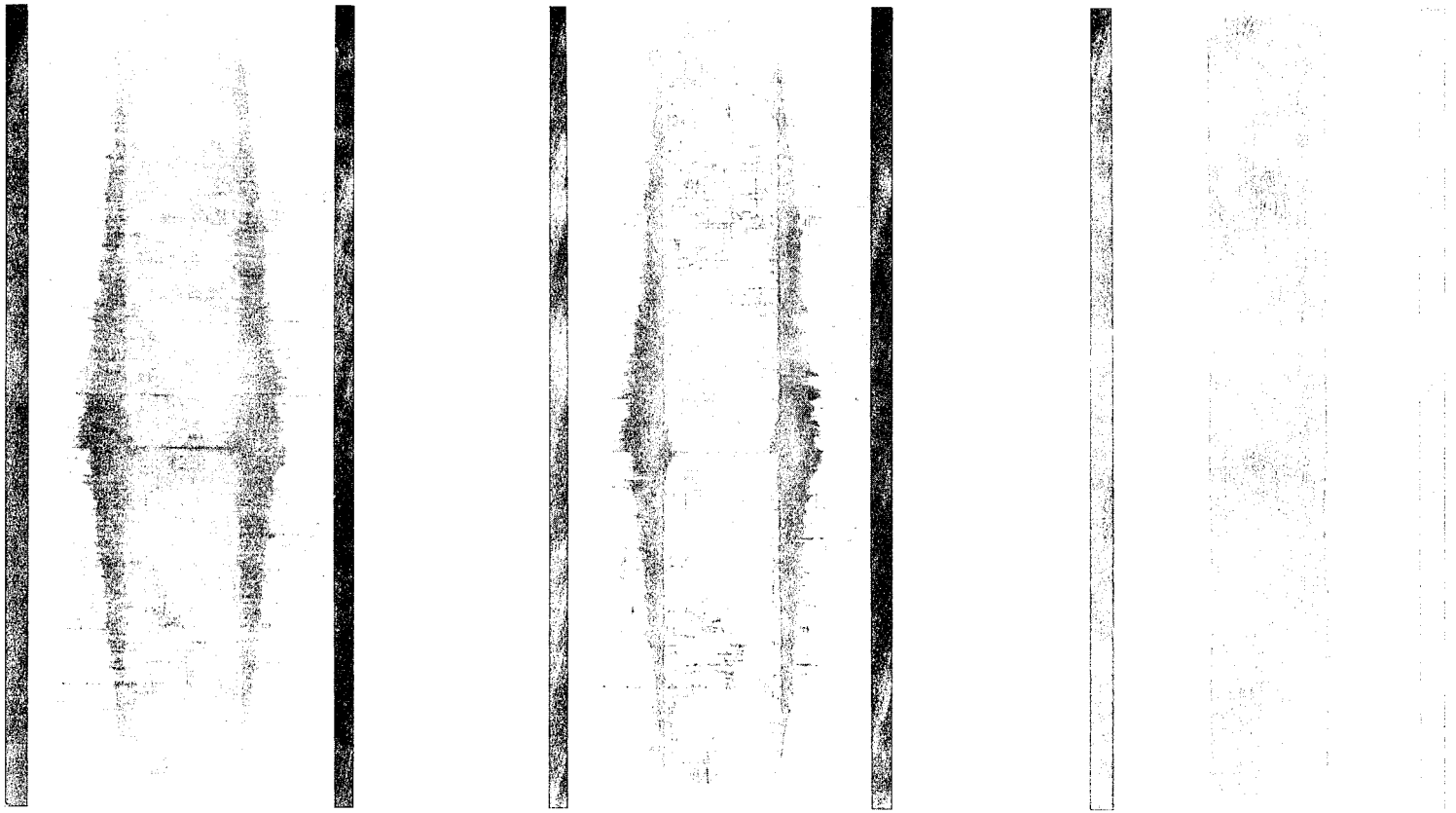

FIGURE 12.

DELAMINATIONS AND SPLITS DEVELOPED IN 90/0/0/90, 1003 SCOTCHPLY WITH TWO-PLY DEEP SURFACE CRACK.

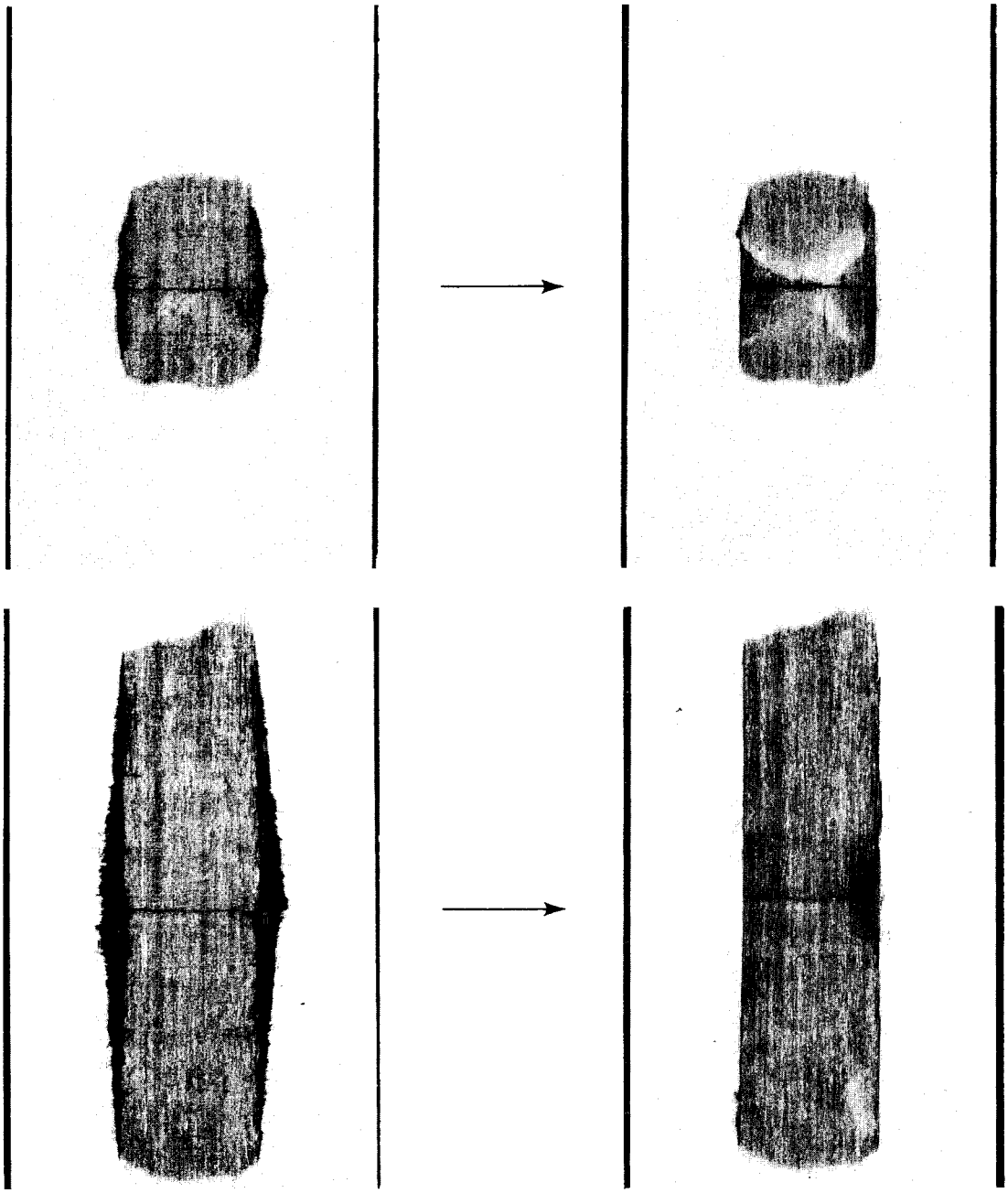

(a) After peeling off of first layer

(b) After slight polishing of (a)

FIGURE 13.

LONG VERTICAL SPLITS AT BOTH CRACK TIPS WITHIN SECOND LAYERS, 90/0/0/90, 1003 SCOTCHPLY WITH TWO-PLY DEEP SURFACE CRACKS.

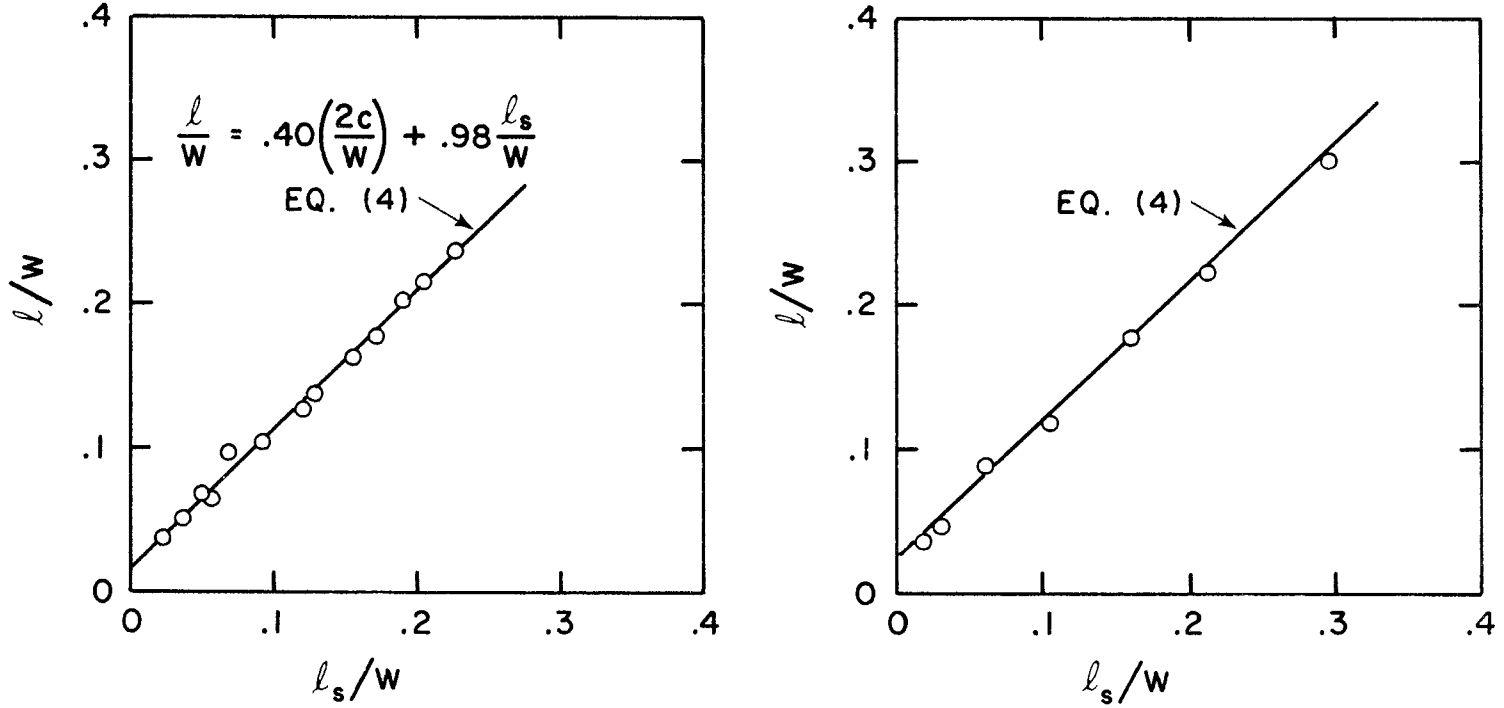

(a) 2c/W = .25

(b) 2c/W = .333

FIGURE 14.

DELAMINATION LENGTH vs. SPLIT LENGTH, 90/0/0/90, TYPE 1003 SCOTCHPLY WITH TWO-PLY DEEP CENTRAL SURFACE CRACKS.

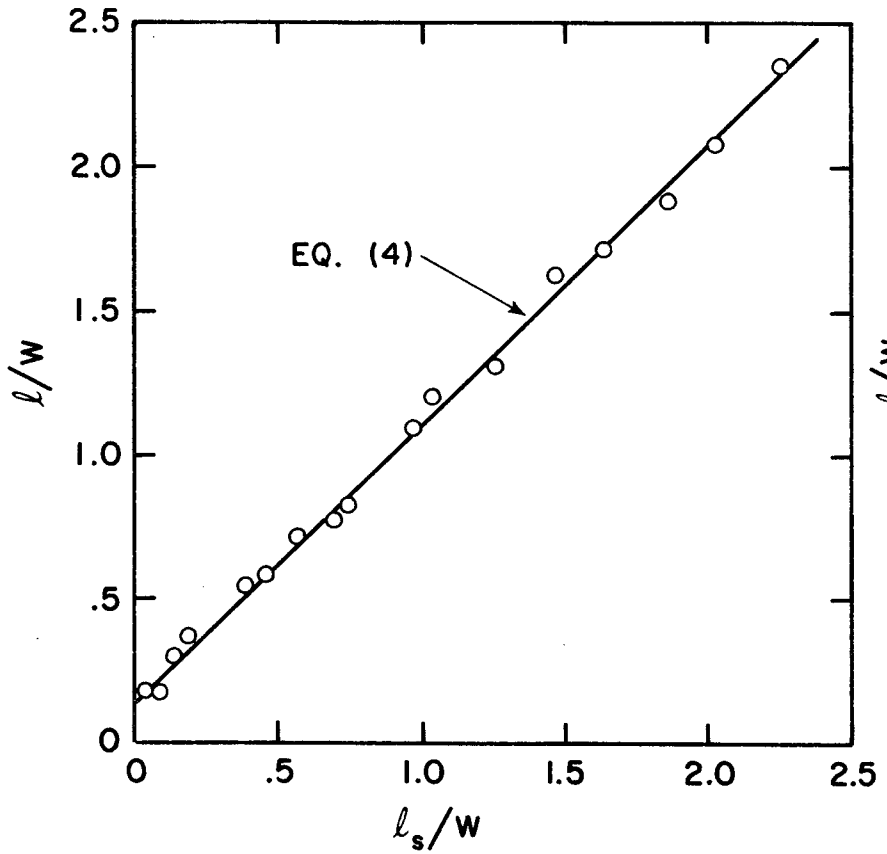

(c) 2c/W = .375

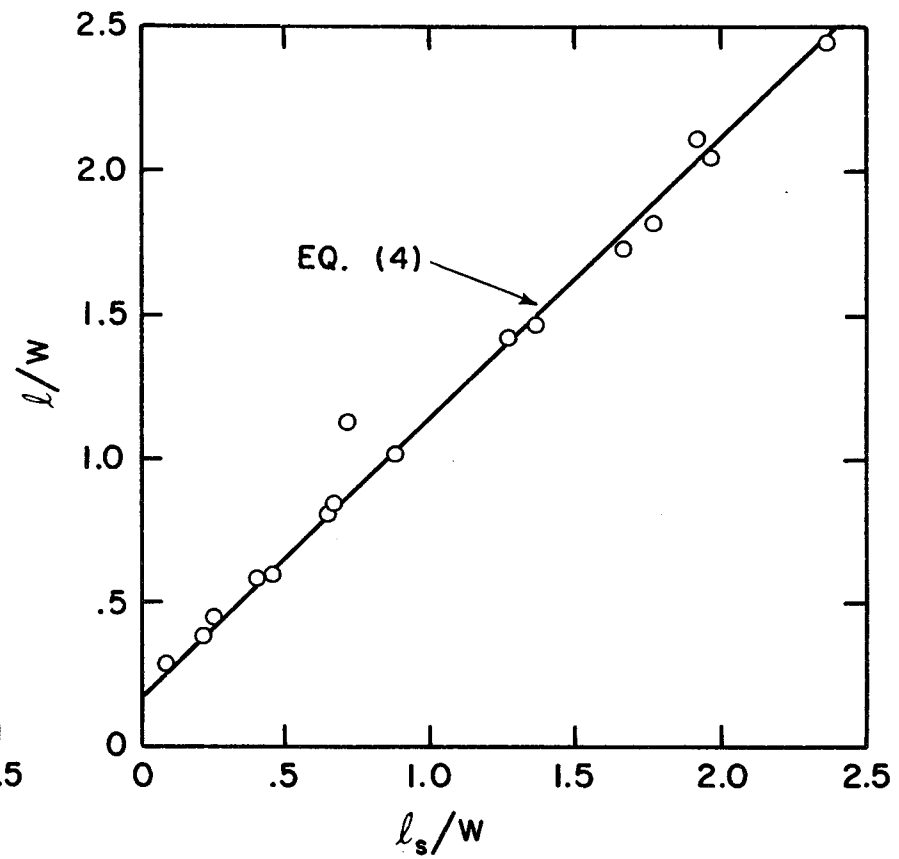

(d) 2c/W = .5

FIGURE 14 (continued)

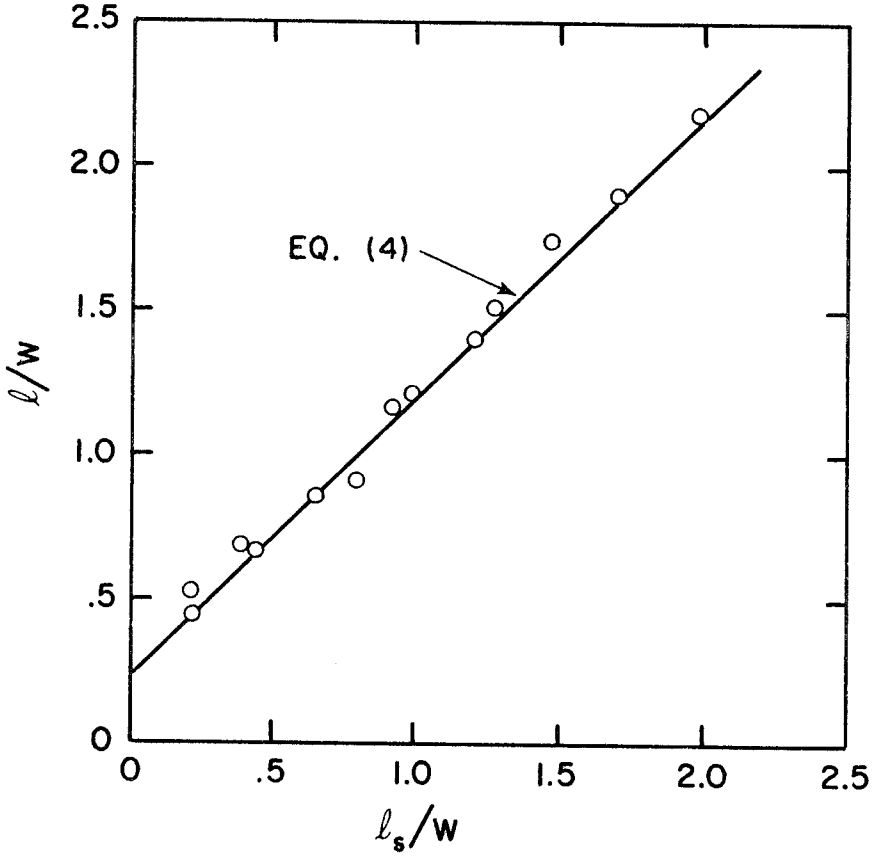

(e) 2c/W = .625

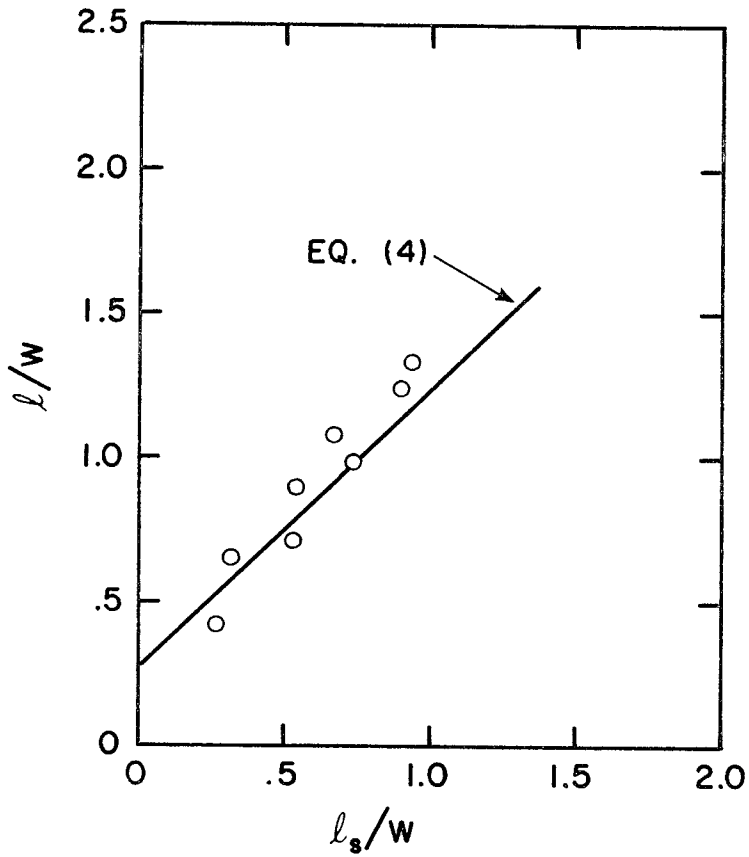

(f) 2c/W = .75

FIGURE 14 (continued).

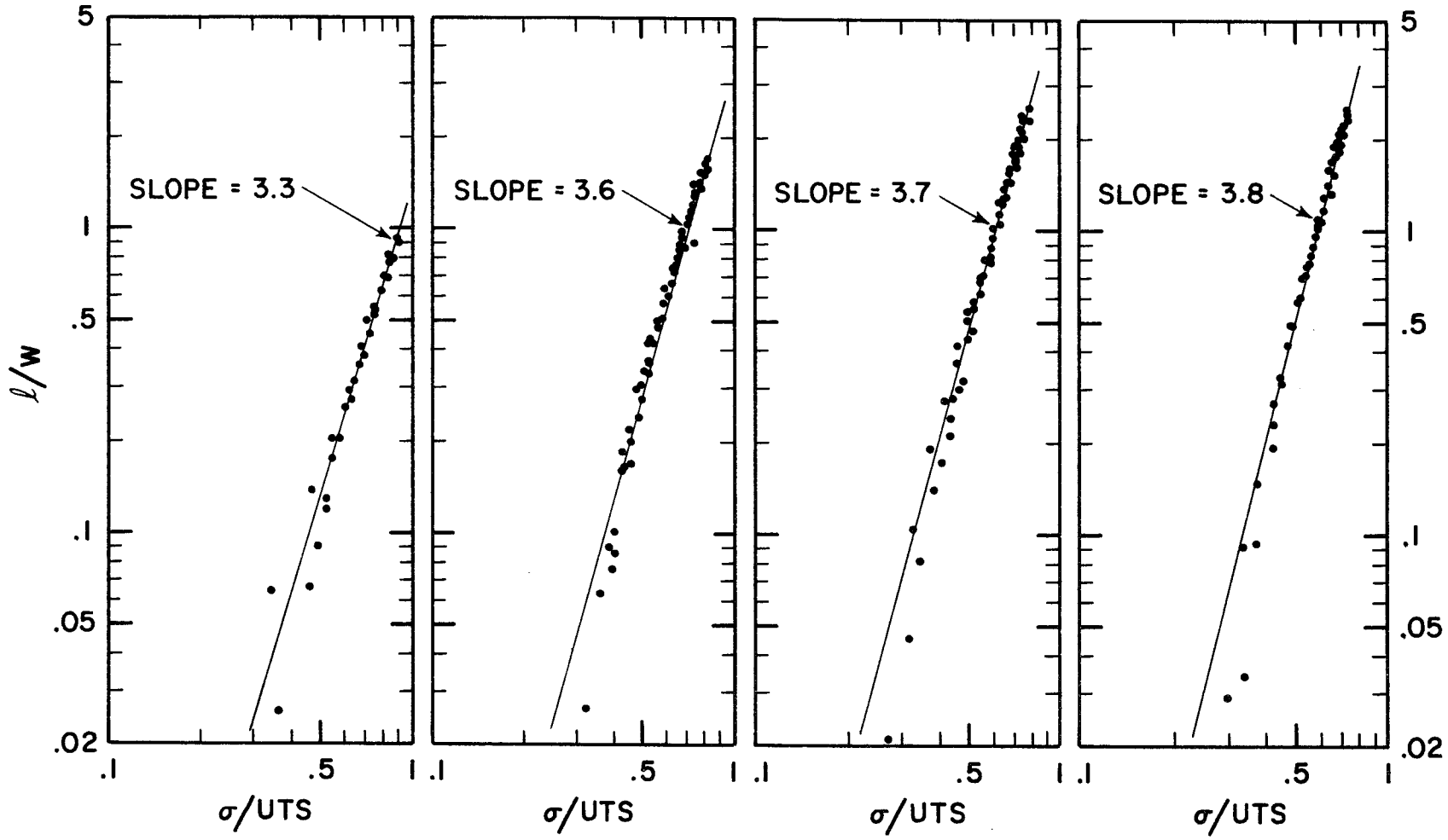

(a) 2c/W = .125 (b) 2c/W = .25 (c) 2c/W = .333 (d) 2c/W = .375

FIGURE 15.

DELAMINATION LENGTH vs. NOMINAL STRESS, 90/0/0/90, TYPE 1003 SCOTCHPLY WITH TWO-PLY DEEP CENTRAL SURFACE CRACKS.

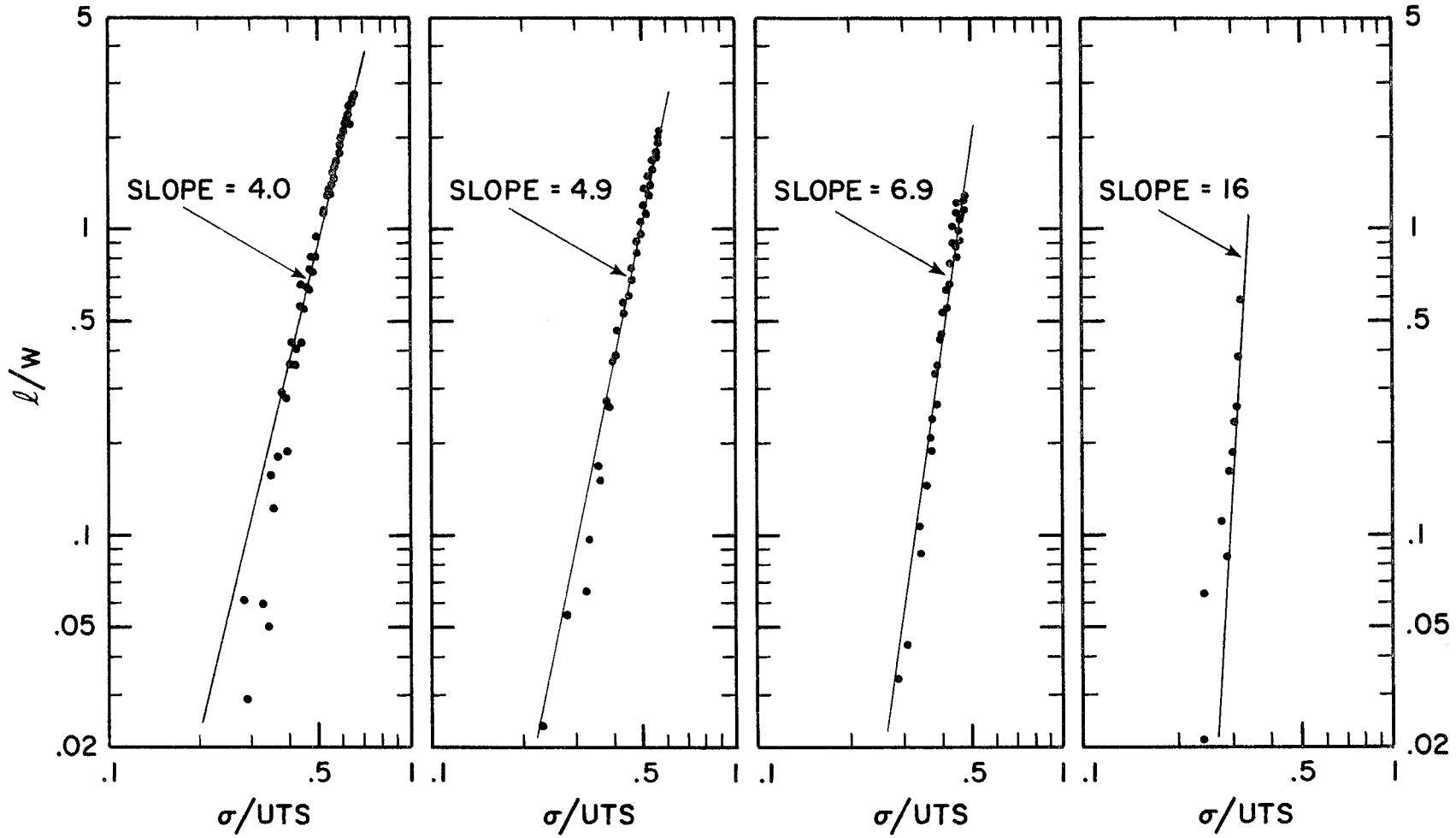

(e) 2c/W = .5 (f) 2c/W = .625 (g) 2c/W = .75 (h) 2c/W = 1.0

FIGURE 15 (continued).

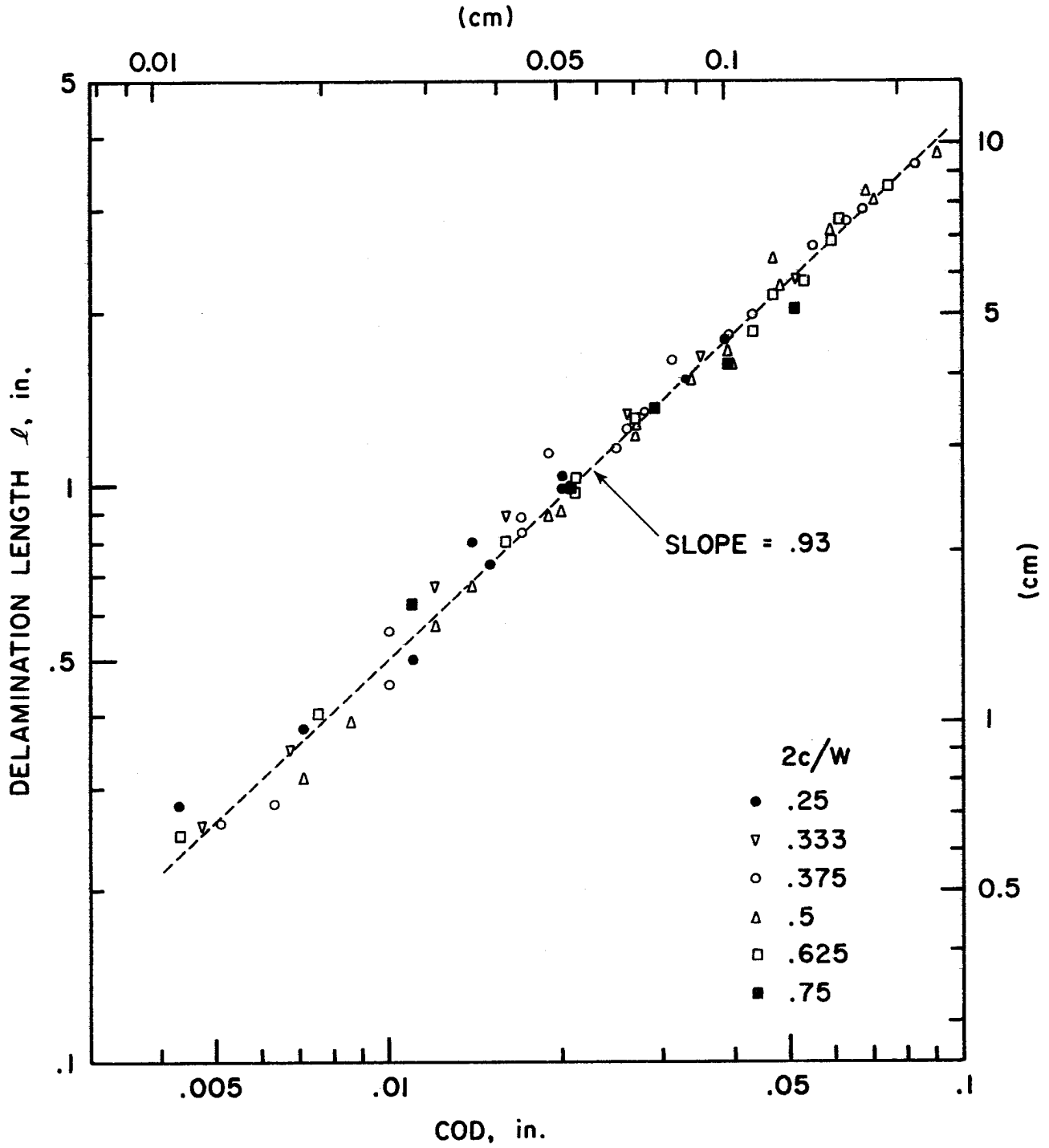

FIGURE 16.

DELAMINATION LENGTH vs. COD, 90/0/0/90 TYPE 1003 SCOTCHPLY WITH TWO-PLY DEEP CENTRAL SURFACE CRACKS.

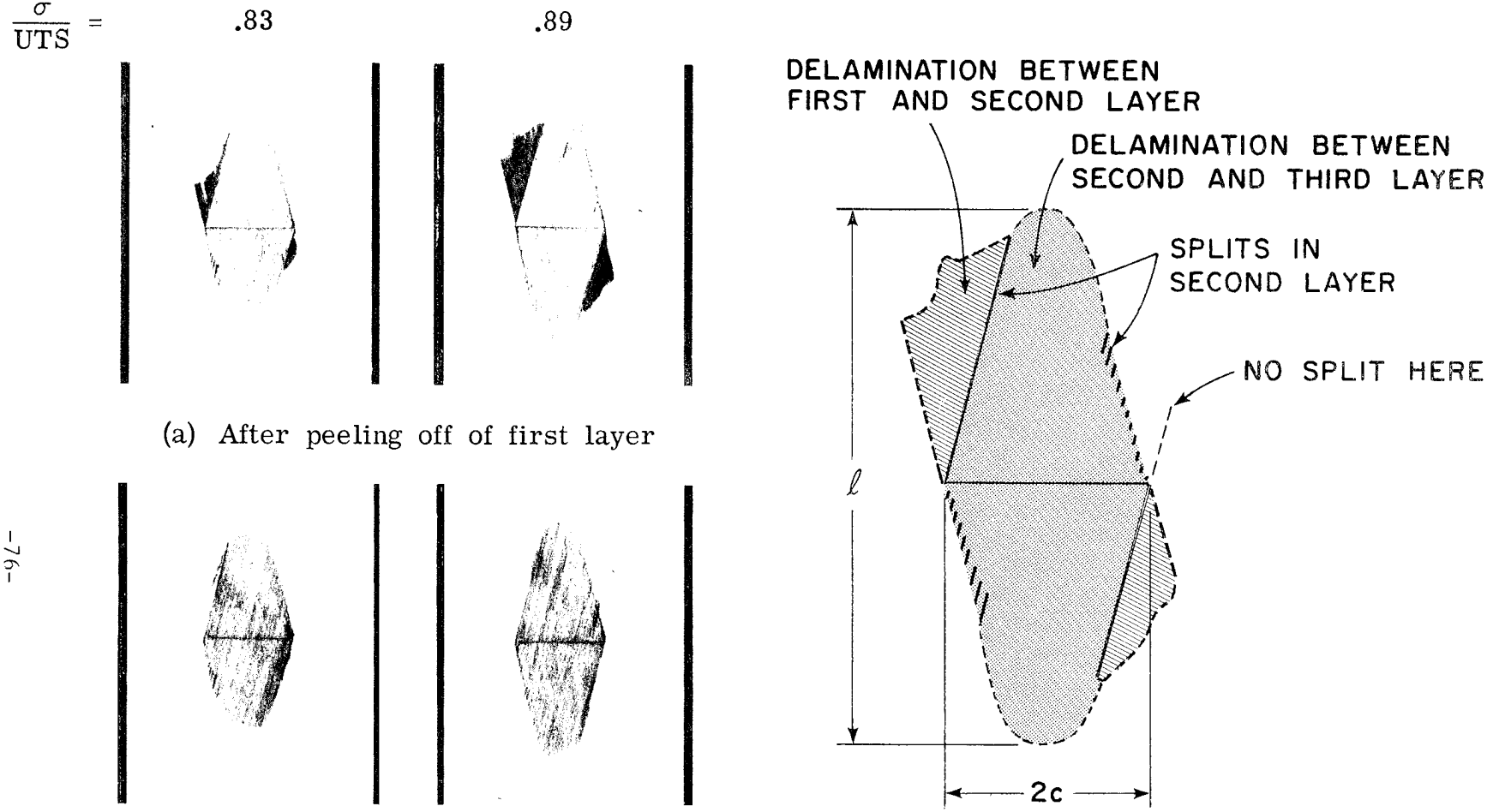

(a) After peeling off of first layer

(b) After slight polishing of (a)

(c) Schematic

FIGURE 17.

DELAMINATIONS AND SPLITS DEVELOPED IN -15/15/15/-15, 1003 SCOTCHPLY CONTAINING SURFACE CRACK.

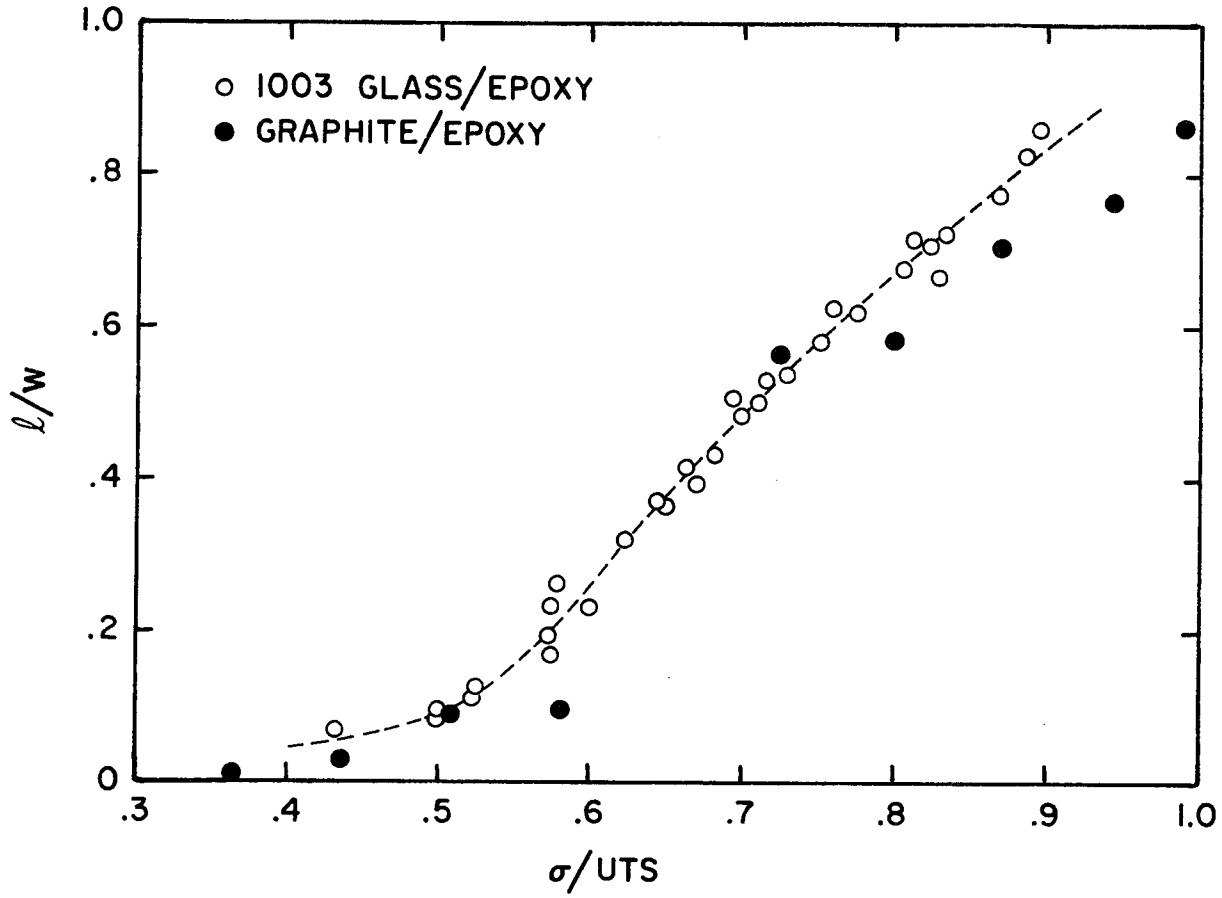

FIGURE 18.

ℓ/W vs. σ/UTS FOR 15/-15/-15/15, 1003 GLASS/EPOXY AND GRAPHITE/EPOXY CONTAINING TWO-PLY DEEP SURFACE CRACKS, 2c/W = .333.

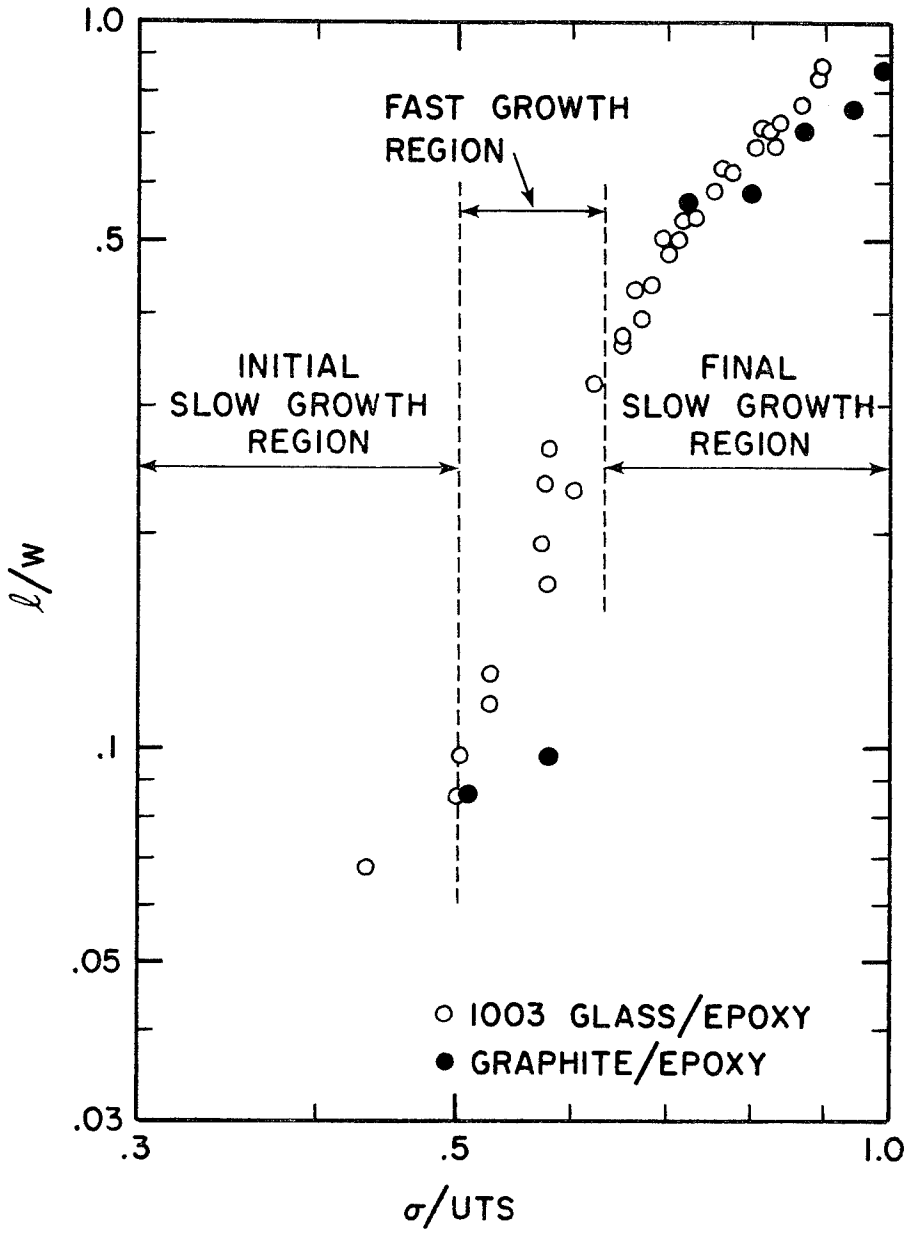

FIGURE 19.

Log ℓ/W vs. Log σ/UTS, 15/-15/-15/15, 1003 GLASS/EPOXY AND GRAPHITE/EPOXY CONTAINING SURFACE CRACKS, $2c/W = .333$.

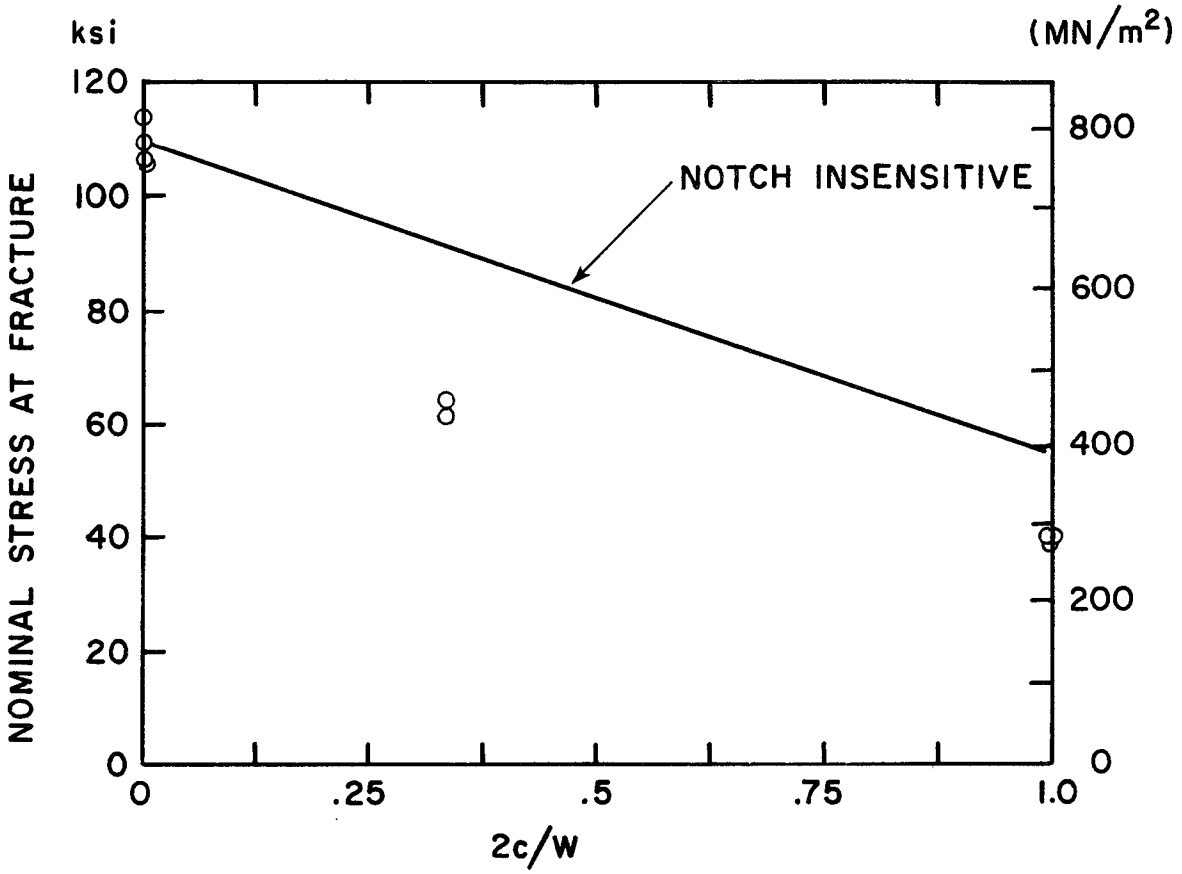

(a) 90/0/0/90, Surface Crack

FIGURE 20.

FRACTURE STRESS vs. 2c/W, GRAPHITE/EPOXY WITH TWO-PLY DEEP SURFACE OR EMBEDDED CRACK.

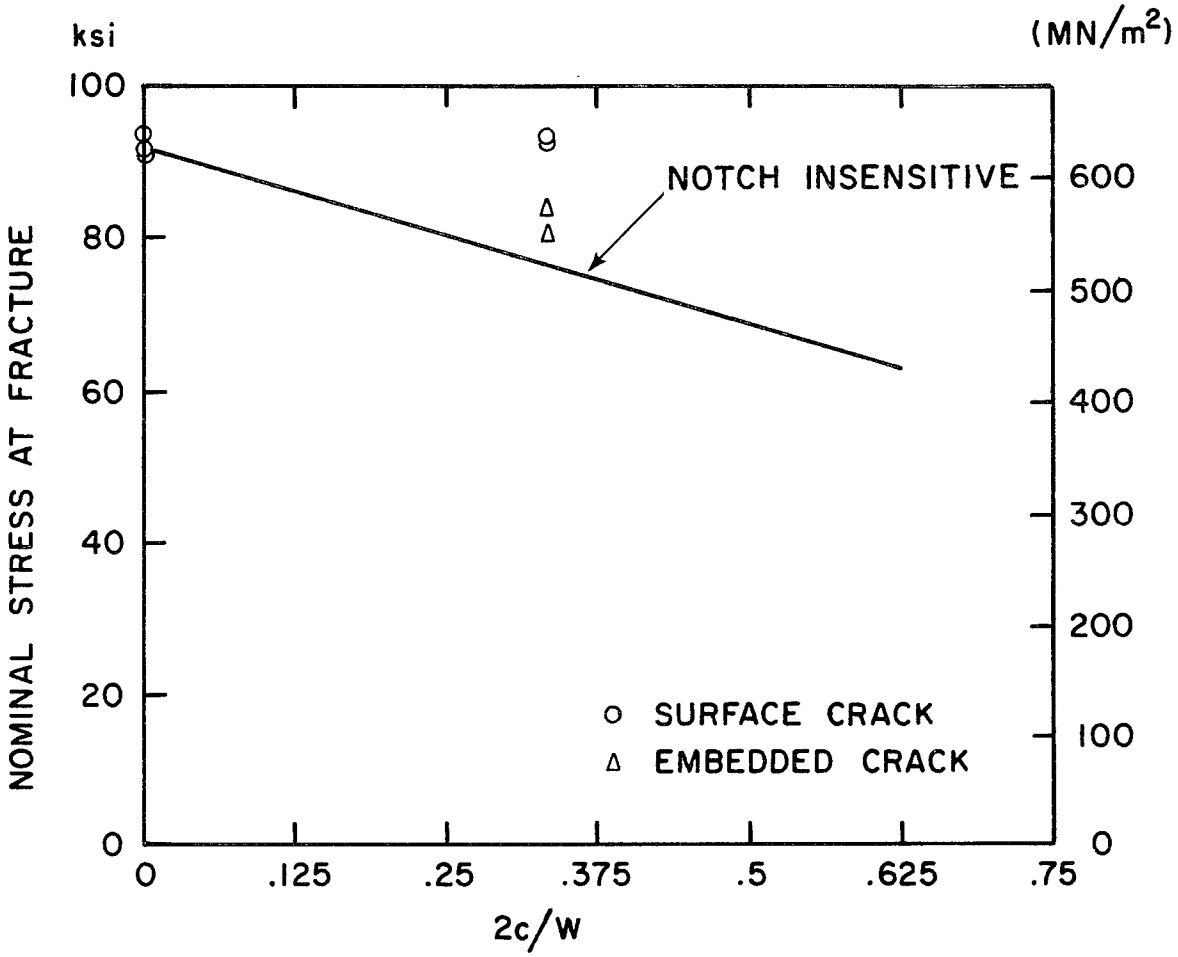

(b) 15/-15/-15/15, Surface or Embedded Crack

FIGURE 20 (continued)

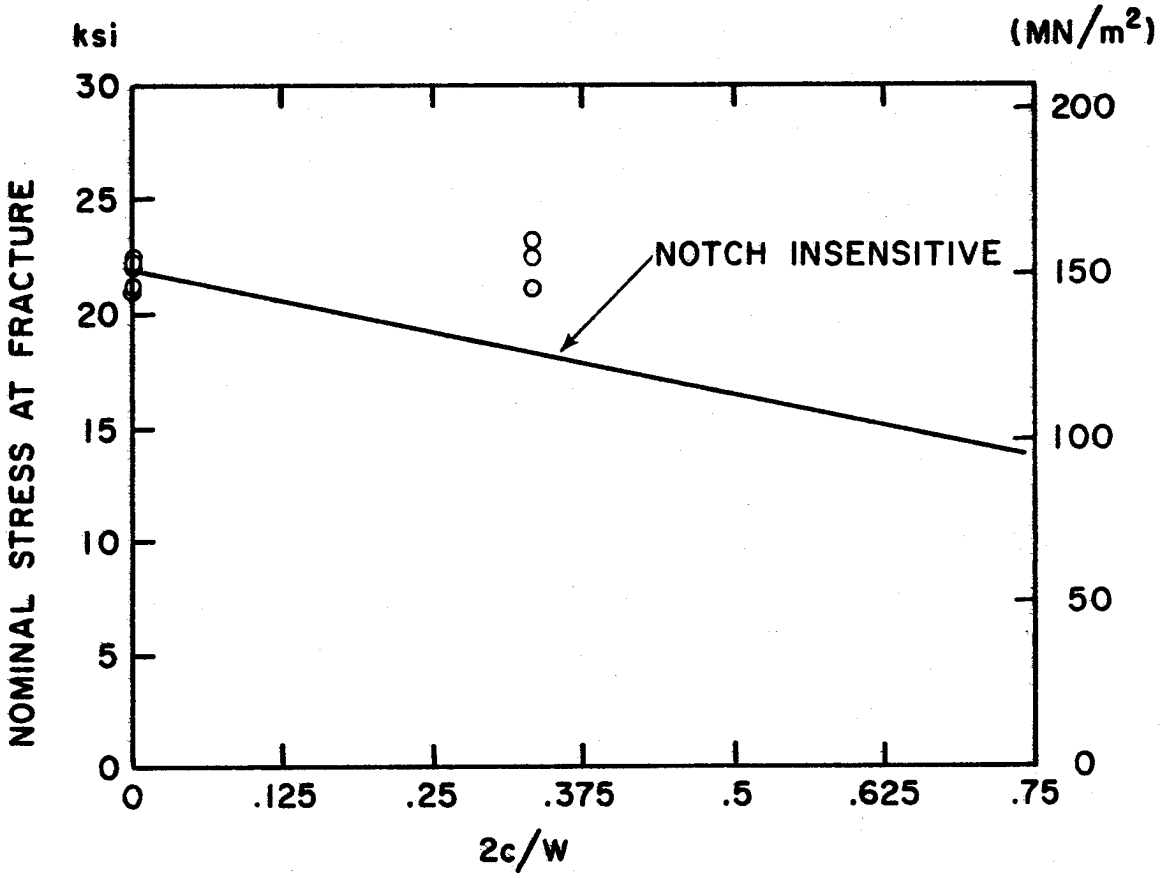

(c) 45/-45/-45/45, Surface Crack

FIGURE 20 (continued).

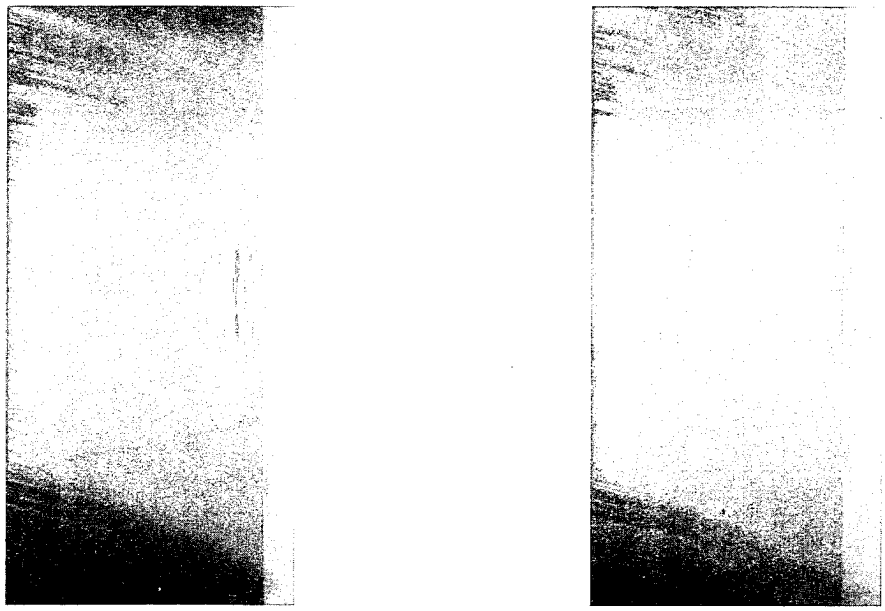

Interface 1-2 Layer 2

Preload: σ/UTS = .53

FIGURE 21.

ONE HALF OF PRELOADED SPECIMEN POLISHED DOWN TO DIFFERENT LEVEL, 90/0/0/90 GRAPHITE/EPOXY WITH TWO-PLY DEEP SURFACE CRACK, 2c/W = .333.

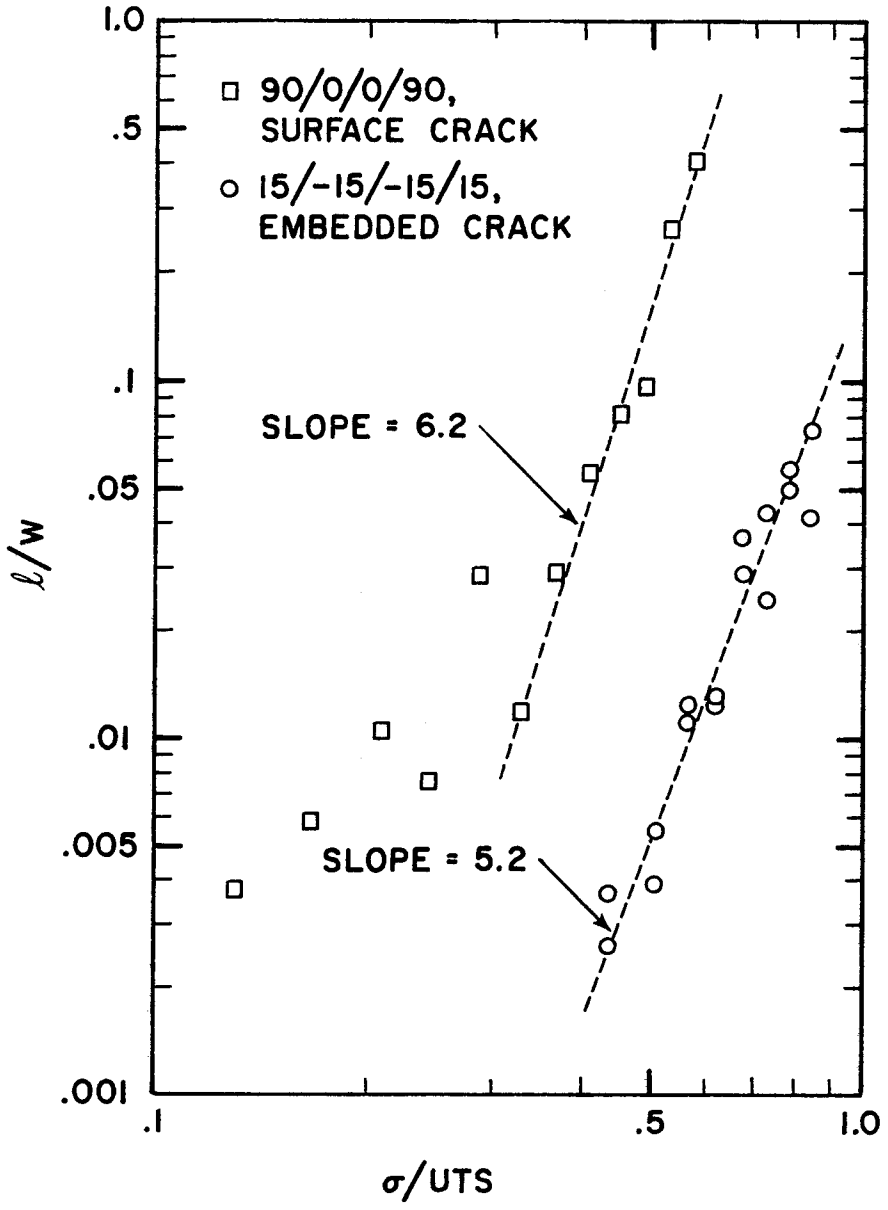

FIGURE 22.

ℓ/W vs. σ/UTS FOR TWO DIFFERENT PLY SEQUENCES OF GRAPHITE/EPOXY CONTAINING PARTIAL THROUGH CRACKS, 2c/W = .333.

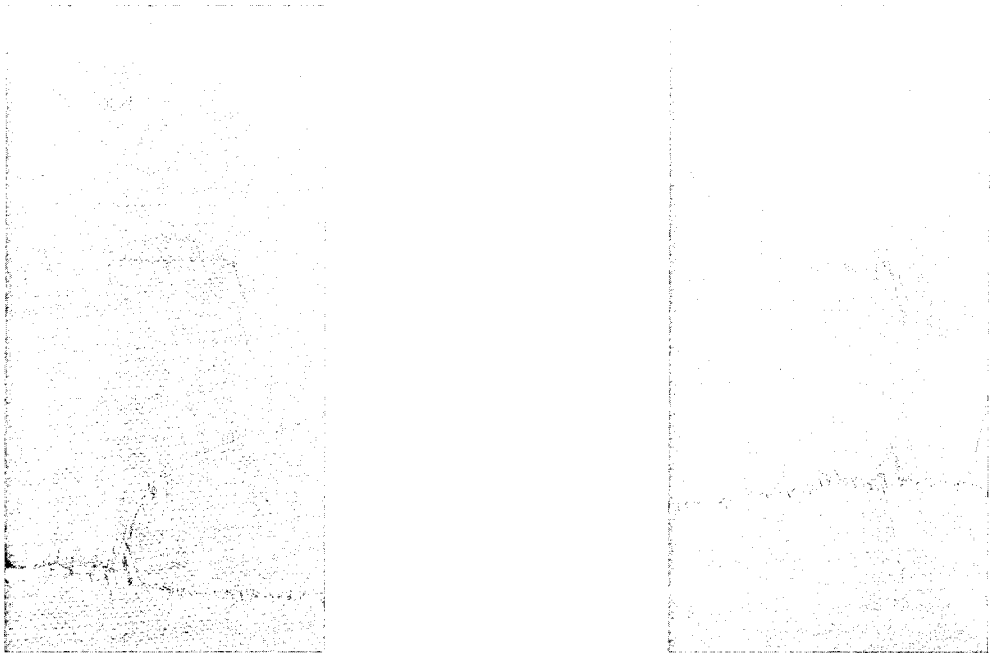

(a) Surface crack

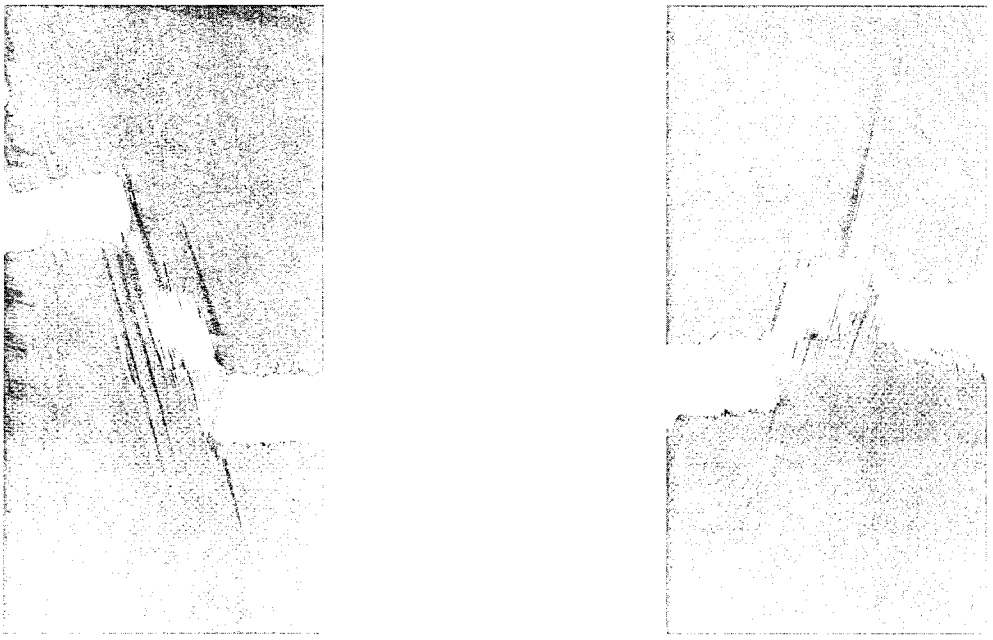

(b) Embedded crack

FIGURE 23.

APPEARANCE OF FRACTURED SPECIMENS CONTAINING SURFACE AND EMBEDDED CRACKS, 15/-15/-15/15 GRAPHITE/EPOXY.

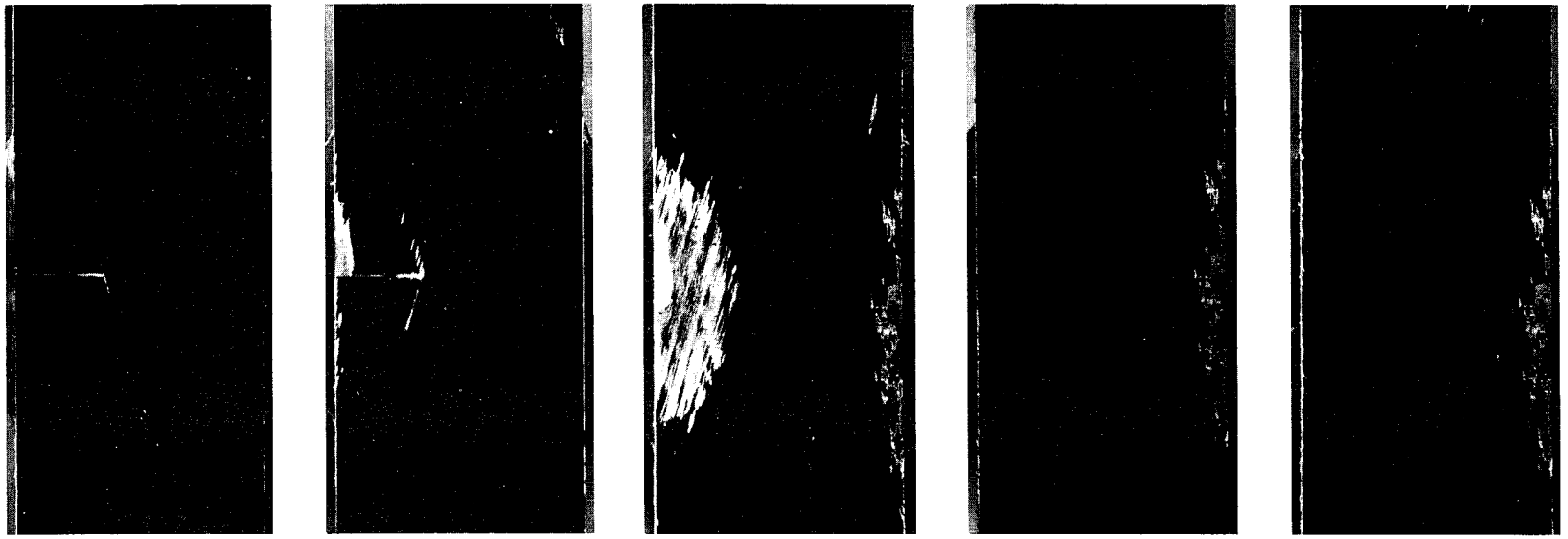

Layer 1 2 Interface 2-3 3 4

(a) Preload: σ/UTS = .80

FIGURE 24.

DAMAGE DEVELOPED AT TWO DIFFERENT LOAD LEVELS IN -15/15/15/-15 GRAPHITE/EPOXY CONTAINING SURFACE CRACKS. (SPECIMENS WERE CUT IN HALF AFTER PRELOADING.)

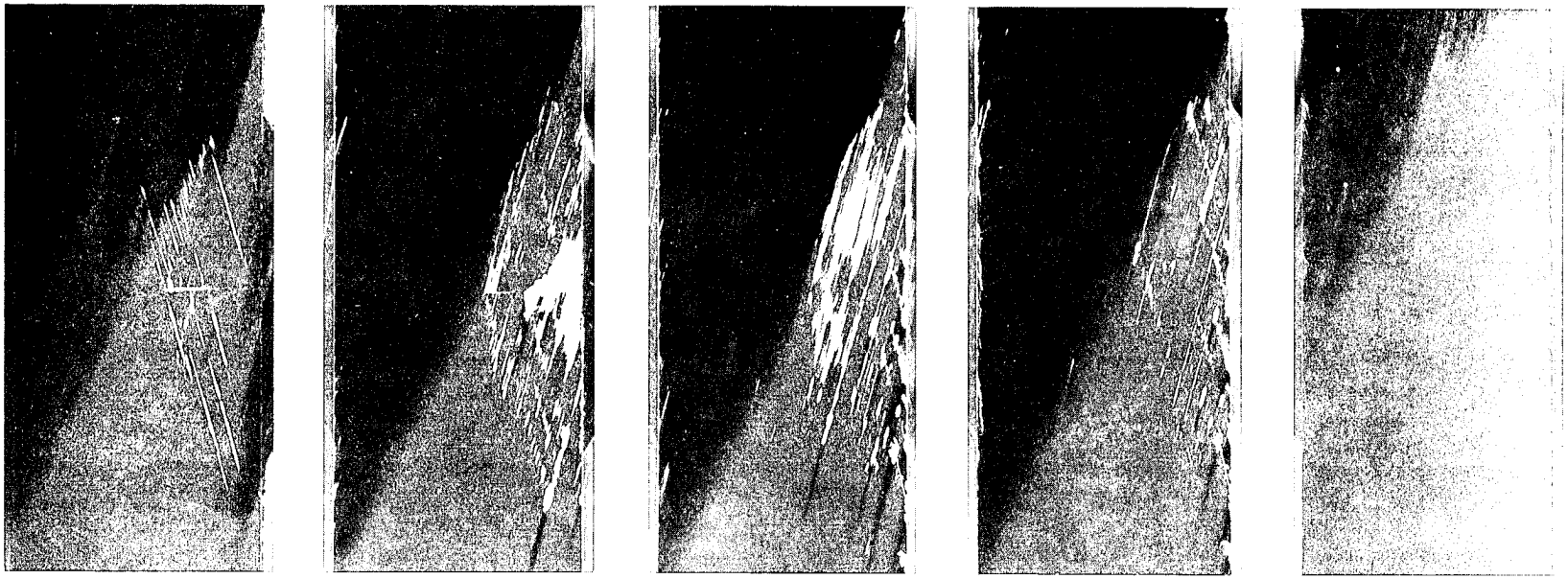

Layer 1 2 Interface 2-3 3 4

(b) Preload: σ/UTS = .98

FIGURE 24 (continued).

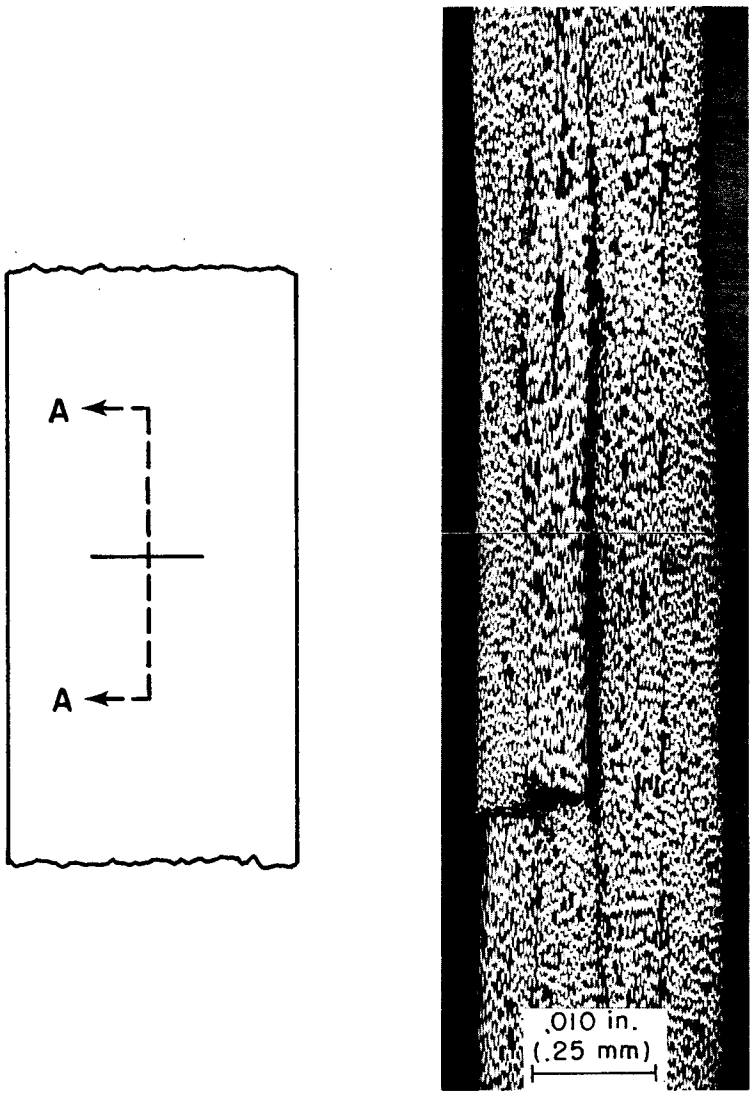

Section A-A

Composite micrograph

FIGURE 25.

INTERLAMINAR DELAMINATION IN 15/-15/-15/15 GRAPHITE/EPOXY SPECIMEN CONTAINING SURFACE CRACK.

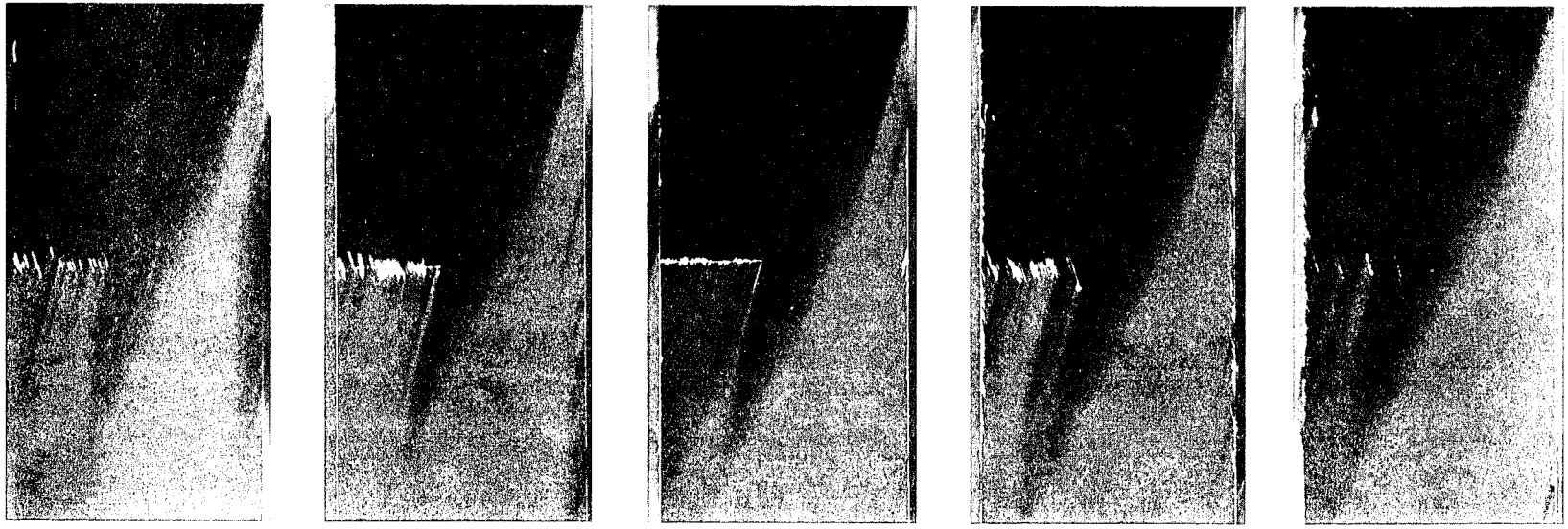

FIGURE 26.

DAMAGE DEVELOPED AT σ/UTS = 0.83 IN -15/15/15/-15 GRAPHITE/EPOXY CONTAINING EMBEDDED CRACKS. (SPECIMENS WERE CUT IN HALF AFTER PRELOADING.)

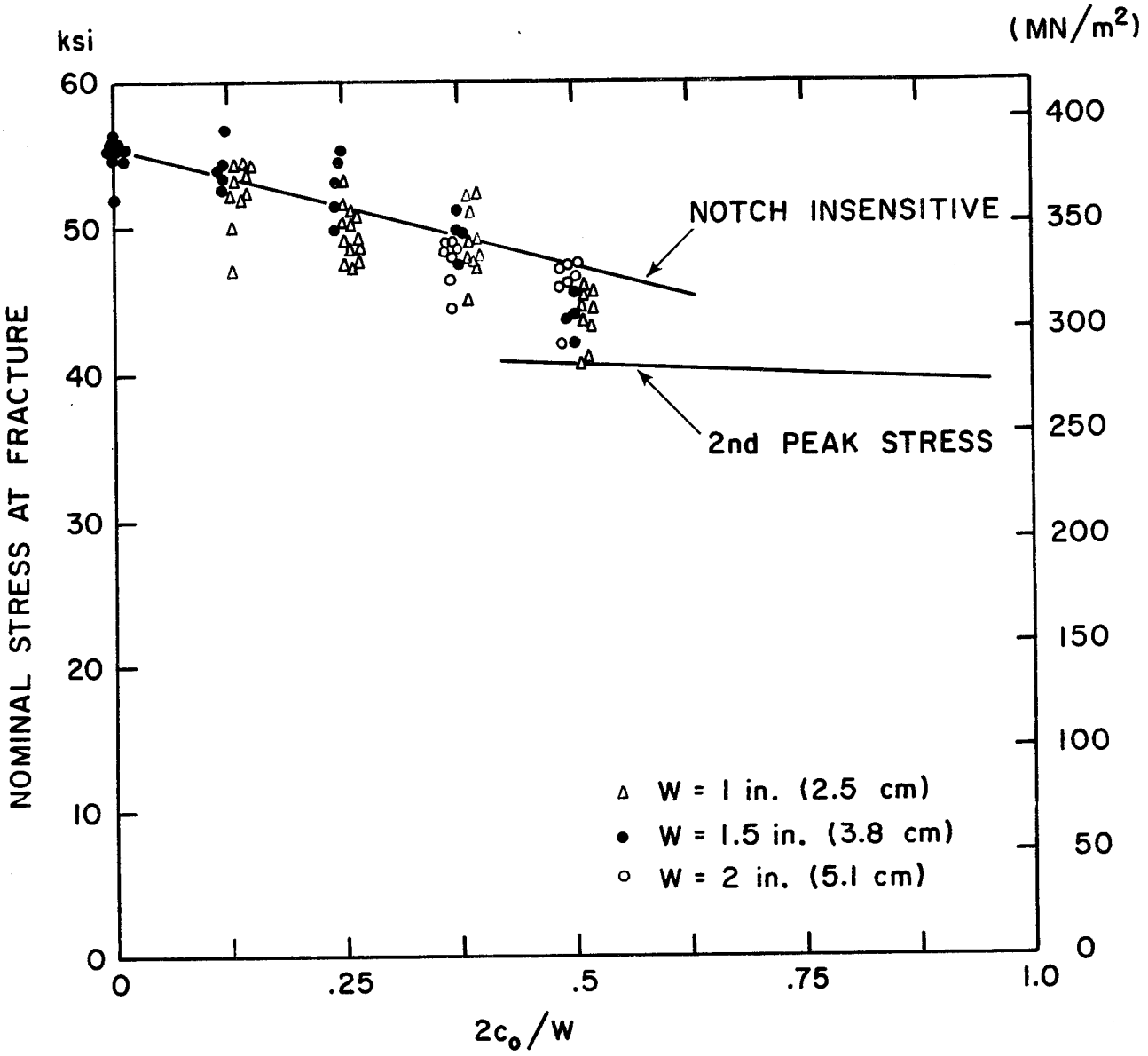

FIGURE 27.

NOMINAL STRESS AT FRACTURE vs. $2c_o/W$, 90/0 (15 LAYERS) TYPE 1002 SCOTCHPLY WITH SURFACE CRACK ON ONE SIDE (LAYERS 1-5 PRECUT).

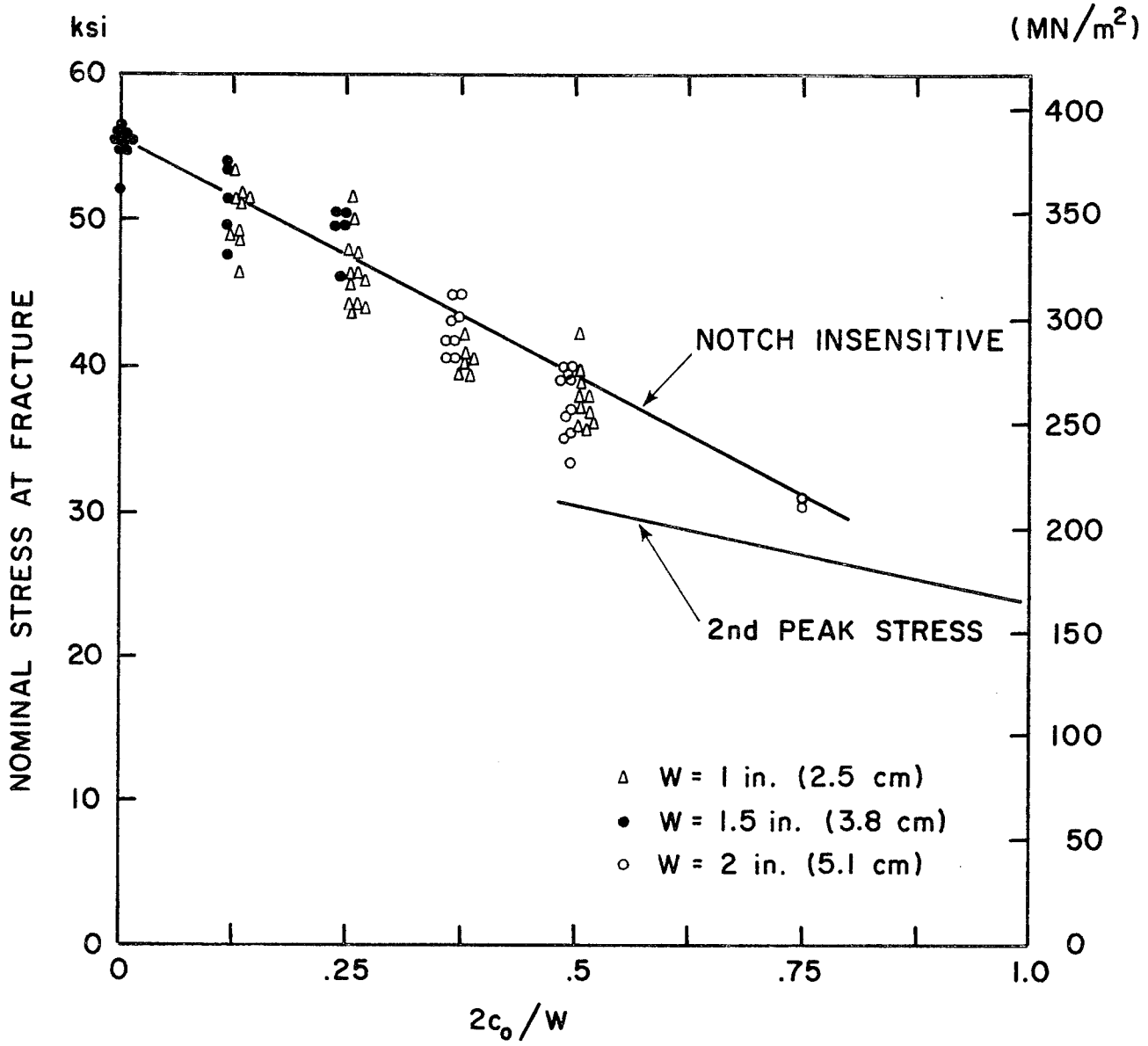

FIGURE 28.

NOMINAL STRESS AT FRACTURE vs. $2c_0/W$, 90/0 (15 LAYERS) TYPE 1002 SCOTCHPLY WITH SURFACE CRACKS ON BOTH SIDES (LAYERS 1-5 AND 11-15 PRECUT).

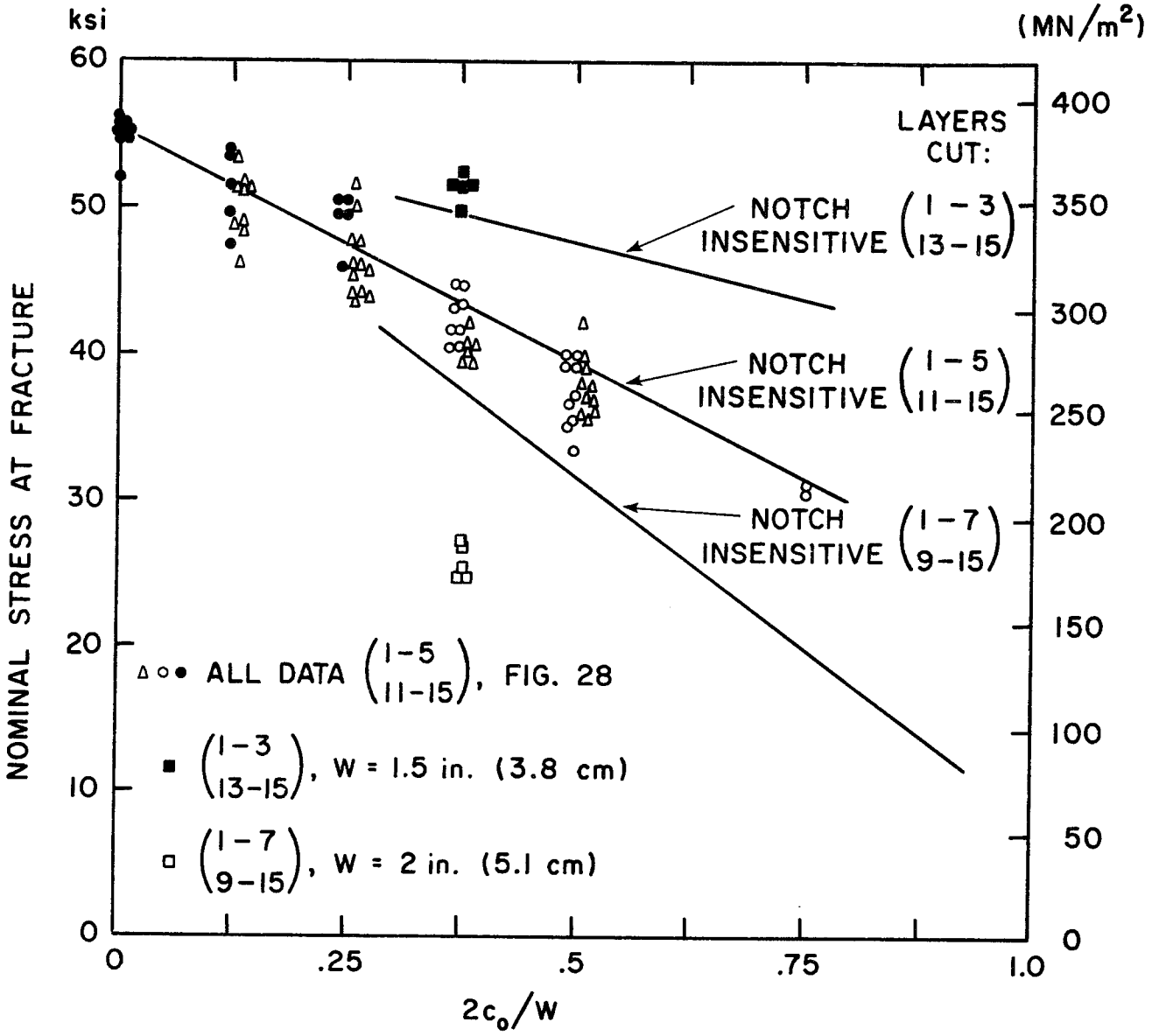

FIGURE 29.

NOTCH SENSITIVITY DEPENDENCE ON CRACK DEPTH IN 90/0, TYPE 1002 SCOTCHPLY WITH SURFACE CRACKS ON BOTH SIDES.

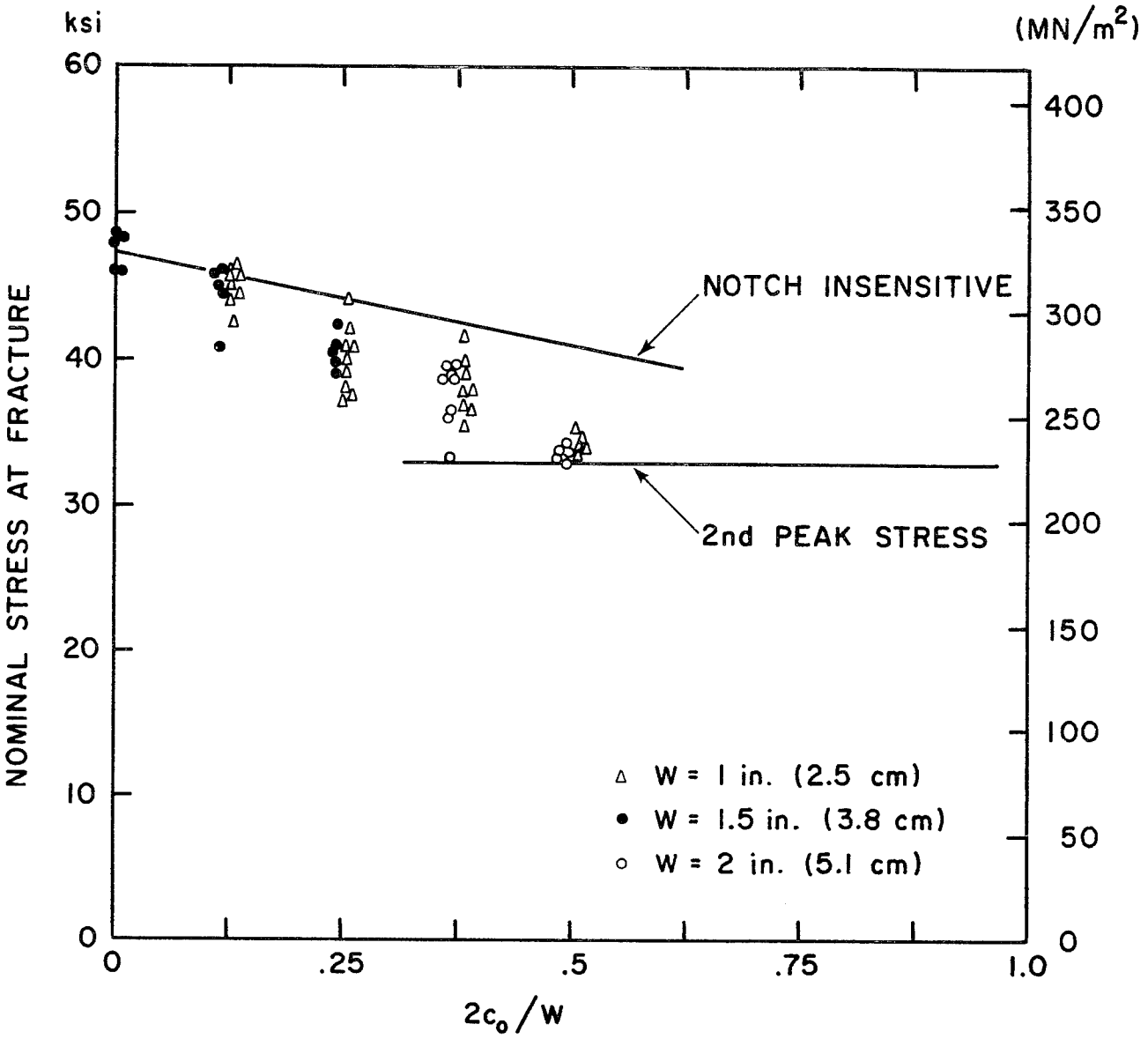

FIGURE 30.

NOMINAL STRESS AT FRACTURE vs. $2c_o/W$, ±60/0 (12 LAYERS) TYPE 1002 SCOTCHPLY WITH SHALLOW SURFACE CRACK ON ONE SIDE (LAYERS 1-4 PRECUT).

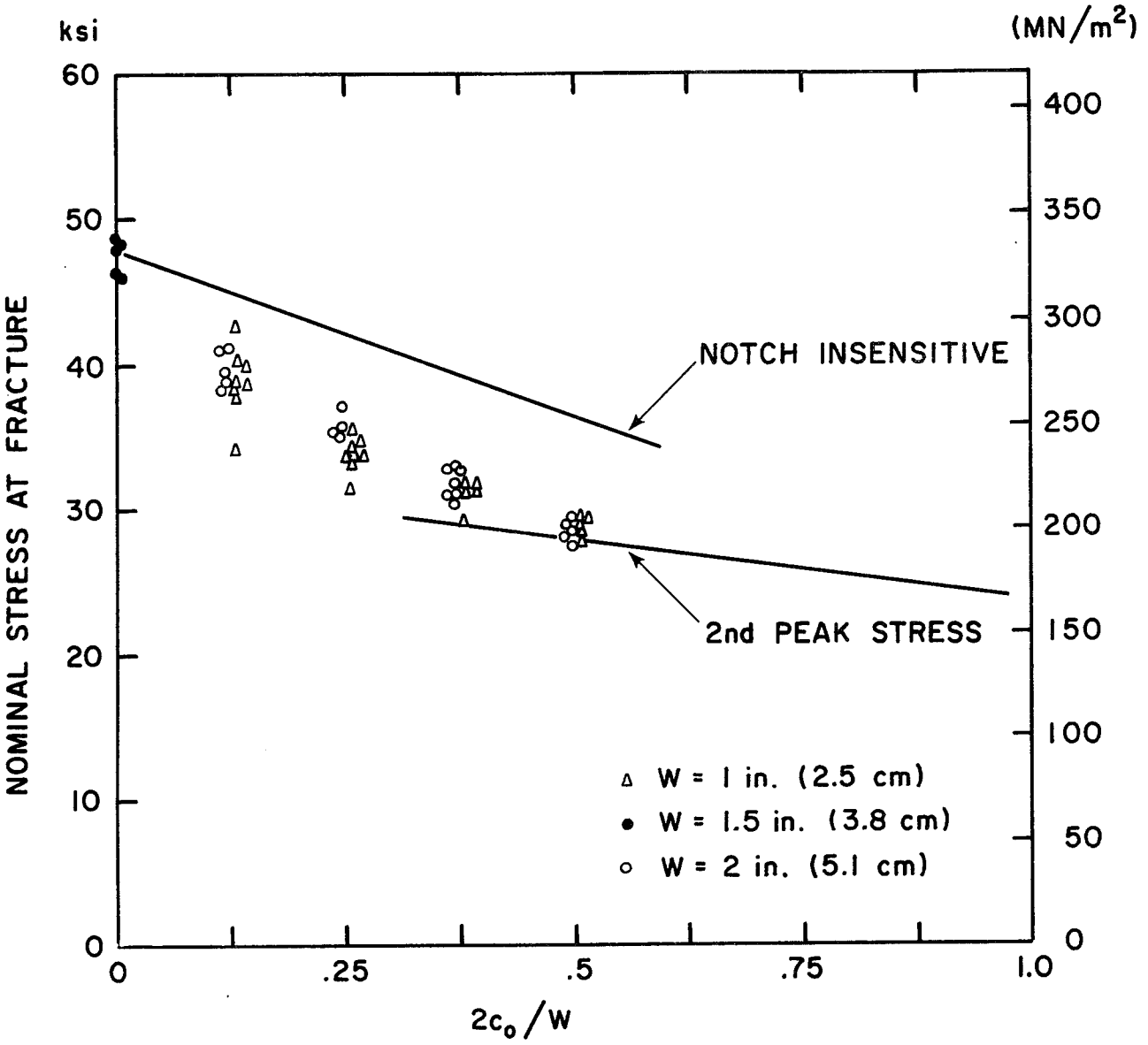

FIGURE 31.

NOMINAL STRESS AT FRACTURE vs. $2c_o/W$, ±60/0 (12 LAYERS) TYPE 1002 SCOTCHPLY WITH DEEP SURFACE CRACK ON ONE SIDE (LAYERS 1-5 PRECUT).

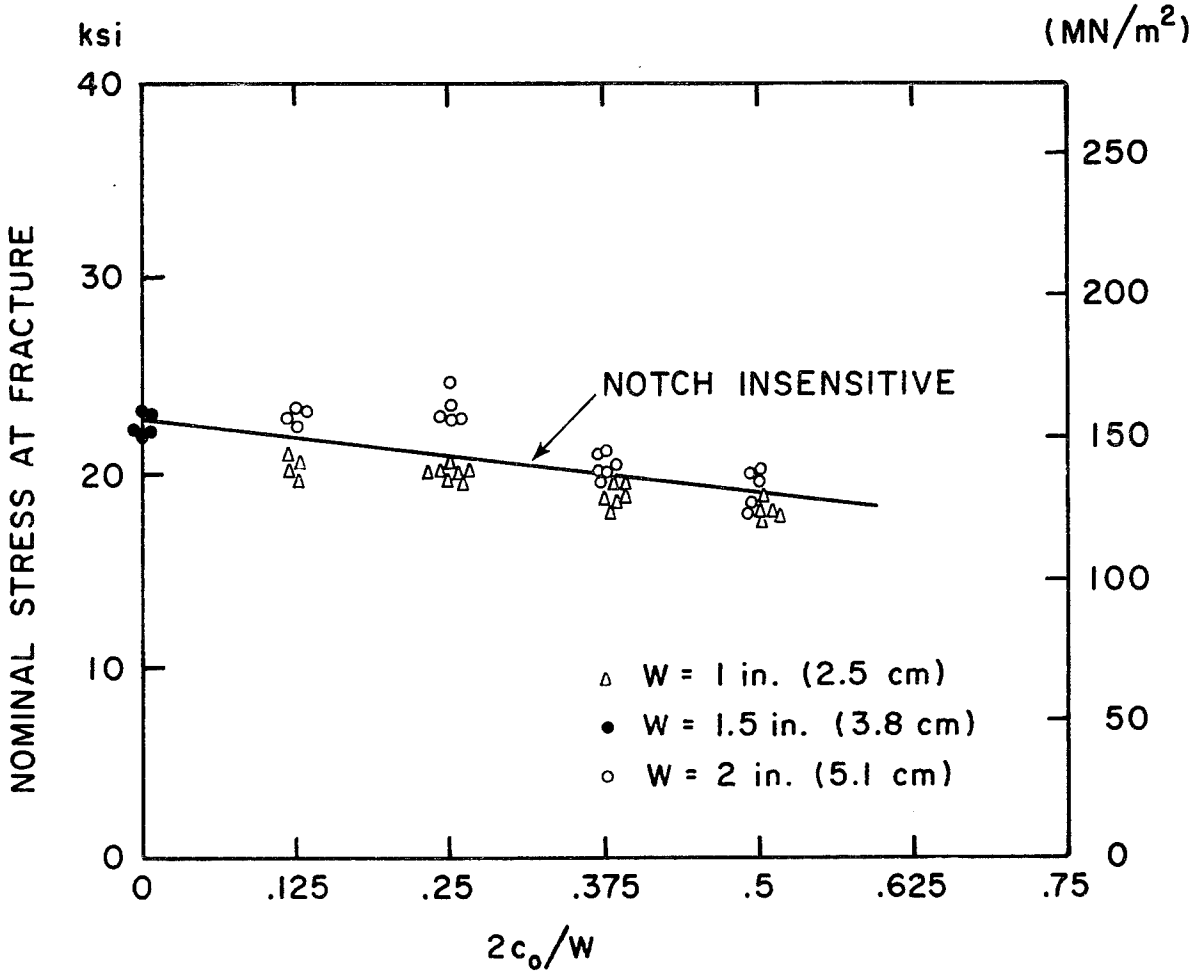

FIGURE 32.

NOMINAL STRESS AT FRACTURE vs. $2c_o/W$, ±45 (16 LAYERS) TYPE 1002 SCOTCHPLY WITH SURFACE CRACK ON ONE SIDE (LAYERS 1-5 PRECUT).

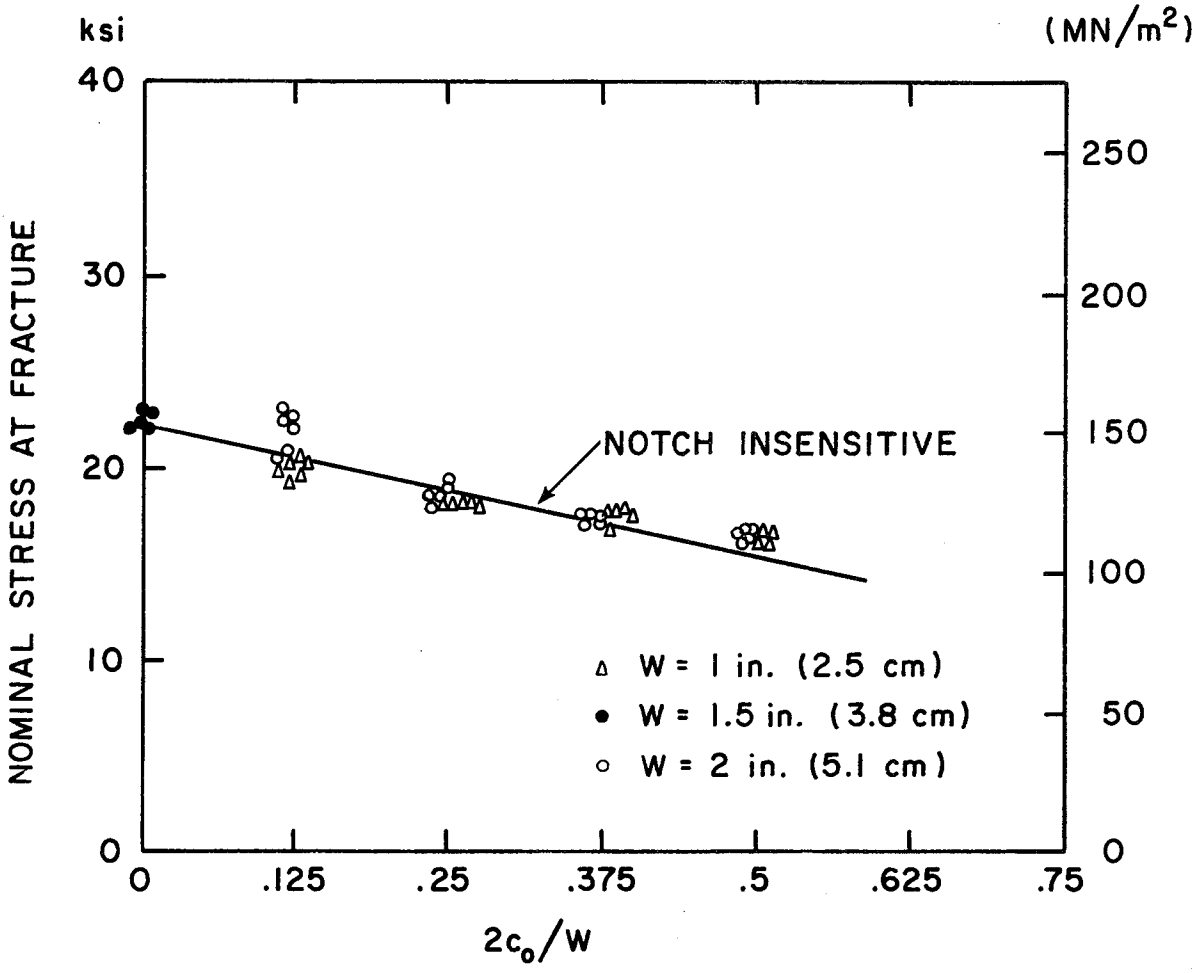

FIGURE 33.

NOMINAL STRESS AT FRACTURE vs. $2c_0/W$, ±45 (16 LAYERS) TYPE 1002 SCOTCHPLY WITH SURFACE CRACKS ON BOTH SIDES (LAYERS 1-5 AND 12-16 PRECUT).

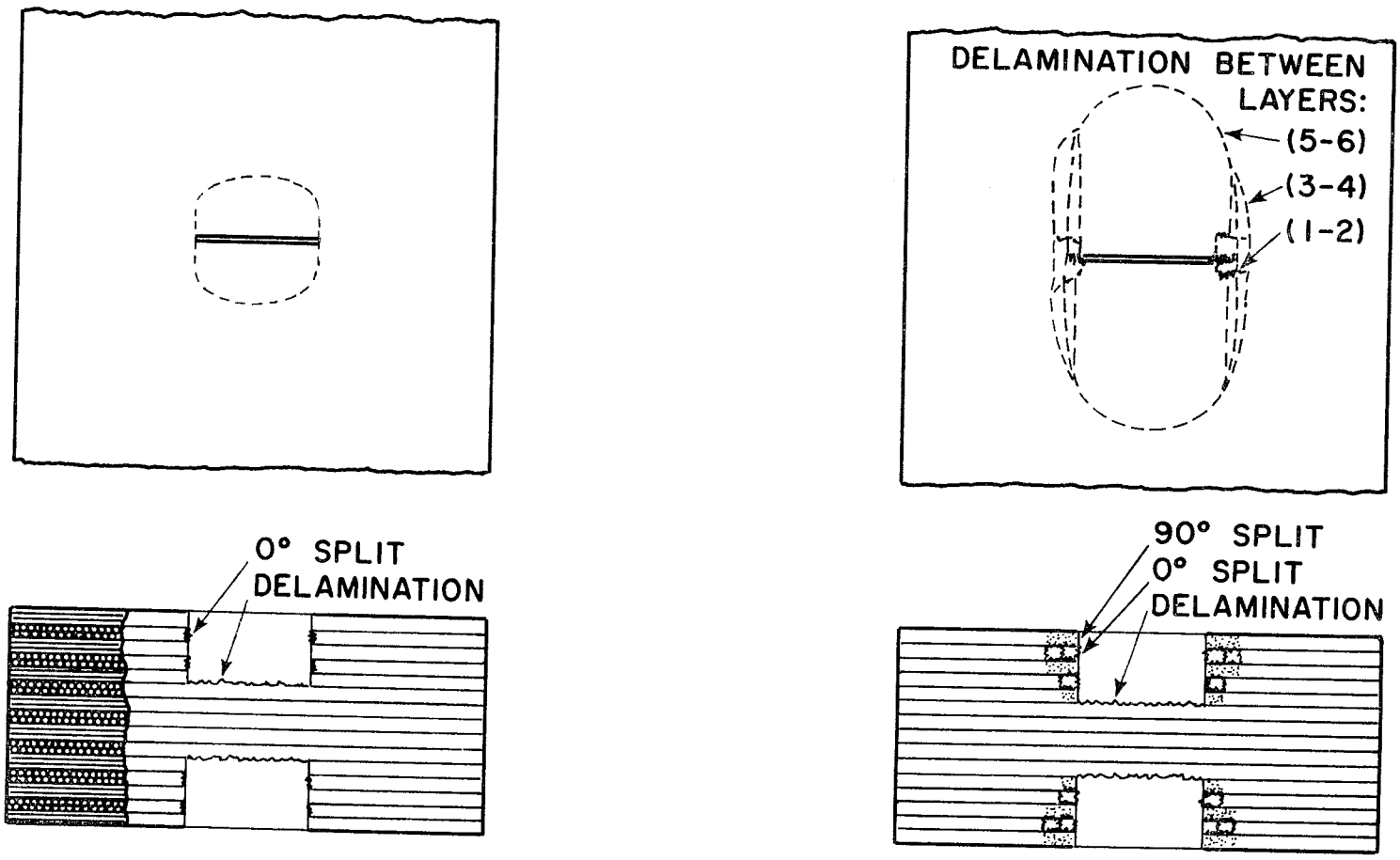

(a) Low load

(b) High load

FIGURE 34.

GROWTH OF DELAMINATIONS AND SPLITS IN 90/0 (15 LAYERS) 1002 SCOTCHPLY CONTAINING SURFACE CRACKS ON BOTH SIDES.

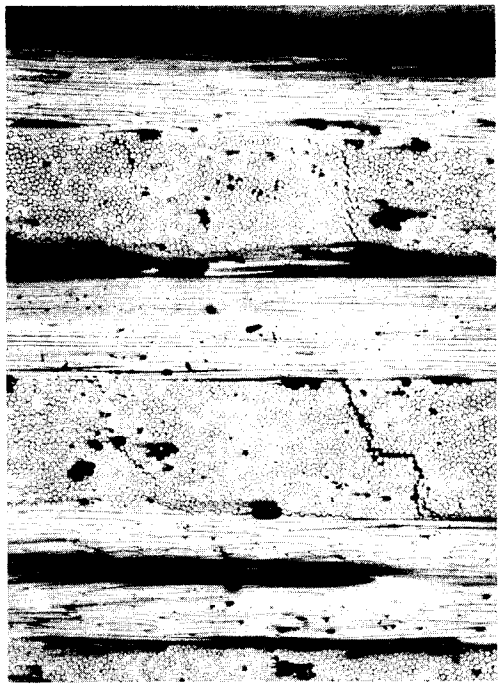

Region A

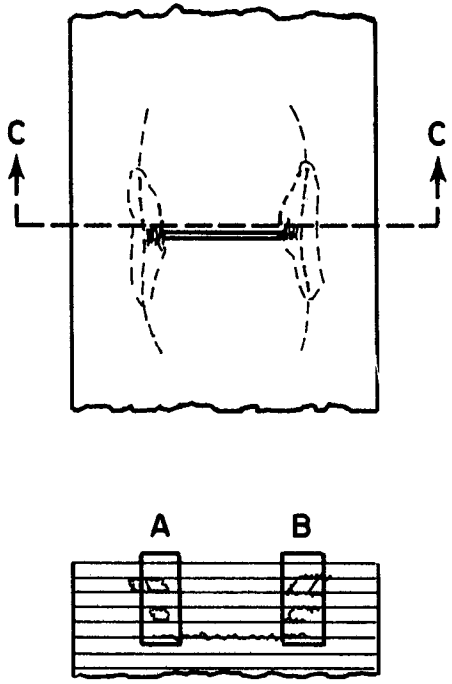

Section C-C

Region B

(c) Micrographs

FIGURE 34 (continued).

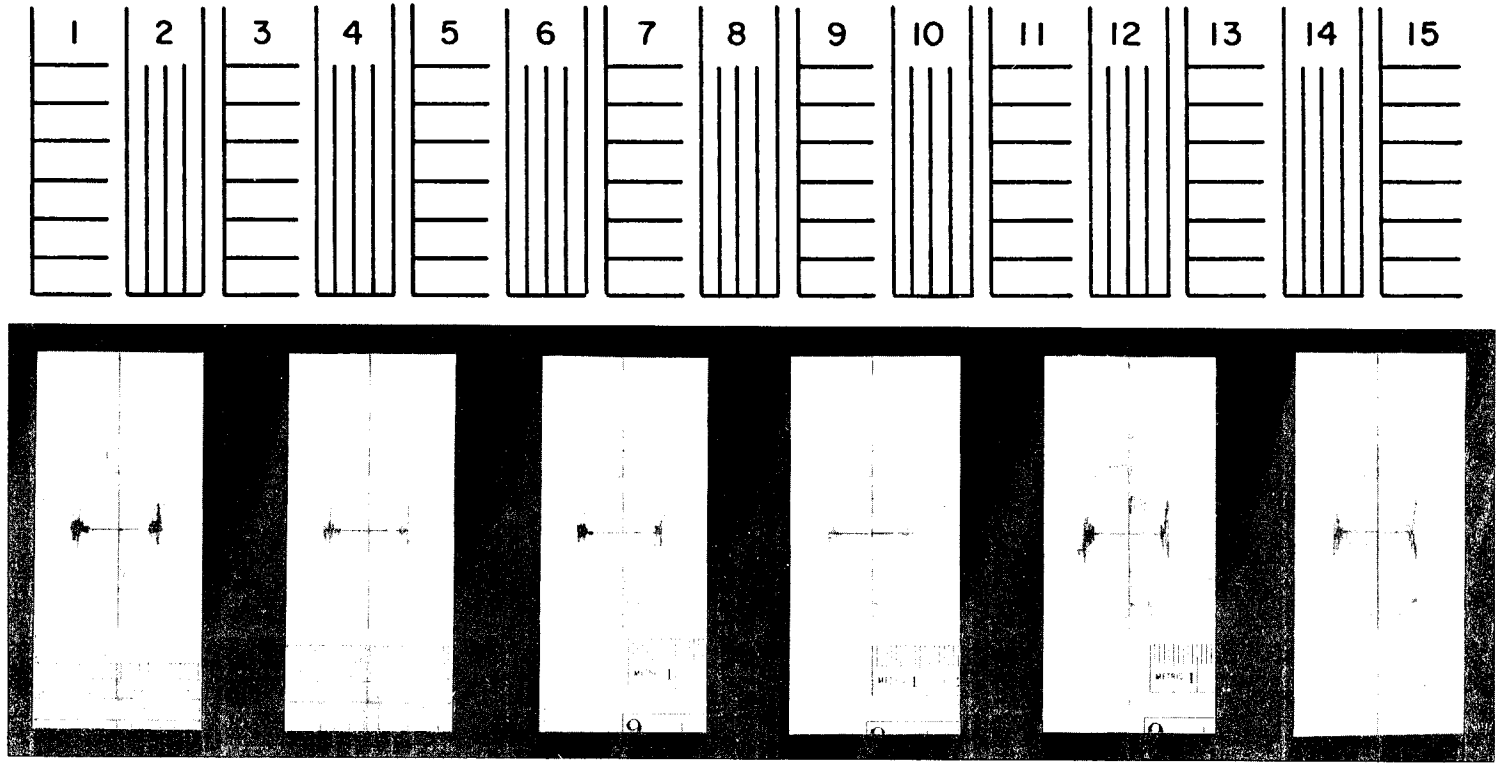

(a) Preload: σ/UTS = .68, W = 1.5 in. (3.81 cm), $2c_o/W$ = .375

FIGURE 35.

DAMAGE DEVELOPED IN 90/0 (15 LAYERS), 1002 SCOTCHPLY CONTAINING FIVE-LAYER DEEP SURFACE CRACKS ON BOTH SIDES.

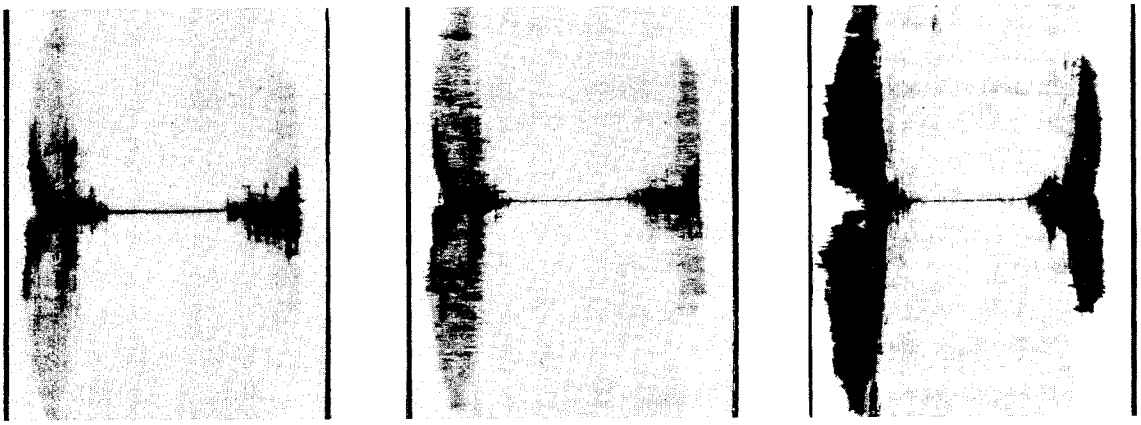

Interface 1-2 2-3 3-4

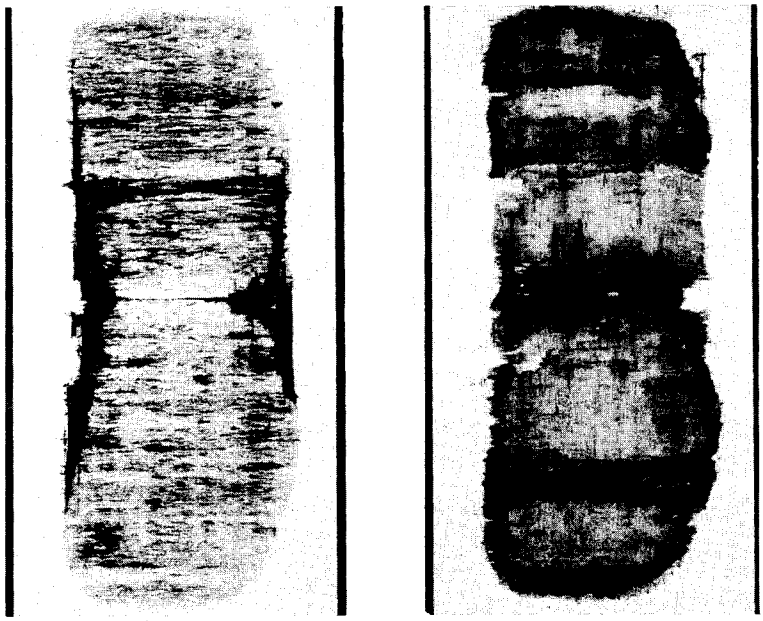

4-5 5-6

(b) Preload: σ/UTS = .79
W = 2 in. (5.1 cm), $2c_o/W$ = .375

FIGURE 35 (continued).

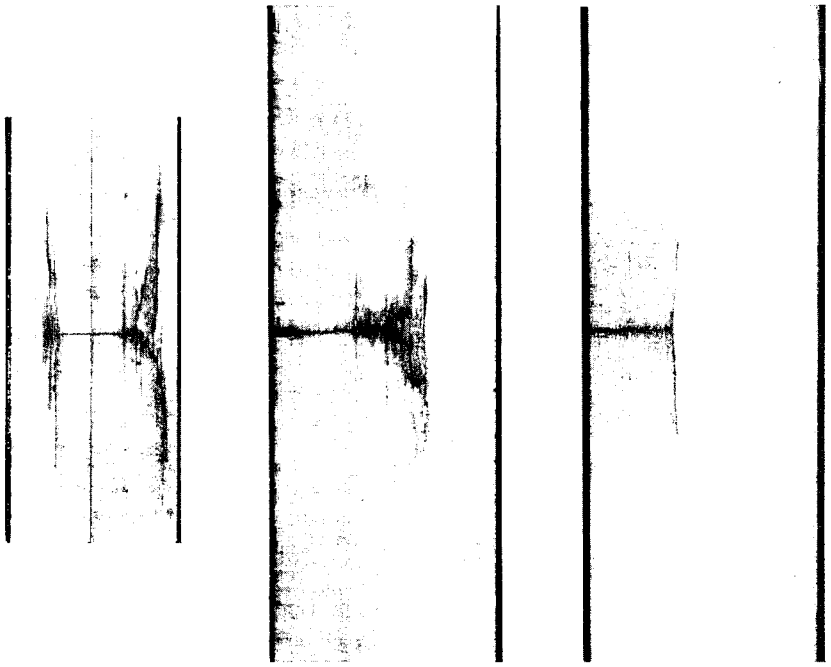

FIGURE 36.

PHOTOGRAPHS SHOWING LOCATIONAL COINCIDENCE BETWEEN LAST SPLITS FROM SURFACE CRACK TIPS WITHIN FOURTH LAYER AND VERTICAL BOUNDARIES OF DELAMINATION BETWEEN LAYERS 4 AND 5, 90/0 (15 LAYERS) 1002 SCOTCHPLY.

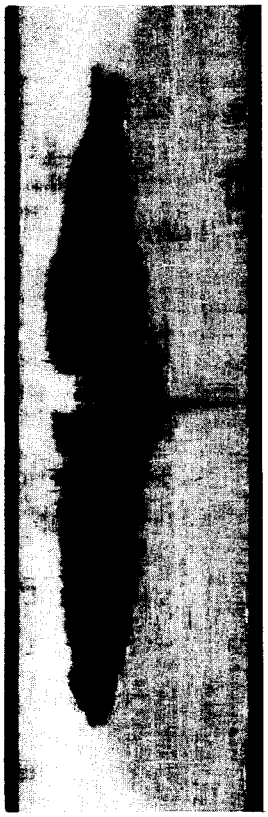

FIGURE 37.

SHAPE OF CRACK TIP DELAMINATION AT INTERFACE (3-4), 90/0 (15 LAYERS), 1002 SCOTCHPLY WITH SURFACE CRACK.

-60/0/60

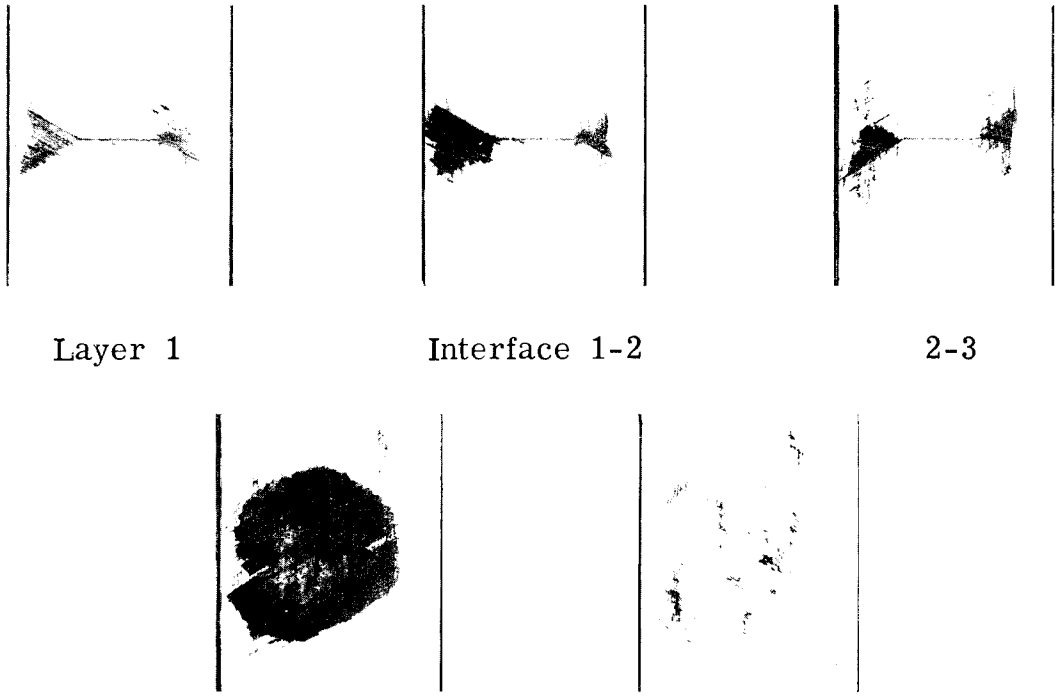

Preload: σ/UTS = .76

FIGURE 38.

DAMAGE DEVELOPED IN ±60/0 (12 LAYERS), 1002 SCOTCHPLY CONTAINING FOUR-LAYER DEEP SURFACE CRACK, W = 2 in. (5.1 cm), $2c_o/W$ = .375.

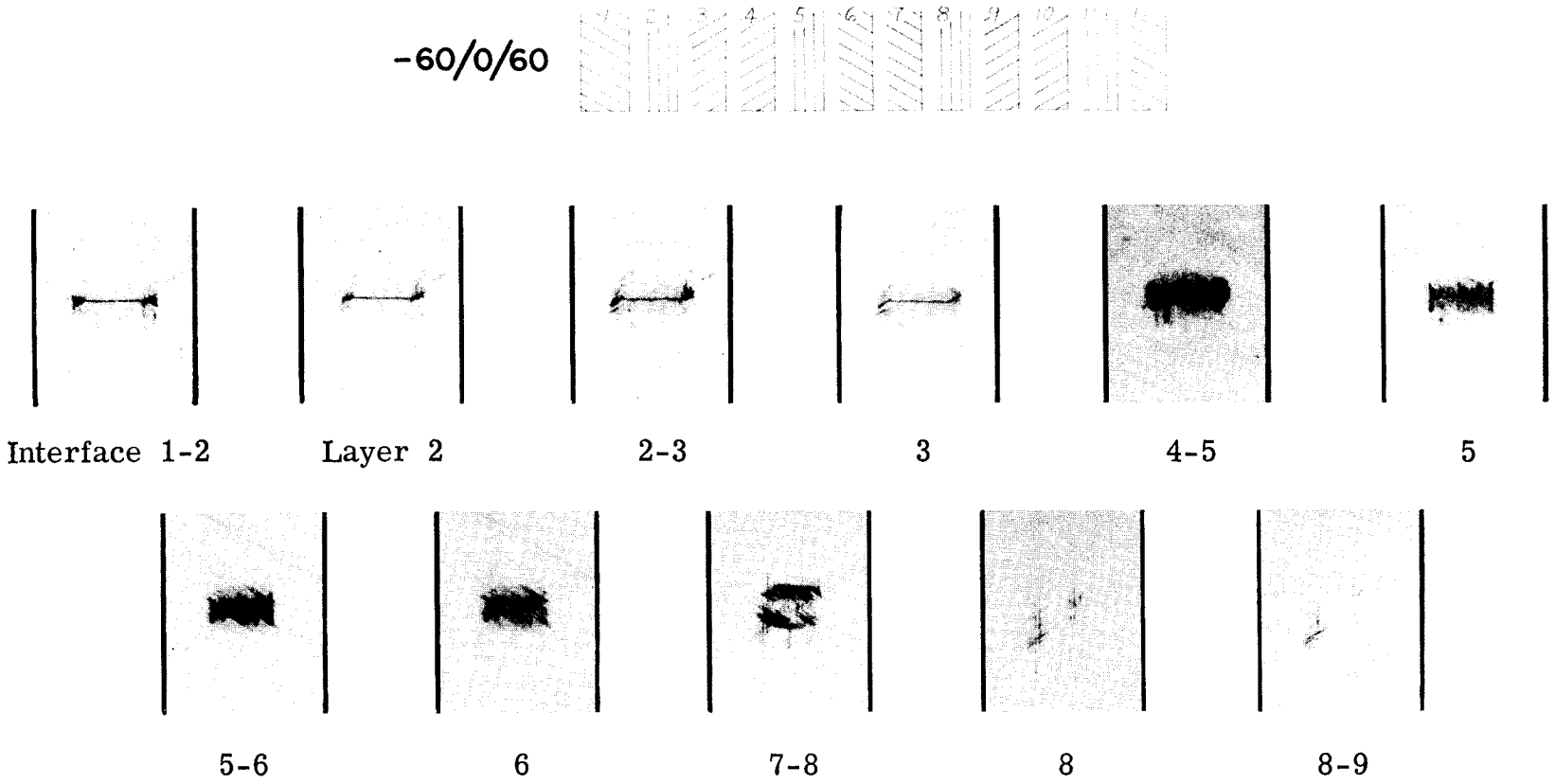

Preload: σ/UTS = .57

FIGURE 39.

DAMAGE DEVELOPED IN ±60/0 (12 LAYERS), 1002 SCOTCHPLY CONTAINING FIVE-LAYER DEEP SURFACE CRACK, W = 2 in. (5.1 cm), $2c_o/W$ = .375.

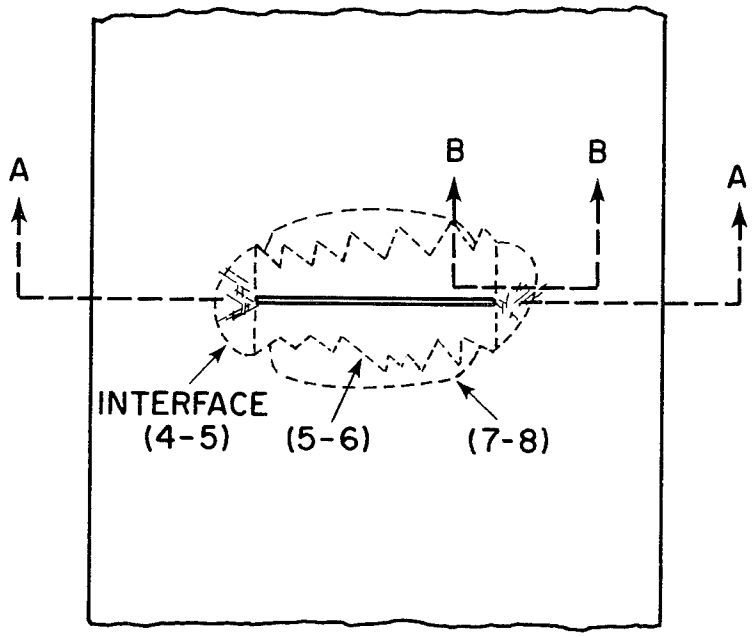

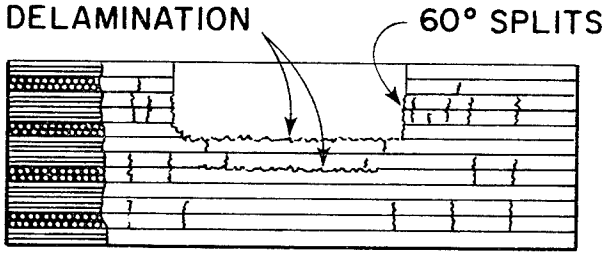

SECTION A-A

(a) Schematic

FIGURE 40.

SCHEMATIC AND MICROGRAPHS OF DAMAGED REGION, 60/0/-60 (12 LAYERS) 1002 SCOTCHPLY CONTAINING FIVE-LAYER DEEP SURFACE CRACK.

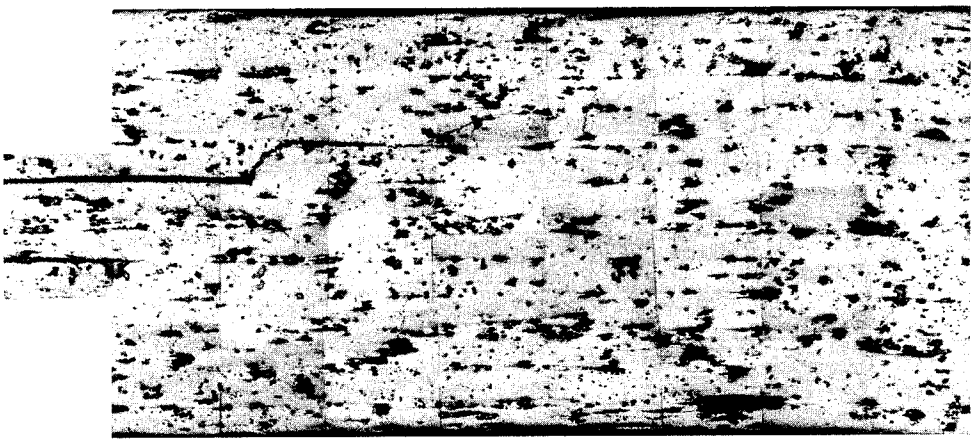

(b) Section B-B

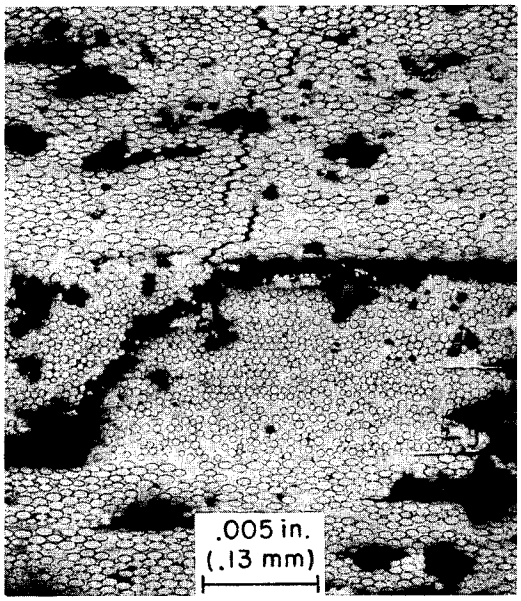

(c) Enlargement of 0° split region in (b)

FIGURE 40 (continued).

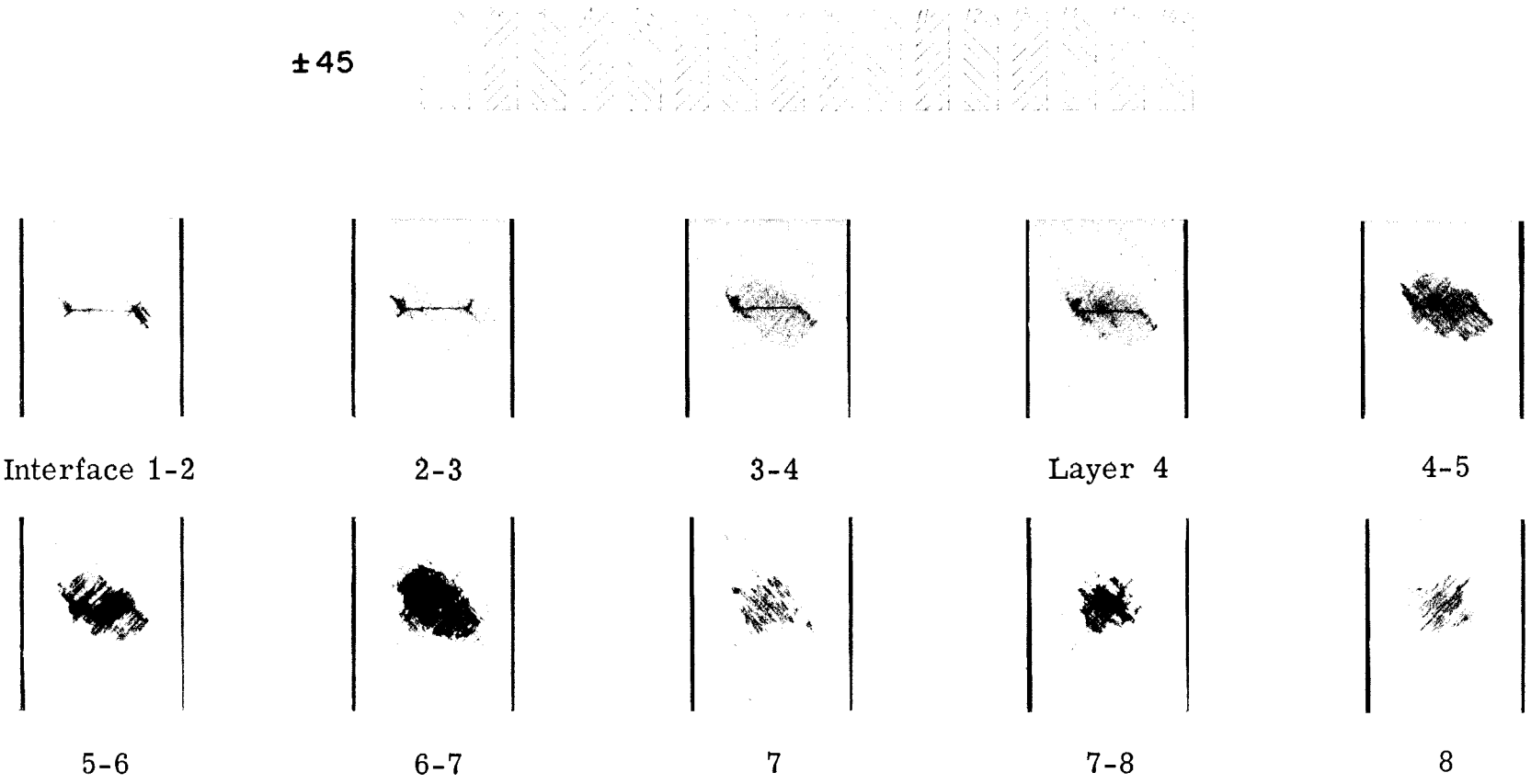

Preload: σ/UTS = .74

FIGURE 41.

DAMAGE DEVELOPED IN ±45 (16 LAYERS), 1002 SCOTCHPLY CONTAINING FIVE-LAYER DEEP SURFACE CRACKS ON BOTH SIDES, W = 2 in. (5.1 cm), $2c_o/W$ = .375.

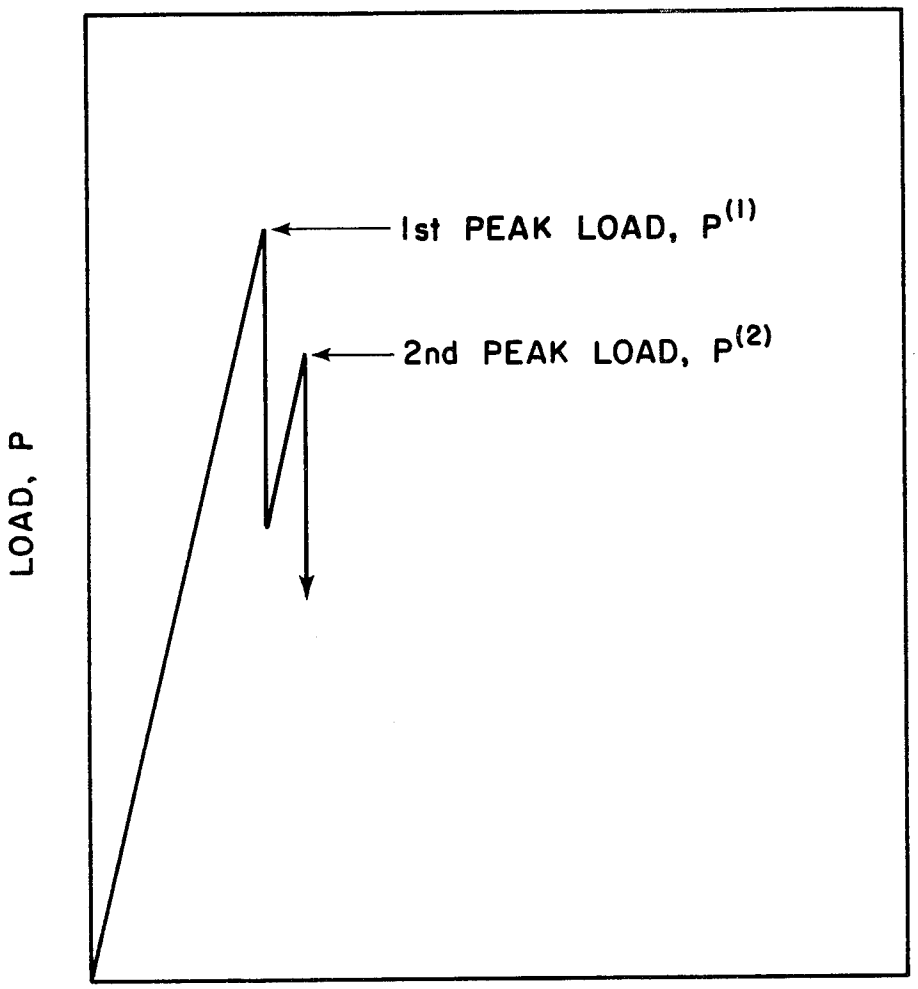

FIGURE 42.

TWO DISTINCT PEAKS REFLECTED IN LOAD-EXTENSION CURVE FOR COMPOSITE SPECIMENS CONTAINING SURFACE CRACKS.

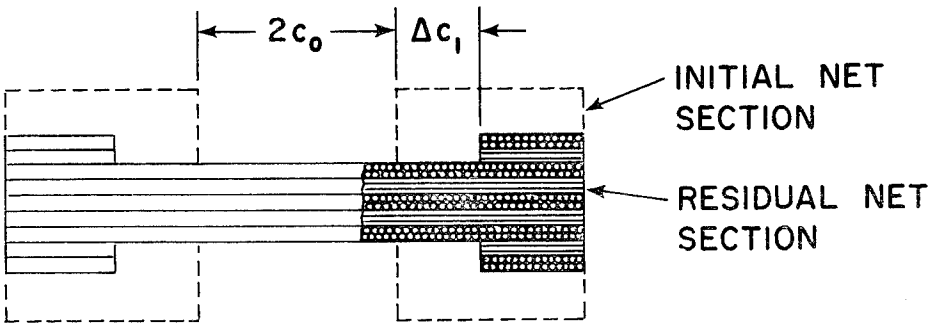

(a) 90/0 (15 layers) with five-layer deep surface cracks on both sides

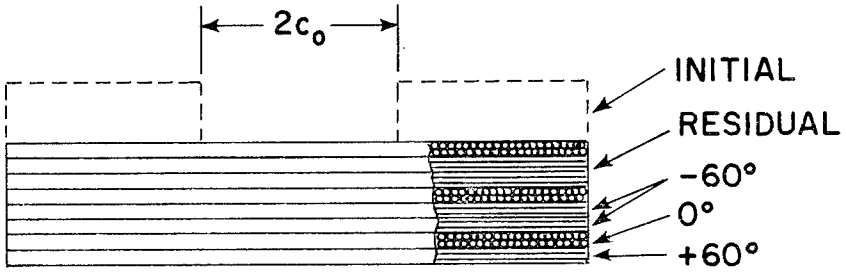

(b) 60/0/-60 (12 layers) with four-layer deep surface crack

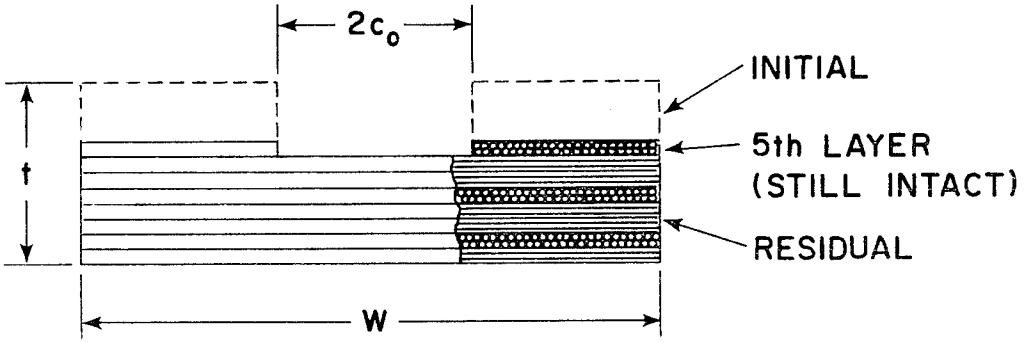

(c) 60/0/-60 (12 layers) with five-layer deep surface crack

FIGURE 43.

NET SECTIONS REMAINING INTACT AFTER FIRST PEAK AND PERSISTING UNTIL FINAL FRACTURE, MULTI-LAYERED 1002 SCOTCHPLY WITH SURFACE CRACKS.

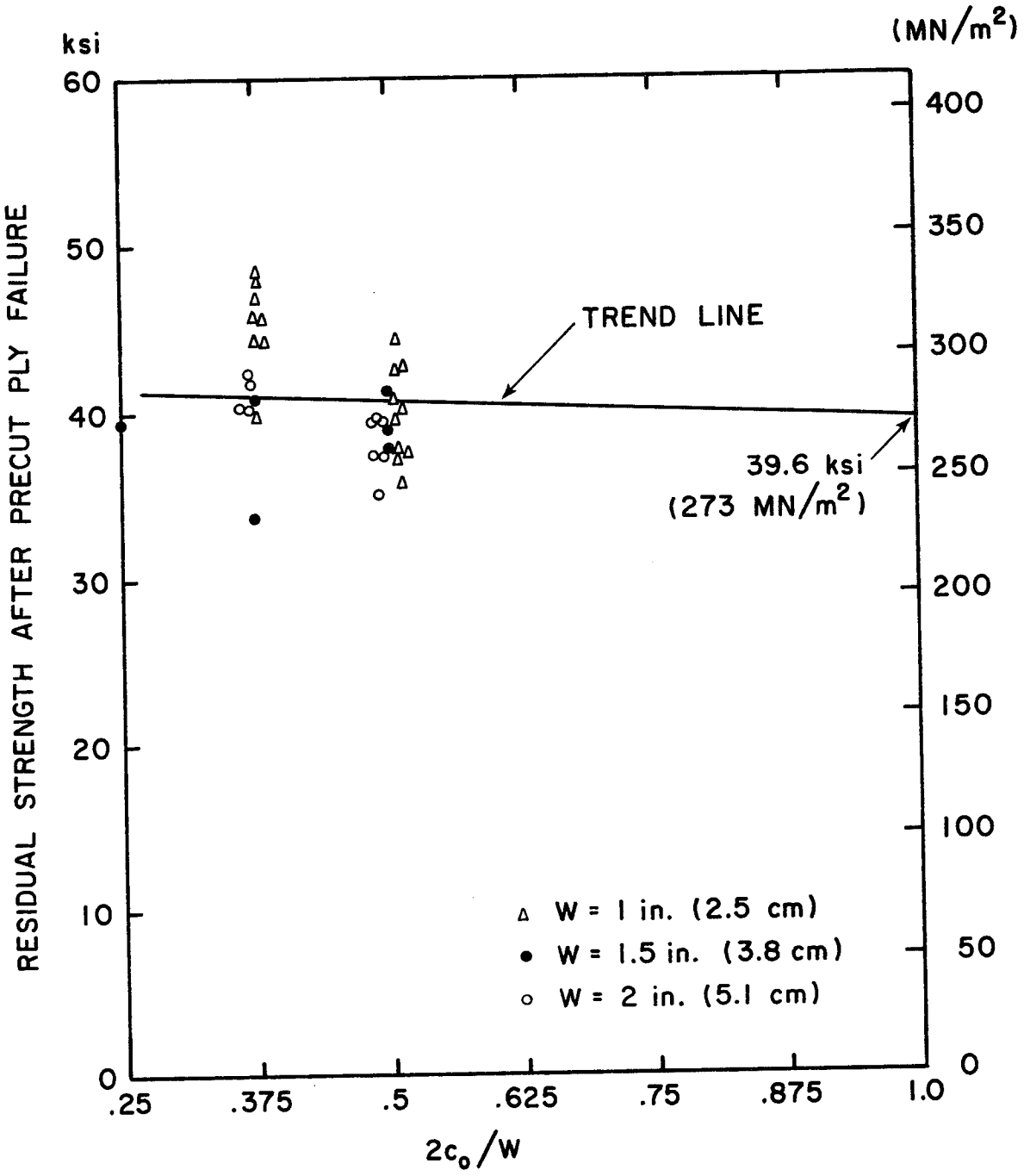

FIGURE 44.

RESIDUAL STRENGTH AFTER PRECUT PLY FAILURE vs. $2c_0/W$, 90/0 (15 LAYERS) TYPE 1002 SCOTCHPLY WITH SURFACE CRACK ON ONE SIDE (LAYERS 1-5 PRECUT).

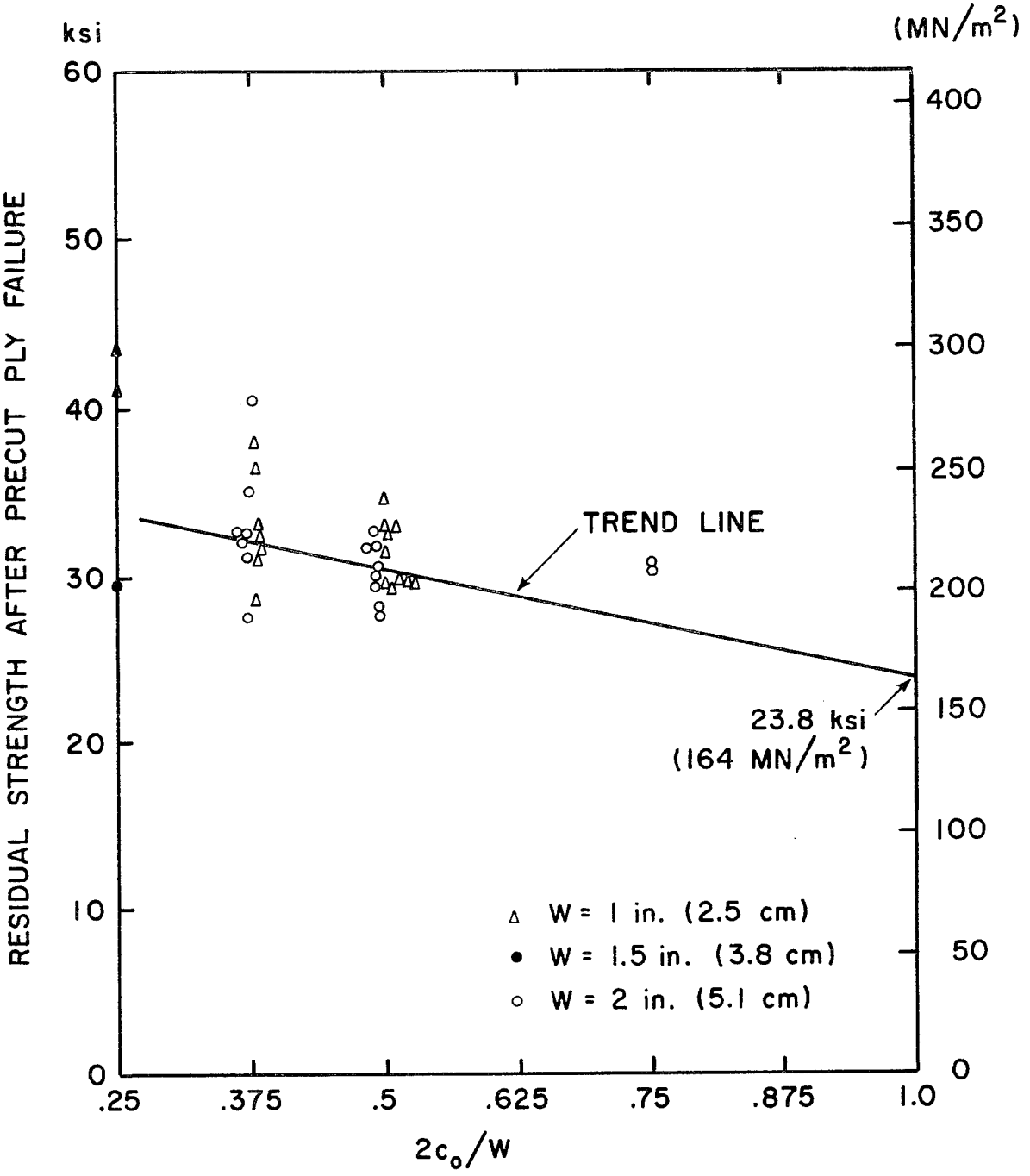

FIGURE 45.

RESIDUAL STRENGTH AFTER PRECUT PLY FAILURE vs. $2c_o/W$, 90/0 (15 LAYERS) TYPE 1002 SCOTCHPLY WITH SURFACE CRACKS ON BOTH SIDES (LAYERS 1-5 AND 11-15 PRECUT).

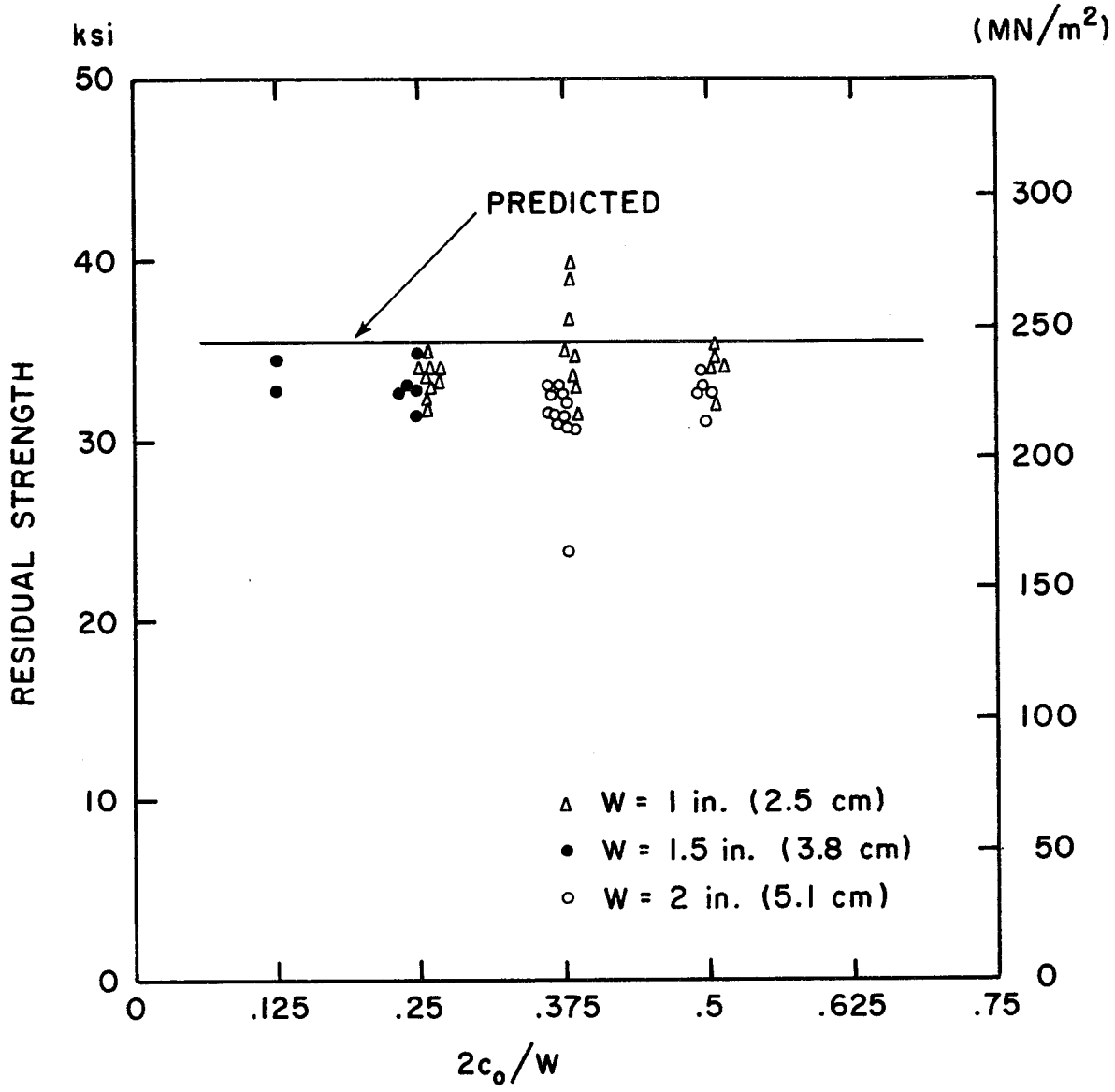

FIGURE 46.

RESIDUAL STRENGTH AFTER PRECUT PLY FAILURE vs. $2c_o/W$, ±60/0 (12 LAYERS) TYPE 1002 SCOTCHPLY WITH SHALLOW SURFACE CRACK ON ONE SIDE (LAYERS 1-4 PRECUT).

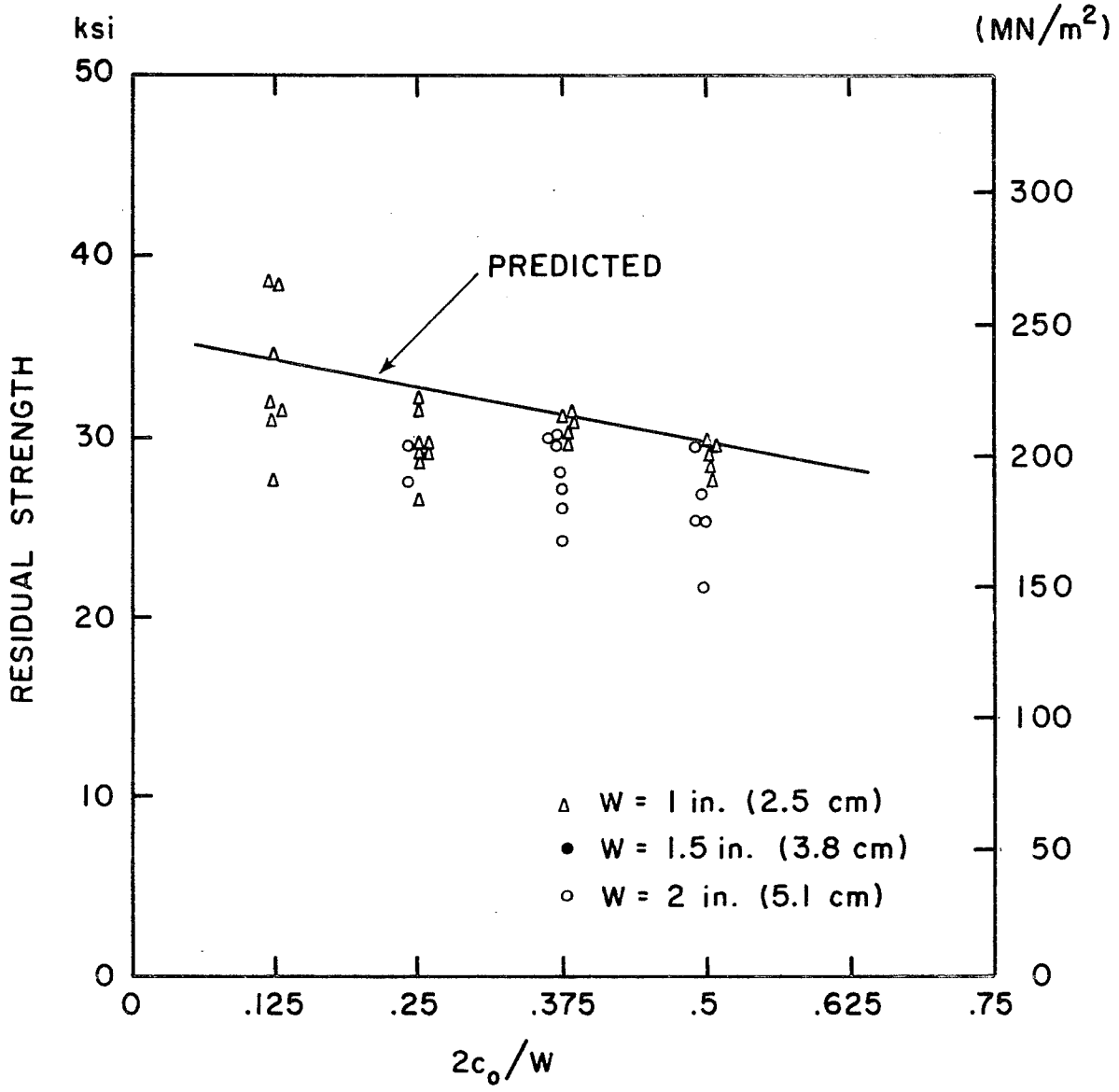

FIGURE 47.

RESIDUAL STRENGTH AFTER PRECUT PLY FAILURE vs. $2c_0/W$, ±50/0 (12 LAYERS) TYPE 1002 SCOTCHPLY WITH SURFACE CRACK ON ONE SIDE (LAYERS 1-5 PRECUT).

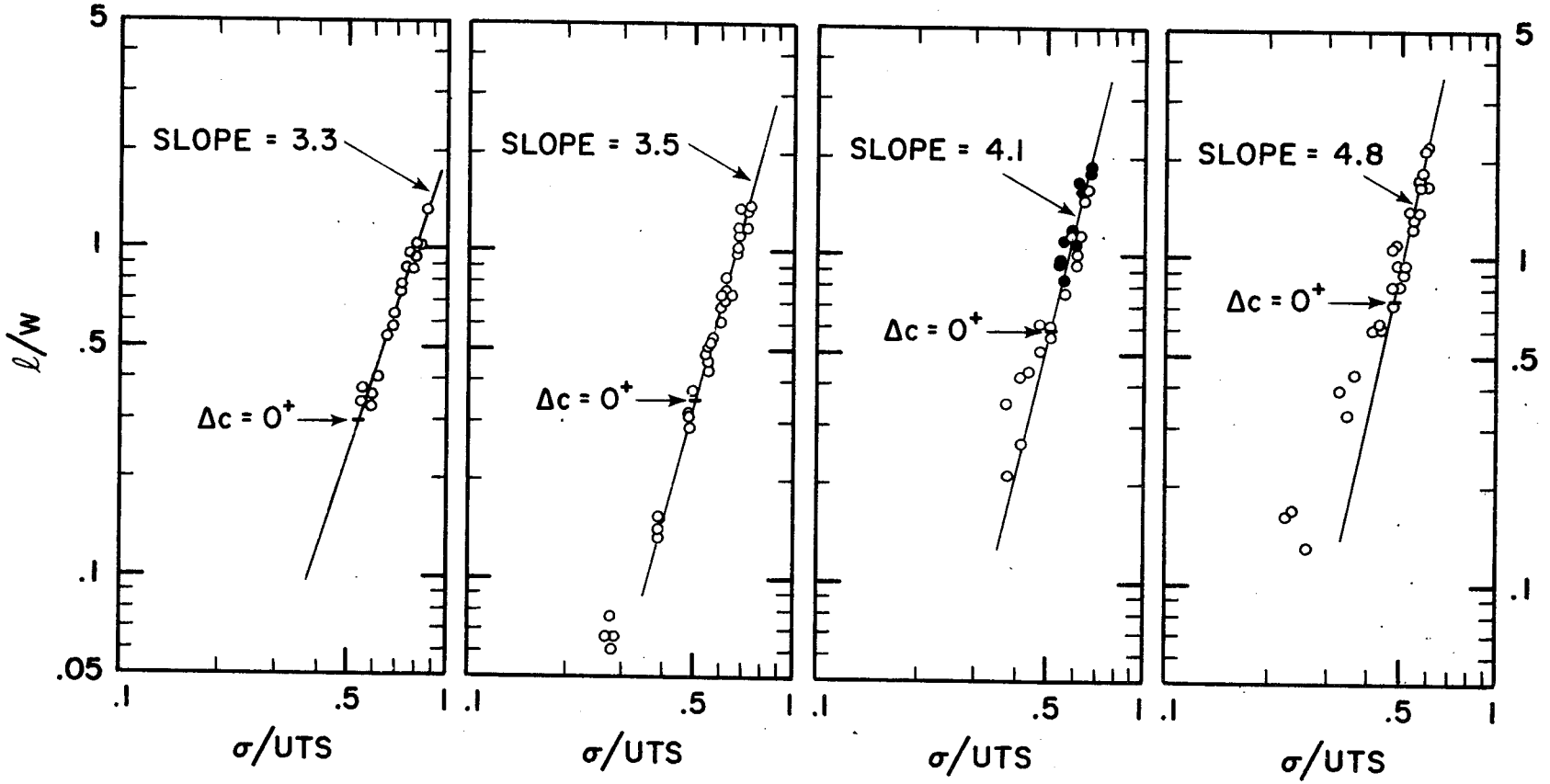

(a) Type 1003 $2c_0/W = .25$

(b) Type 1002 $2c_0/W = .375$

(c) Type 1003 $2c_0/W = .5$

(d) Type 1003 $2c_0/W = .625$

FIGURE 48.

DELAMINATION LENGTH, ℓ/W vs. NOMINAL STRESS, σ/UTS, 90/0 (15 LAYERS) TYPE 1002 AND 1003 SCOTCHPLIES WITH FIVE-LAYER DEEP SURFACE CRACKS ON BOTH SIDES, W_{AV} = 2 in. (5.1 cm) (o) AND 1 in. (2.5 cm) (●).

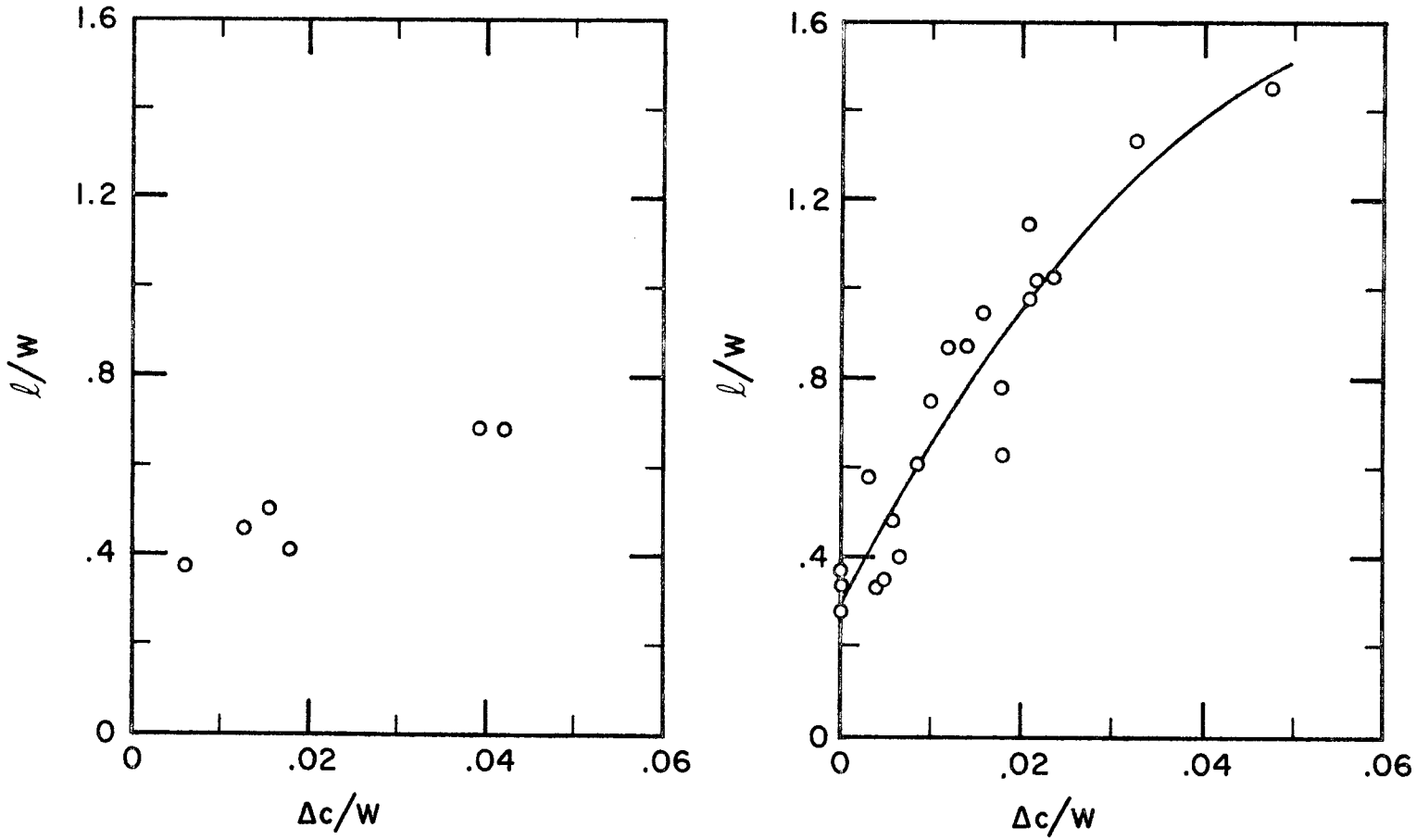

(a) $2c_o/W = .125$, Type 1003

(b) $2c_o/W = .25$, Type 1003

FIGURE 49.

EXTENT OF DELAMINATION, ℓ/W vs. MAIN CRACK EXTENSION WITHIN FOURTH LAYER, $\Delta c/W$, FOR 90/0 (15 LAYERS) GLASS/EPOXY CONTAINING FIVE-LAYER DEEP SURFACE CRACKS ON BOTH SIDES.

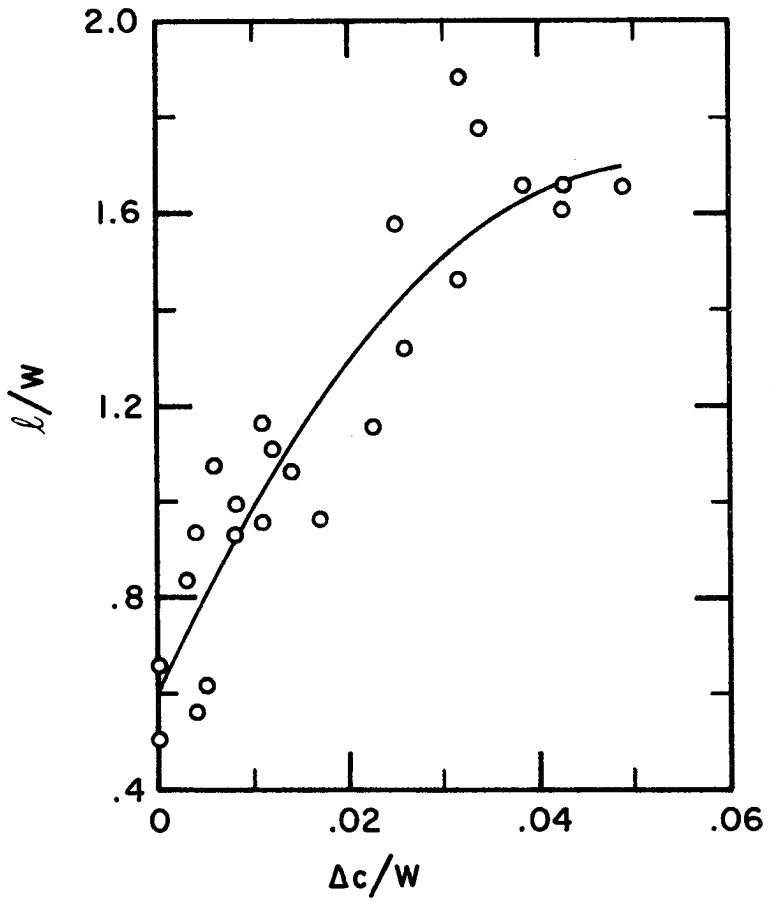

(c) $2c_o/W$ = .5, Type 1003

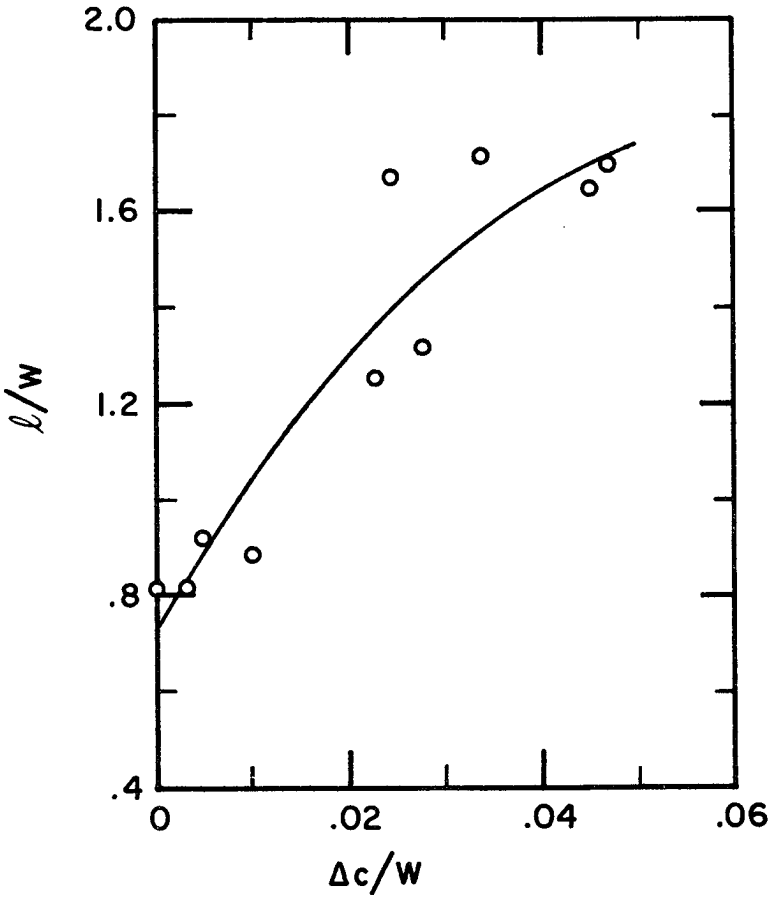

(d) $2c_o/W$ = .625, Type 1003

FIGURE 49 (continued)

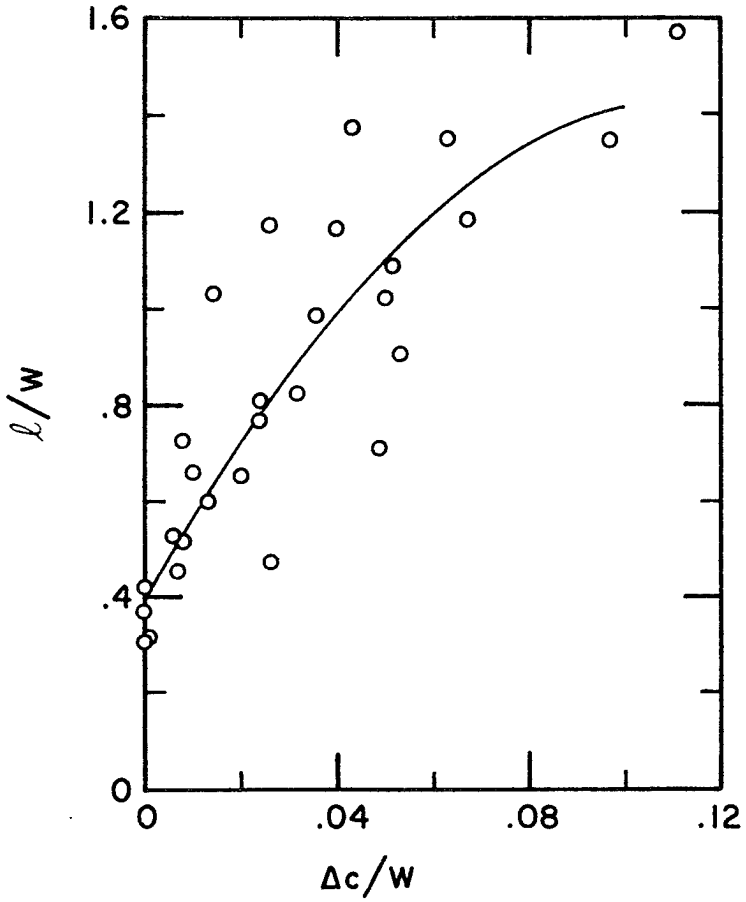

(e) $2c_o/W$ = .375, Type 1002

FIGURE 49 (continued).

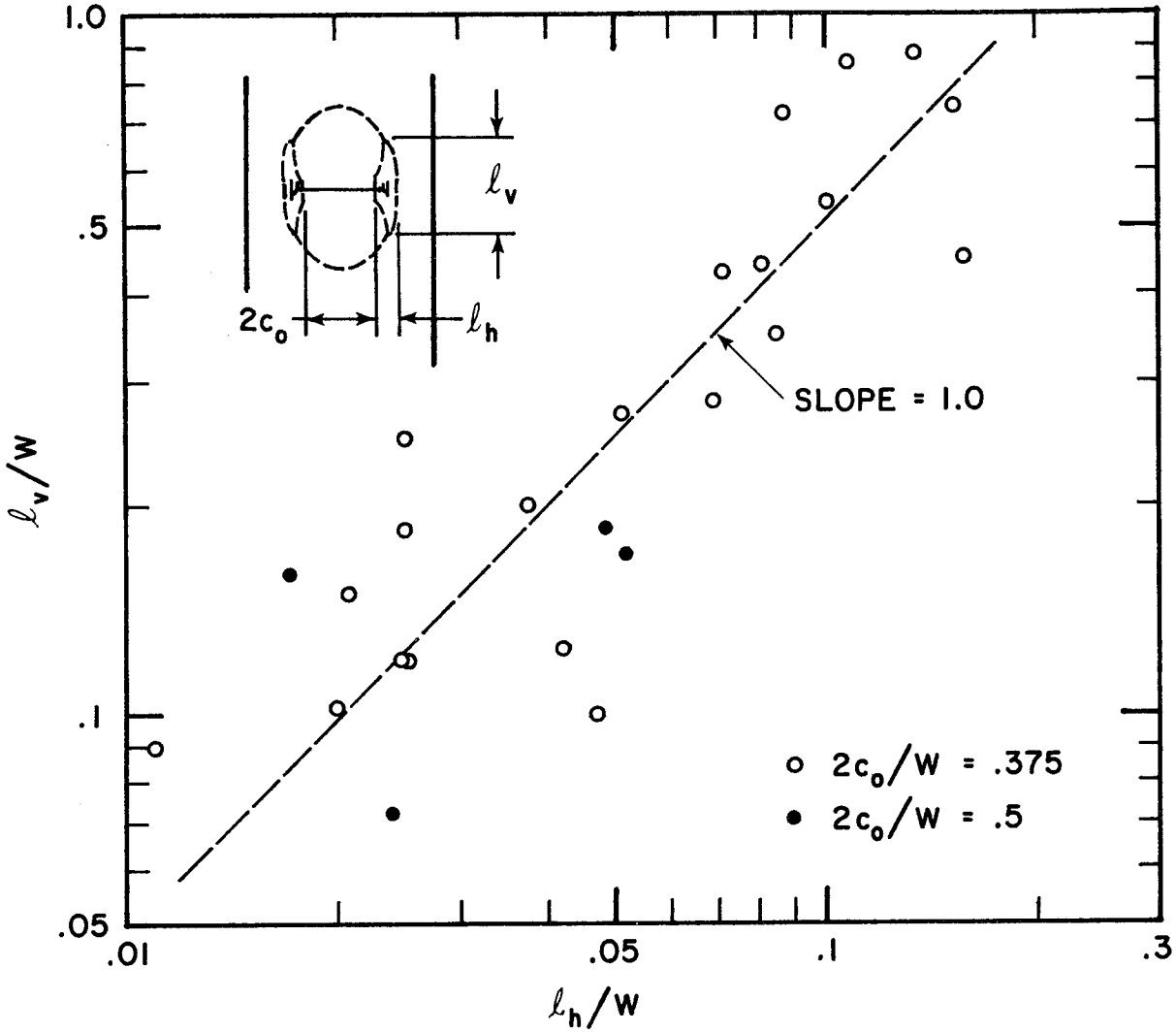

FIGURE 50.

SIZE OF DELAMINATION AT INTERFACE BETWEEN THIRD AND FOURTH LAYERS, 90/0, 1002 SCOTCHPLY WITH FIVE-LAYER DEEP SURFACE CRACKS ON BOTH SIDES, W = 1.5 in. (3.81 cm).

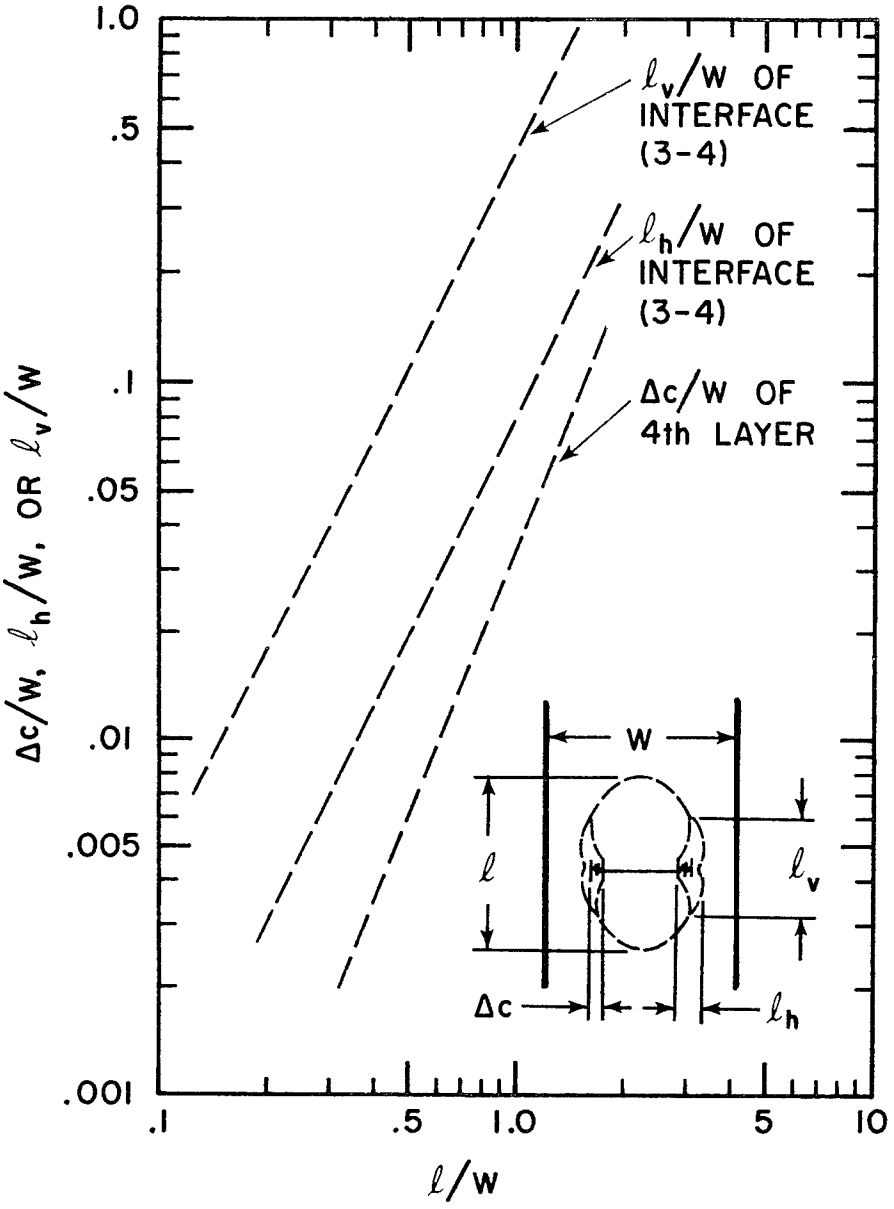

FIGURE 51

APPROXIMATE INTER-RELATIONS AMONG ℓ/W, $\Delta c/W$, ℓ_h/W, AND ℓ_v/W, 90/0, 1002 SCOTCHPLY WITH FIVE-LAYER DEEP SURFACE CRACKS ON BOTH SIDES, W = 1.5 in. (3.81 cm), $2c_o/W$ = .375.

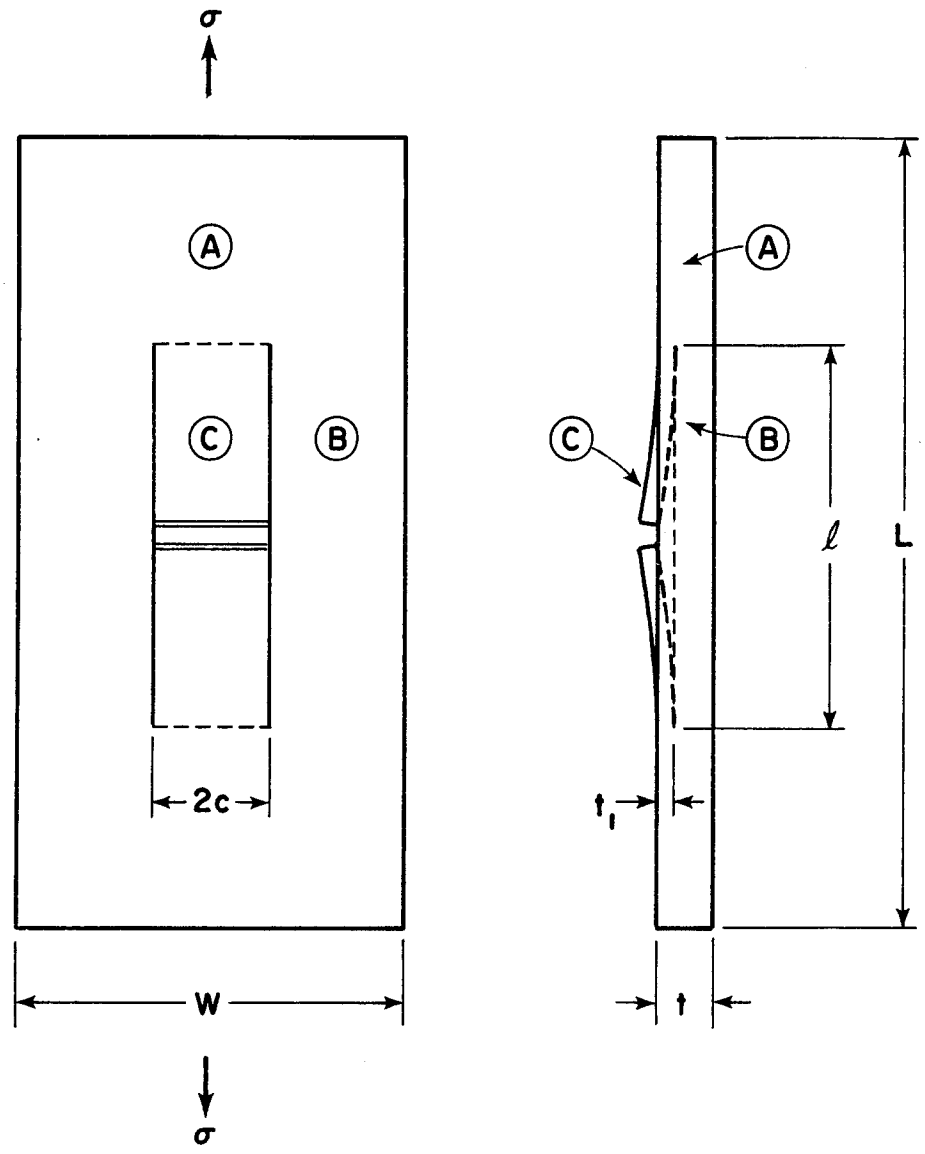

FIGURE 52.

MODEL FOR UNIDIRECTIONAL COMPOSITE CONTAINING SURFACE CRACK.

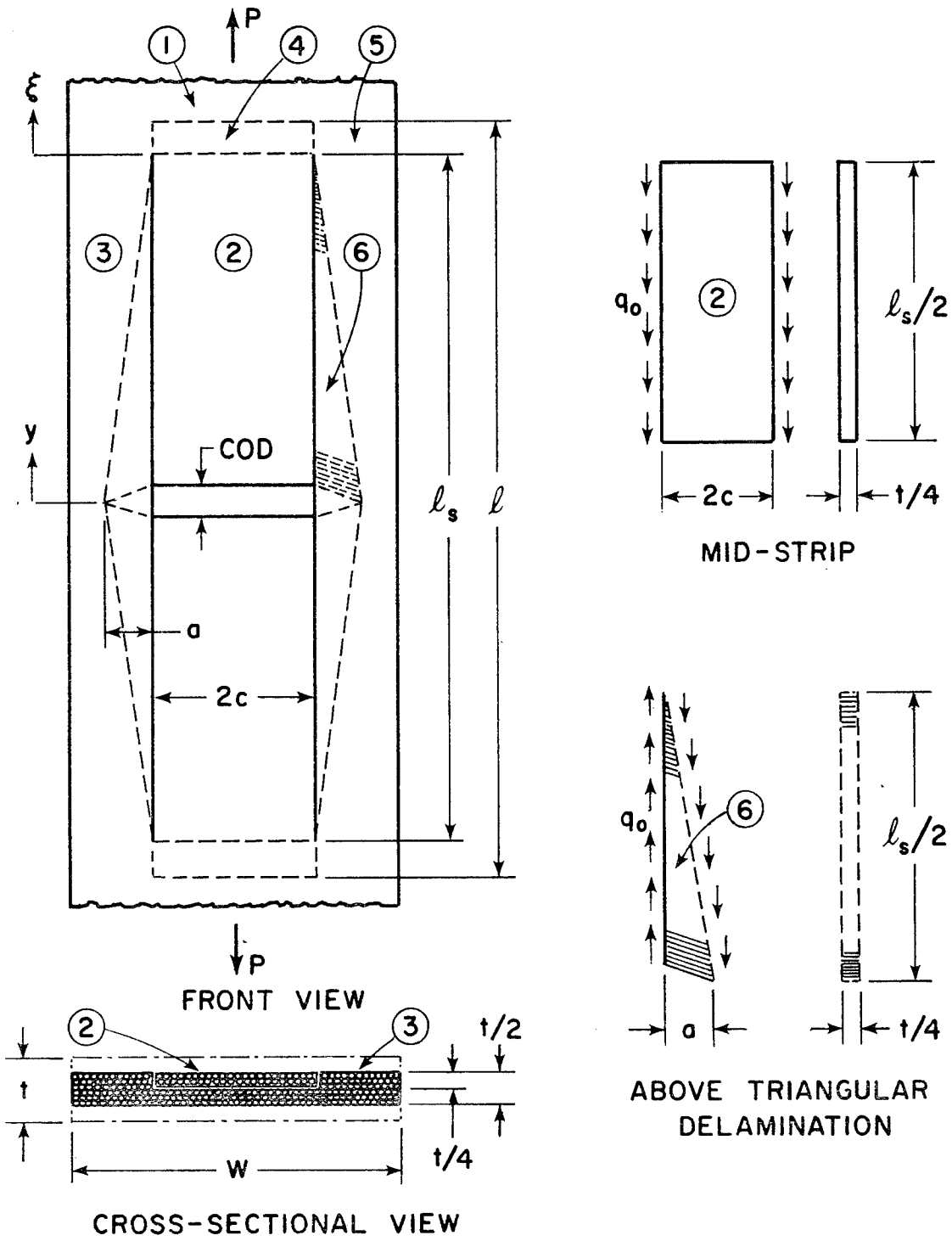

(a) Schematics

FIGURE 53.

SCHEMATICS OF MODEL AND DESCRIPTION OF EACH REGION, 90/0/0/90, 1003 SCOTCHPLY WITH TWO-PLY DEEP SURFACE CRACK.

Region 1:

Uniform thickness, $t/2$

Uniform stress, $\sigma_{1L} = P/(\frac{t}{2} W)$

Region 2:

Tongue-shaped mid-strip

Uniform thickness, $t/4$

Constant stress, q_o, acts on split surfaces

Region 3:

Same cross-sectional area as Region 1 minus Region 2

Constant force, $(q_o \frac{t}{4})$ per unit height acts along the boundary of Region 6

Regions 4 and 5:

Have same cross-sectional areas as Regions 2 and 3, respectively

Region 6:

Consists of outermost 90° layer above triangular delamination

Uniform shear stress, q_o, acts along the boundaries

(b) Description of regions

FIGURE 53 (continued).

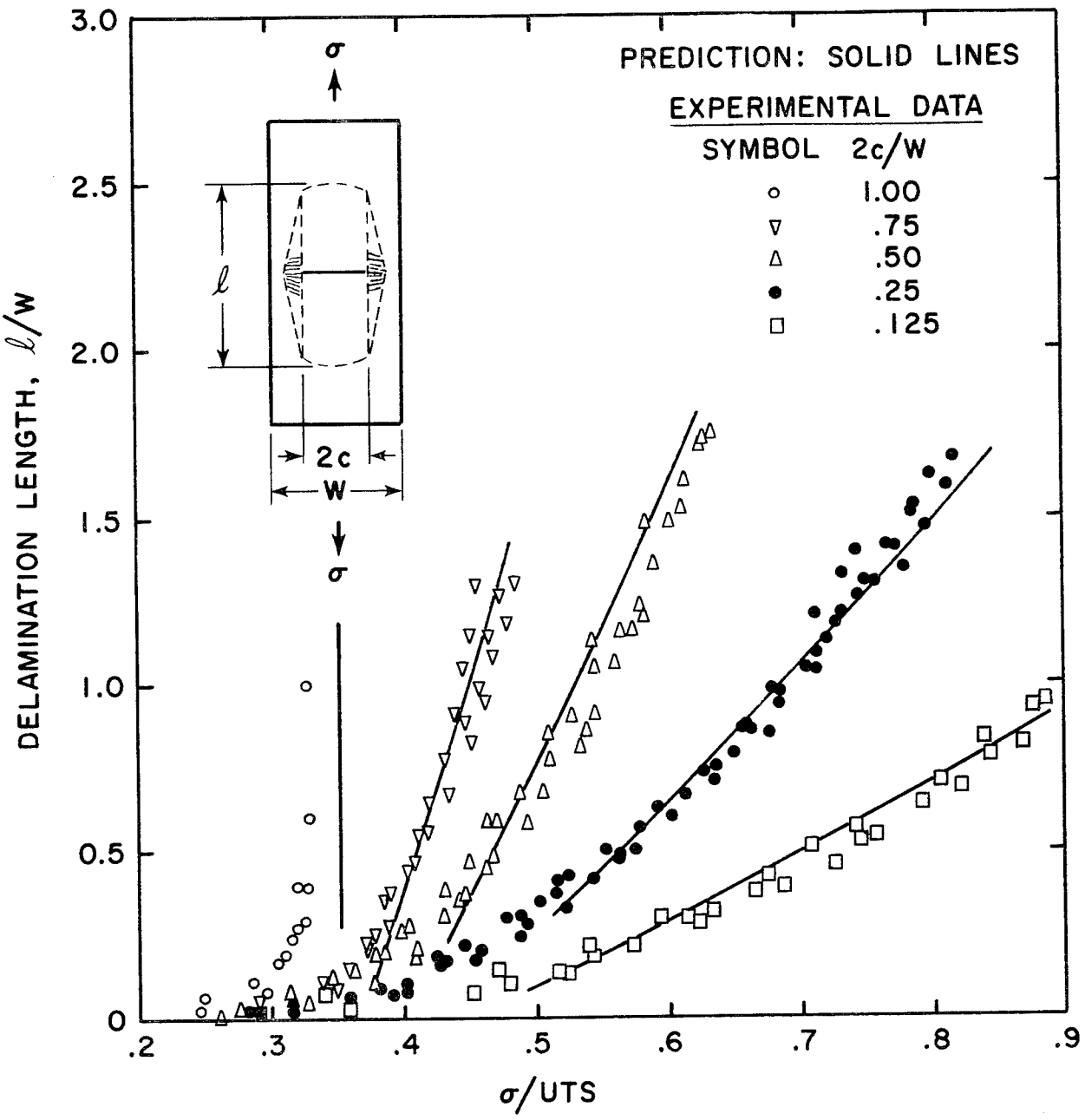

FIGURE 54.

COMPARISON OF PREDICTED AND MEASURED DELAMINATION GROWTH CURVES FOR VARIOUS CRACK LENGTHS, 90/0/0/90 TYPE 1003 SCOTCHPLY GLASS/EPOXY.

INTERIM REPORT DISTRIBUTION LIST

NSG 3044

SURFACE CRACK GROWTH IN FIBER COMPOSITES

Advanced Research Projects Agency
Washington, DC 20525
Attn: Library

Advanced Technology Center, Inc.
LTV Aerospace Corporation
P. O. Box 6144
Dallas, TX 75222
Attn: D. H. Petersen
W. J. Renton

Air Force Flight Dynamics Laboratory
Wright-Patterson Air Force Base, Ohio 45433
Attn: L. J. Obery (TBP)
G. P. Sendeckyj (FBC)
R. S. Sandhu
J. C. Halpin

Air Force Materials Laboratory
Wright-Patterson Air Force Base, Ohio 45433
Attn: J. D. Ray (LTN)
H. S. Schwartz (LN)
T. J. Reinhart (MBC)
G. P. Peterson (LC)
E. J. Morrisey (LAE)
S. W. Tsai (MBM)
N. J. Pagano
J. M. Whitney (MBM)

Air Force Office of Scientific Research
Washington, DC 20333
Attn: J. F. Masi (SREP)

Air Force Office of Scientific Research
1400 Wilson Blvd.
Arlington, VA 22209
Attn: SIGL

Air Force Rocket Propulsion Laboratory
Edwards, CA 93523
Attn: Library

Babcock and Wilcox Company
Advanced Composites Department
P.O. Box 419
Alliance, Ohio 44601
Attn: R. Young

Bell Helicopter Company
P.O. Box 482
Ft. Worth, TX 76101
Attn: H. Zinberg

The Boeing Company
P.O. Box 3999
Seattle, WA 98124
Attn: J. T. Hoggatt, MS 88-33
T. R. Porter

The Boeing Company
Vertol Division
Morton, PA 19070
Attn: R. A. Pinckney
E. C. Durchlaub

Battelle Memorial Institute
Columbus Laboratories
505 King Avenue
Columbus, OH 43201
Attn: E. F. Rybicki
L. E. Hulbert

Brunswick Corporation
Defense Products Division
P.O. Box 4594
43000 Industrial Avenue
Lincoln, NE 68504
Attn: R. Morse

Chemical Propulsion Information Agency
Applied Physics Laboratory
8621 Georgia Avenue
Silver Spring, MD 20910
Attn: Library

Commander
Natick Laboratories
U.S. Army
Natick, MA 01762
Attn: Library

Commander
Naval Air Systems Command
U.S. Navy Department
Washington, DC 20360
Attn: M. Stander, AIR-43032D

Commander
Naval Ordnance Systems Command
U.S. Navy Department
Washington, DC 20360
Attn: B. Drimmer, ORD-033
M. Kinna, ORD-033A

Cornell University
Dept. Theoretical & Applied Mech.
Thurston Hall
Ithaca, NY 14853
Attn: F. C. Moon

Defense Metals Information Center
Battelle Memorial Institute
Columbus Laboratories
505 King Avenue
Columbus, OH 43201

Department of the Army
U.S. Army Material Command
Washington, DC 20315
Attn: AMCRD-RC

Department of the Army
U.S. Army Aviation Materials Laboratory
Ft. Eustis, VA 23604
Attn: I. E. Figge, Sr.
Library

Department of the Army
U.S. Army Aviation Systems Command
P.O. Box 209
St. Louis, MO 63166
Attn: R. Vollmer, AMSAV-A-UE

Department of the Army
Plastics Technical Evaluation Center
Picatinny Arsenal
Dover, NJ 07801
Attn: H. E. Pebly, Jr.

Department of the Army
Watervliet Arsenal
Watervliet, NY 12189
Attn: G. D'Andrea

Department of the Army
Watertown Arsenal
Watertown, MA 02172
Attn: A. Thomas

Department of the Army
Redstone Arsenal
Huntsville, AL 35809
Attn: R. J. Thompson, AMSMI-RSS

Department of the Navy
Naval Ordnance Laboratory
White Oak
Silver Spring, MD 20910
Attn: R. Simon

Department of the Navy
U.S. Naval Ship R&D Laboratory
Annapolis, MD 21402
Attn: C. Hersner, Code 2724

Director
Deep Submergence Systems Project
6900 Wisconsin Avenue
Washington, DC 20015
Attn: H. Bernstein, DSSP-221

Director
Naval Research Laboratory
Washington, DC 20390
Attn: Code 8430
I. Wolock, Code 8433

E. I. DuPont DeNemours and Co.
DuPont Experimental Station
Wilmington, DE 19898
Attn: C. H. Zweben

Fiber Science, Inc.
245 East 157th Street
Gardena, CA 90248
Attn: E. Dunahoo

General Dynamics
P.O. Box 748
Ft. Worth, TX 76100
Attn: M. E. Waddoups
Library

General Dynamics/Convair
P.O. Box 1128
San Diego, CA 92112
Attn: J. L. Christian

General Electric Co.
Evendale, OH 45215
Attn: C. Stotler
R. Ravenhall
R. Stabrylla

General Motors Corporation
Detroit Diesel-Allison Division
Indianapolis, IN 46244
Attn: M. Herman

Grumman Aerospace Corporation
Bethpage, Long Island, NY 11714
Attn: S. Dastin
J. B. Whiteside

Hamilton Standard Division
United Aircraft Corporation
Windsor Locks, CT 06096
Attn: W. A. Percival

Hercules, Inc.
Allegheny Ballistics Laboratory
P.O. Box 210
Cumberland, MD 21052
Attn: A. A. Vicario

Illinois Institute of Technology
10 West 32 Street
Chicago, IL 60616
Attn: L. J. Broutman

IIT Research Institute
10 West 35 Street
Chicago, IL 60616
Attn: I. M. Daniel

Jet Propulsion Laboratory
4800 Oak Grove Drive
Pasadena, CA 91103
Attn: A. C. Knoell
Library

Lawrence Livermore Laboratory
P.O. Box 808, L-421
Livermore, CA 94550
Attn: T. T. Chiao
E. M. Wu
R. H. Toland

Lockheed-Georgia Co.
Advanced Composites Information Center
Dept. 72-14, Zone 402
Marietta, GA 30060
Attn: T. M. Hsu

Lockheed Missiles and Space Co.
P.O. Box 504
Sunnyvale, CA 94087
Attn: R. W. Fenn

Lockheed-California
Burbank, CA 91503
Attn: J. T. Ryder
R. L. Vaughn

McDonnell Douglas Aircraft Corporation
P.O. Box 516
Lambert Field, MS 63166
Attn: J. C. Watson

McDonnell Douglas Aircraft Corporation
3855 Lakewood Blvd.
Long Beach, CA 90810
Attn: L. B. Greszczuk

Material Sciences Corporation
1777 Walton Road
Blue Bell, PA 19422
Attn: B. W. Rosen

NASA-Ames Research Center
Moffett Field, CA 94035
Attn: Library
D. P. Williams

NASA-Flight Research Center
P.O. Box 273
Edwards, CA 93523
Attn: Library

NASA-George C. Marshall Space Flight Center
Huntsville, AL 35812
Attn: C. E. Cataldo, S&E-ASTN-MX
Library

NASA-Goddard Space Flight Center
Greenbelt, MD 20771
Attn: Library

NASA-Langley Research Center
Hampton, VA 23365
Attn: E. E. Mathauser, MS 188a
R. A. Pride, MS 188a
M. C. Card
Library

NASA-Lewis Research Center
21000 Brookpark Road
Cleveland, OH 44135
Attn: Contracting Officer, MS 500-313
Tech. Report Control, MS 5-5
Technical Utilization, MS 3-19
AFSC Liaison, MS 501-3
Rel. and Quality Assur., MS 500-211
R. H. Kemp, MS 49-3
R. F. Lark, MS 49-3
J. C. Freche, MS 49-1
R. H. Johns, MS 49-3
N. T. Saunders, MS 105-1
C. C. Chamis, MS 49-3 (13 copies)
T. T. Serafini, MS 49-1
Library, MS 60-3 (2 copies)

NASA-Lyndon B. Johnson Space Center
Houston, TX 77001
Attn: S. Glorioso, SMD-ES52
Library

NASA Scientific and Tech. Information Facility
P. O. Box 33
College Park, MD 20740
Attn: Acquisitions Branch (10 copies)

National Aeronautics & Space Administration
Office of Advanced Research and Technology
Washington, DC 20546
Attn: M. J. Salkind, Code RWS

National Aeronautics & Space Administration
Office of Technology Utilization
Washington, DC 20546

National Bureau of Standards
Eng. Mech. Section
Washington, DC 20234
Attn: R. Mitchell

National Technology Information Service
Springfield, VA 22151 (6 copies)

National Science Foundation
Engineering Division
1800 G Street, NW
Washington, DC 20540
Attn: Library

Northrop Space Laboratories
3401 West Broadway
Hawthorne, CA 90250
Attn: R. M. Verette

Pratt & Whitney Aircraft
East Hartford, CT 06108
Attn: A. J. Dennis

Rockwell International
Los Angeles Division
International Airport
Los Angeles, CA 90009
Attn: L. M. Lackman
D. Y. Konishi

Sikorsky Aircraft Division
United Aircraft Corporation
Stratford, CT 06602
Attn: Library

Southwest Research Institute
8500 Culebra Road
San Antonio, TX 78284
Attn: P. H. Francis

Space and Missile Systems Organization
Air Force Unit Post Office
Los Angeles, CA 90045
Attn: Technical Data Center

Structural Composites Industries, Inc.
6344 N. Irwindale Avenue
Azusa, CA 91702
Attn: E. E. Morriss

TRW, Incorporated
23555 Euclid Avenue
Cleveland, OH 44117
Attn: W. E. Winters

Union Carbide Corporation
P.O. Box 6116
Cleveland, OH 44101
Attn: J. C. Bowman

United Technologies Research Center
East Hartford, CT 06108
Attn: R. C. Novak

University of Dayton Research Institute
Dayton, OH 45409
Attn: W. S. Blain

University of Delaware
Mechanical and Aerospace Engineering
Newark, DE 19711
Attn: B. R. Pipes

University of Oklahoma
School of Aerospace Mechanical and
Nuclear Engineering
Norman, OK 73069
Attn: C. W. Bert

University of Wyoming
College of Engineering
University Station Box 3295
Laramie, WY 82071
Attn: D. F. Adams

U. S. Army Materials and Mechanics
Research Center
Watertown Arsenal
Watertown, MA 02172
Attn: E. M. Lenoe
D. W. Oplinger

V. P. I. and S. U.
Dept. of Eng. Mech.
Blacksburg, VA 24061
Attn: R. H. Heller
H. J. Brinson
C. T. Herakovich